INVESTIGATION OF THE STRESS INTENSITY FACTORS AT SHARP CORNERS OF ARBITRARY CUTOUTS IN FINITE PLATES

A THESIS

Presented to

The Faculty of the Division of Graduate Studies

By

Wen-mo Chen

In Partial Fulfillment

of the Requirements for the Degree

Doctor of Philosophy

in the School of Aerospace Engineering

Georgia Institute of Technology

June, 1977

INVESTIGATION OF THE STRESS INTENSITY FACTORS

AT SHARP CORNERS OF ARBITRARY CUTOUTS

IN FINITE PLATES

Approved:

Dr. C. V. Smith, Chairman

Dr. J. M. Anderson

Dr. R. L. Carlson

Date approved by Chairman: 7 July 1977

ACKNOWLEDGMENTS

I would express my sincere appreciation to Dr. C. V. Smith for his instruction throughout the preparation of this work.

I would like to acknowledge the financial support under the Tuition Assistant Plan from Bell Aerospace Textron. My deepest appreciation goes to Mr. Hugh F. Farabaugh, Director, Employee Relations and Services and Mr. Robert G. Moore, Assistant Director, Engineering Technology for their permission to utilize Bell's Computer facility. Completion of this work would have been impossible without their support.

Sincere thanks are extended to Dr. J. M. Anderson, Dr. M. P. Stallybrass, Dr. R. L. Carlson and Dr. S. Atluri, for their reading of my dissertation.

My sincere appreciation goes to my wife, Pi-Ian, for her constant encouragement and devotion during the entire period of study. My deep gratitude also goes to my mother, Mrs. Chu-ying Chen, for her financial support through the early years of my education.

My thanks also go to Mrs. Claudine Taylor for typing the final manuscript.

TABLE OF CONTENTS

TABLE OF CONTENTS (Continued)

LIST OF TABLES

LIST OF TABLES (Continued)

LIST OF SYMBOLS

Symbol	Definition
$f(\theta)$	Part of stress function dependent upon θ only
$f^n(\theta)$	The n^{th} order derivative of $f(\theta)$
i	Imaginary unit = $\sqrt{-1}$
ℓ	Notch length
ℓ_x, ℓ_y or n_{ij}	The direction cosines of the unit normal
m, n	Positive integer
$\{\delta\}$	Nodal displacement along S_u
$\{\delta_R\}$	Rigid body displacements matrix
$\{\delta_s\}$	Symmetric nodal displacements matrix
$\{\delta_a\}$	Antisymmetric nodal displacements matrix
r, θ	Plane polar coordinates
r_b	Radial coordinate on the boundary
t	Thickness of singular element
u_r, u_θ	Displacement components in polar coordinates
u_x^p, u_y^p	Boundary displacement components in cartesian coordinates
w	Plate width
x, y	Cartesian coordinates
$[B]$	Surface traction matrix along S_u
$[B_s]$	Part of [B] due to symmetric stresses
$[B_a]$	Part of [B] due to antisymmetric stresses
$\{C\}$	Matrix of stress coefficients
$\{C_s\}$	Matrix of symmetric stress coefficients

LIST OF SYMBOLS (Continued)

Symbol	Definition
C_a	Matrix of antisymmetric stress coefficients
C_1, C_2, C_3, C_4	Integration constants
C_{an}	Antisymmetric stress coefficient
C_{sn}	Symmetric stress coefficient
$[D]$	Linear interpolations of $\{q\}$ along S_u
E	Young's modulus
G	Shear modulus of rigidity
$[H]$	Matrix defined by equation (3.5)
IP	Imaginary part of eigenvalue
$[K]$	Stiffness matrix of singular element
$[K_s]$	Part of [K] due to symmetric stresses
$[K_a]$	Part of [K] due to antisymmetric stresses
K_a	Sliding mode stress intensity factor
K_s	Opening mode stress intensity factor
$[L]$	Stress series matrix
$[L_s]$	Part of [L] due to symmetric stresses
$[L_a]$	Part of [L] due to antisymmetric stresses
$[N]$	Elasticity matrix containing the appropriate material properties
P	Load
RP	Real part of eigenvalue
S_u	The surface where displacements are prescribed
$\{S\}$	The surface traction on S_u
$[TS]$	Stress transformation matrix

LIST OF SYMBOLS (Continued)

Symbol	Definition
$[T]$	Matrix defined by equation (3.12)
$\{u^p\}$	Boundary displacement matrix, specified on S_u
U_c	Complementary strain energy
U_j^p	The displacement on S_u
V	Volume
V_c	Potential of external loads
X_r , X_θ	Components of body force (per unit volume)
α	Eigenvalues
α_{an}	Antisymmetric eigenvalues
α_{sn}	Symmetric eigenvalues
β_n	Stress coefficients of a special triangular element
∇	Laplace operator
$\epsilon_r, \epsilon_\theta, \gamma_{r\theta}$	Plane polar strain components
θ_o	Vertex angle
μ	Poisson's ratio
π_c	The total complementary energy
σ_{ij}	Stress tensor
$\sigma_r, \sigma_\theta, \tau_{r\theta}$	Plane polar stress components
$\sigma_r^b, \sigma_\theta^b, \tau_{r\theta}^b$	Plane polar stress components on boundary
$\sigma_x, \sigma_y, \tau_{xy}$	Plane cartesian stress components
$\sigma_x^b, \sigma_y^b, \tau_{xy}^b$	Plane cartesian stress components along boundary
φ	Airy stress function
φ_a	Antisymmetric part of stress function
φ_s	Symmetric part of stress function

LIST OF SYMBOLS (Concluded)

Symbol	Definition
$[\ ]$	Row-column matrix
$\{\ \}$	Column matrix
$[\ ]^T$	Transpose of a matrix

LIST OF ILLUSTRATIONS

LIST OF ILLUSTRATIONS (Continued)

LIST OF ILLUSTRATIONS (Continued)

LIST OF ILLUSTRATIONS (Concluded)

SUMMARY

In a two-dimensional formulation of linear elasticity, the stress field at a sharp corner of an arbitrary notch angle as shown in Figure 1 is known to have singularities of order $r^{\alpha-1}$, where α depends upon notch angle between two stress-free edges. The purpose of this study is to determine the associated stress intensity factors at interior sharp corners in a finite plate subject to in-plane loading. This is done with the finite element method because of the ease of treating discontinuous stresses at sharp corners and stress-free boundary conditions at free edges.

In order to apply the finite element method, the stiffness matrix for singular elements as shown in Figure 2 is formulated by utilizing the principle of stationary complementary energy. The assumed stress expressions are obtained by solving the biharmonic governing differential equation and satisfying the stress-free boundary conditions.

The shapes of the singular elements, square with 9 nodes for $0° \leq$ notch angle $< 90°$ and rectangular with 7 nodes for $90° \leq$ notch angle $< 180°$, are chosen to fit conveniently in finite element models making use of the most common constant strain triangular membrane element. The stiffness matrices for the singular and triangular elements are derived based on the assumption that boundary displacements between two nodes are linear so that the compatibility along interelement boundaries is maintained.

The conventional procedures to predict stress intensity factors

for hairline crack have been found to be limited, inaccurate, and uneconomical. The singular element can be used to replace highly detailed conventional element models at sharp corners, with very significant economies both in data preparation and computer time. Thus an engineer, without being extensively trained in fracture mechanics, can utilize the singular element in the finite element model to determine stress intensity factors, which are the controlling variables for predicting crack propagation. The procedure to predict crack-growth rates is first to determine the stress intensity factors at the sharp corner where a crack is initiated. After the crack is formed, it is then necessary to introduce a crack element to recalculate the stress intensity factors at the crack tip. However, the present effort is concerned only with the development of a singular element to determine the stress intensity factors at sharp corners; the subjects of crack initiation and propagation are excluded in this study.

The most accurate stiffness matrix presented in this dissertation is obtained when the number of assumed stress states equals the number of displacement degrees of freedom. Stiffness matrices are also derived based on an assumed stress state which includes only the singular terms in the assumed stress series. This eliminates the need for complex eigenvalues and leads to a much easier and a cheaper solution. The accuracy of this simple procedure is determined by comparison to the results of the more accurate solution, and both approximate solutions are compared to other existing solutions when such are available.

In order to investigate the effect of notch angle on stress intensity factors at sharp corners, a number of finite element models are

constructed for double-edge notch (Figures 10, 12 and 14) and single-edge notch (Figures 16, 18 and 20) finite plates with notch angles being equal to 0°, 60° and 90°. Additional study is extended to finite plates with center hairline crack (Figures 30 and 34), single-edge crack (Figure 36) and a rectangular cutout (Figures 38, 40, 42, 44, 46, 48 and 50). It is noted that the singular elements are placed wherever the sharp corners appear, and the triangular elements are attached adjacent to those singular elements. The accuracy and efficiency of the singular element is demonstrated by determining the stress intensity factors of simple crack configurations for which there are existing solutions.

CHAPTER I

INTRODUCTION

The requirement of minimum possible weight in aircraft structure has led to the use of very high strength material which has been found to behave in a brittle manner in the presence of small flaws. As a result, rather than fail by yielding, service failure can occur by brittle fracture at stresses below the design yield strength of the material. This brittle fracture will initiate at points of high stress. One location of these high stresses is at the tip of a hairline crack where the stress field theoretically has a singularity of order $r^{-0.5}$, where r is distance from the crack tip and the corresponding strain energy density has a singularity of order r^{-1}. Physically these stress singularities imply high stress concentration in the neighborhood of the tip; and these high stresses will, in general, cause material yielding which violates some of the basic assumptions of linear theory of elasticity. However, it will be shown in Chapter III that mathematically the total strain energy evaluated over a volume around the neighborhood of the crack tip has a finite value of order r^{1}. Therefore the principle of complementary strain energy can be used to calculate stresses and displacements within the elastic domain.

The stress fields near a crack tip in a flat plate can be divided into three basic types: (1) the opening mode, I, is associated with in-plane stresses and displacements which are symmetric with respect to the crack line; (2) the sliding mode, II, is associated with in-plane stresses

and displacements which are antisymmetric with respect to the crack line; (3) the tearing mode, III, is characterized by displacements perpendicular to the plate which are antisymmetric with respect to the crack line. The most general crack-tip deformation and stress field can be described by combining the three modes.

This study is limited to plannar problems leading to modes I and II. The strengths of the singularities, which are proportional to the coefficients of the singular terms in the stress state, are called stress intensity factors; in this dissertation, they are denoted by K_s and K_a for modes I and II, respectively.

Since K_s and K_a have been discovered to be the controlling parameters for predicting crack propagation, their calculation has been the starting point for most routine fracture mechanics analyses; and much effort has gone into determining the magnitudes of K_s and K_a for various geometric configurations and external loadings. This is a difficult problem in the theory of elasticity due to complications caused by the traction free surfaces of the crack, and exact solutions exist only for cracks in infinite domains.

For finite plates, a numerical technique which has been very popular is the finite element method, which can easily handle the traction free boundary conditions in a plate with arbitrary geometry and loading. Early application of this procedure employed many conventional elements surrounding the crack tip. The stress intensity factors were estimated either by extrapolating crack-opening displacement or near-tip stresses [1,2] or by numerically computing the variation in strain energy with change in crack length [3,4]. It was discovered that these procedures

required highly detailed models in the neighborhood of the crack tip, which were uneconomical both in data preparation and computer time.

Recent efforts have been concentrated on replacing the highly detailed models around the tip with a so-called singular element which has the characteristic crack tip singularity embedded in it. There have been many different types of singular elements, based on different assumptions with different theoretical formulations; a few will be summarized in what follows.

Hardy [5] developed a stiffness matrix for an eight node rectangular cracked element with sixteen degrees of freedom consisting of the first thirteen symmetric deformation modes of the Williams' eigenfunction expansion for the crack-tip stress field plus the three rigid-body displacements. Generalized coordinate displacement models were utilized in the finite-element displacement method for the development of the singular elements. The principal disadvantage of the resulting high order cracked element is that there is no interelement displacement compatibility. However, Hardy demonstrated the capability and efficiency of his element incorporated with conventional constant strain elements to calculate stress-intensity factors for a number of simple structural configurations with accuracy in result within one percent.

Atluri's [1] finite element procedure is based on the assumed displacement hybrid model. The theoretical basis of the assumed displacement hybrid model is a modified principle of minimum potential energy. In the mathematical formulation of the displacement model for analyzing cracked structures, the vanishing of the variation of the functional in the modified minimum potential energy principle leads to

the following conditions:

(1) The stresses generated by the interior displacement satisfy the local equilibrium equations in the element;

(2) Values of interior displacements at interelement boundaries coincide with the interelement boundary displacements;

(3) The boundary tractions coincide with the tractions generated at interelement boundaries by the interior displacement.

Atluri also considered the question of convergence of the finite element solution for smaller singular elements. He concluded that an optimum singular element size exists, and the method yields reasonable results in prediction of the stress intensity factors provided that the sizes of singular elements are chosen through experience and the regular elements are also spaced appropriately.

Walsh [8] utilized the conventional finite element displacement method to generate the stiffness matrix of a special crack element consisting of two regions; the stress and displacement distribution in the inner region is defined by the singular stress field associated with the crack tip. The outer region consists of a conventional finite element mesh that is constrained to satisfy nodal compatibility and equilibrium conditions on the interface between the two regions.

It seems that in Walsh's formulation of the stiffness matrix, neither compatibility nor equilibrium is satisfied along the boundary between the singular element and the remainder of the structure. However, the accuracy of the special cracked element is demonstrated by analyzing

for the stress intensity factors of simple crack configurations for which there are existing solutions.

Byskov [9] utilized the same approach as Hardy's generalized coordinate displacement method to derive the stiffness matrix of a four node triangular cracked element with eight degrees of freedom. Instead of applying William's stress series, Byskov used Muskhelishvili's complex stress function to obtain a set of stresses which satisfy interior equilibrium and stress-free boundary conditions on cracked edges. However, the conditions of equilibrium and compatibility along the boundary between the triangular cracked and conventional elements are not satisfied. In order to gain some idea of the convergence of the method, he tried three meshes (C = coarse, M = medium, F = fine) of strips with edge crack and concluded that non-monotonic convergence is obvious from the results obtained from the three meshes.

Hilton [10] developed a technique for using the dominant singular solution in conjunction with the finite element to predict plastic stress and strain intensity factors for the problems of a semi-infinite body with an edge crack in a far out-of-plane shearing field and an infinite plate under plane stress conditions containing a finite line crack in a remote tensile field. In the small scale yielding range, when the plastic zone about the crack tip is small in comparison with the crack length, the plastic intensity factors can be related directly to the elastic stress intensity factor. For the larger scale yielding range, the plastic zone is no longer small compared to the crack length; and the elastic stress intensity factor is no longer relevant without some modification, described as follows.

The plane containing a hairline crack is divided into two regions of elastic and plastic zones. The plastic zone is further subdivided into elastic-plastic and fully plastic regions. The fully plastic area is bounded by a circular arc centered at the crack tip; and an additional circular arc bounding the elastic-plastic zone is centered at the intersection of the axes and crack line with a sufficient radius so that the plastic region is contained within it. The dominant singular solution for small scale yielding is used to describe the solution on and within the fully plastic region. The elastic-plastic region is divided into a triangular grid pattern, and the finite element technique is utilized to connect the singular solution to the elastic field.

The variational principle of minimum potential energy for deformation theory plasticity forms the basis for this method. The equilibrium equations are obtained from the minimization of modified potential energy functional. This leads to a set of nonlinear algebraic equations for plastic strain intensity factor and the nodal displacements, and an iterative procedure is used to solve them.

Tong, et al. [16] utilized the hybrid functional to construct a special super-element to be used for crack problems in plane elasticity. The approach made use of complex variable techniques developed by Bowie [17] in his modified boundary collocation method for hairline crack problems. He introduced the concepts used in the hybrid stress model and the hybrid displacement model; that is, the unknowns consist of stress parameters, as well as nodal displacements. Furthermore, he showed that under certain conditions the hybrid functional can be reduced to a relatively simple boundary integral

It is interesting to note that in fact this boundary integral actually can be derived from the complementary strain energy functional which is used in present study to formulate the stiffness matrix for a singular element. The major difference between Pin Tong's approach and the present study is that the former is restricted to analyze the hairline problems with the need of a number of terms in the assumed stresses equal to the total degree of freedom of the super element minus the number of rigid body modes, while the latter provides a convenient way to calculate stress intensity factors for any notch angles by adopting only singular terms. A further discussion is given in Appendix C.

All the previous work on determining stress intensity factors has been limited to the crack, which might be described as a notch with zero opening angle. However, there is another location of high stresses in a plate under in-plane loading, and that is at sharp re-entry corners or notches of nonzero opening angle, as shown in Figure 1. The effect of the local stress state has been studied by Williams [11], England [12] and Karp [13], who showed that there are stress singularities of order $r^{\alpha-1}$, where α depends upon the notch angle and the character of the stress state. One can again define three types of stress states which contain singularities: (1) mode I, symmetric about the notch bisector (x-axis in Figure 1); (2) mode II, antisymmetric about the notch bisector; and (3) mode III, nonplanar and antisymmetric about the notch bisector. For modes I and II, the strength of the singularities will again be defined as proportional to the singular terms in the stress state and will be denoted by K_s and K_a respectively.

The primary purpose of this study is to determine these stress

intensity factors, K_s and K_a, at interior sharp corners in finite plates subjected to in-plane loading. This will be achieved with the finite element method, which requires the development of a new singular element which contains the proper singularity for an arbitrary notch angle. This element can then be combined with conventional nonsingular elements and other singular elements as required to provide an estimate for the stress intensity factors for a plate with arbitrary geometry and loadings.

The only existing finite element for arbitrary notch angle is due to Tong [19], who considered the problem of solving Laplace's equation in a two-dimensional domain with sharp re-entry corners. He developed a ten node superelement which contains the proper singularity at the notch tip. This problem is much more simple than the two-dimensional elasticity problem considered in this dissertation.

CHAPTER II

STRESS STATE IN THE NEIGHBORHOOD OF A NOTCH

The stresses in the neighborhood of a notch are obtained by solving the biharmonic governing differential equation for two dimensional problems in linear elasticity and satisfying the traction-free boundary conditions along radial edges. The resulting characteristic equations are solved for the eigenvalues. This procedure to obtain the stress expressions is briefly described in the following.

Development of Equations

The polar coordinates as shown in Figure 1 are used to derive the governing differential equation because it is more convenient to deal with traction-free boundary conditions by using polar coordinates; the origin lies at the tip of the notch and the x-axis bisects the notch angle. The two equations of equilibrium along the radial and tangential directions are

$$\frac{\partial \sigma_r}{\partial r} + \frac{1}{r}\frac{\partial \tau_{r\theta}}{\partial \theta} + \frac{\sigma_r - \sigma_\theta}{r} + X_r = 0$$

$$\frac{1}{r}\frac{\partial \sigma_\theta}{\partial \theta} + \frac{\partial \tau_{r\theta}}{\partial r} + 2\frac{\tau_{r\theta}}{r} + X_\theta = 0 \qquad (2.1)$$

In the absence of body forces X_r and X_θ, the equilibrium equations are satisfied by expressing the stresses in terms of the Airy stress function, φ, as follows:

$$\sigma_r = \frac{1}{r}\frac{\partial \varphi}{\partial r} + \frac{1}{r^2}\frac{\partial^2 \varphi}{\partial \theta^2}$$

$$\sigma_\theta = \frac{\partial^2 \varphi}{\partial r^2} \tag{2.2}$$

$$\tau_{r\theta} = \frac{1}{r^2}\frac{\partial \varphi}{\partial \theta} - \frac{1}{r}\frac{\partial^2 \varphi}{\partial r \partial \theta} = -\frac{\partial}{\partial r}\left(\frac{1}{r}\frac{\partial \varphi}{\partial \theta}\right)$$

The linearized strain-displacement relations for plane problems are

$$\epsilon_r = \frac{\partial u_r}{\partial r} \tag{2.3}$$

$$\epsilon_\theta = \frac{u_r}{r} + \frac{1}{r}\frac{\partial u_\theta}{\partial \theta} \tag{2.4}$$

$$\gamma_{r\theta} = \frac{1}{r}\frac{\partial u_r}{\partial \theta} + \frac{\partial u_\theta}{\partial r} - \frac{u_\theta}{r} \tag{2.5}$$

Now, from equations (2.3) through (2.5), it can be shown that the strain components satisfy the following compatibility equation

$$\frac{2}{r}\frac{\partial \epsilon_\theta}{\partial r} - \frac{1}{r}\frac{\partial \epsilon_r}{\partial r} + \frac{1}{r^2}\frac{\partial^2 \epsilon_r}{\partial \theta^2} + \frac{\partial^2 \epsilon_\theta}{\partial r^2} = \frac{1}{r^2}\frac{\partial \gamma_{r\theta}}{\partial \theta} + \frac{1}{r}\frac{\partial^2 \gamma_{r\theta}}{\partial r \partial \theta} \tag{2.6}$$

The stress-strain relations in the case of plane stress are

$$\epsilon_r = \frac{\sigma_r - \mu \sigma_\theta}{E} \tag{2.7}$$

$$\epsilon_\theta = \frac{\sigma_\theta - \mu \sigma_r}{E} \tag{2.8}$$

$$\gamma_{r\theta} = \frac{\tau_{r\theta}}{G} = \frac{2(1+\mu)}{E} \tau_{r\theta} \tag{2.9}$$

Substitution of these relations into equation (2.6) gives

$$\frac{\partial^2}{\partial r^2}(\sigma_\theta - \mu \sigma_r) + \frac{1}{r^2}\frac{\partial^2}{\partial \theta^2}(\sigma_r - \mu \sigma_\theta)$$

$$+ \frac{2}{r}\frac{\partial}{\partial r}(\sigma_\theta - \mu \sigma_r) - \frac{1}{r}\frac{\partial}{\partial r}(\sigma_r - \mu \sigma_\theta) \tag{2.10}$$

$$= 2(1+\mu)\frac{1}{r}\frac{\partial^2 \tau_{r\theta}}{\partial r \partial \theta} + 2(1+\mu)\frac{1}{r^2}\frac{\partial \tau_{r\theta}}{\partial \theta}$$

If the stress component $\tau_{r\theta}$ is eliminated from equation (2.10) by use of the equilibrium equations (2.1), it can be shown that equation (2.10) simplifies to

$$\nabla^2(\sigma_r + \sigma_\theta) = 0 \tag{2.11}$$

where $\nabla^2 = \frac{\partial^2}{\partial r^2} + \frac{1}{r}\frac{\partial}{\partial r} + \frac{1}{r^2}\frac{\partial^2}{\partial \theta^2}$ is the Laplace operator in polar coordinates.

Finally substitution of equation (2.2) into equation (2.11) gives the final form of the compatibility equation in terms of the stress function:

$$\left(\frac{\partial^2}{\partial r^2} + \frac{1}{r}\frac{\partial}{\partial r} + \frac{1}{r^2}\frac{\partial^2}{\partial \theta^2}\right)\left(\frac{\partial^2 \varphi}{\partial r^2} + \frac{1}{r}\frac{\partial \varphi}{\partial r} + \frac{1}{r^2}\frac{\partial^2 \varphi}{\partial \theta^2}\right) = 0 \tag{2.12}$$

i.e.,

$$\nabla^2 \cdot \nabla^2 \varphi = 0$$

The fourth order partial differential equation (2.12) can be solved by the separation of variables technique by assuming*

$$\varphi(r,\theta) = r^{\alpha+1} f(\theta) \tag{2.13}$$

Substitute equation (2.13) into the Laplace operator and obtain the following expression

$$\nabla^2\varphi = \frac{\partial^2\varphi}{\partial r^2} + \frac{1}{r}\frac{\partial\varphi}{\partial r} + \frac{1}{r^2}\frac{\partial^2\varphi}{\partial\theta^2}$$

$$= r^{\alpha-1}\left[f''(\theta) + (\alpha+1) f(\theta) + \alpha(\alpha+1) f(\theta) \right]$$

Then the biharmonic equation (2.12) becomes

$$\nabla^4\varphi = \left(\frac{\partial^2}{\partial r^2} + \frac{1}{r}\frac{\partial}{\partial r} + \frac{1}{r^2}\frac{\partial^2}{\partial\theta^2}\right)\left\{ r^{\alpha-1}\left[f''(\theta) + (\alpha+1)^2 f(\theta) \right] \right\}$$

$$= r^{\alpha-3}\left[f^{IV}(\theta) + (\alpha+1)^2 f''(\theta) + (\alpha-1)^2 f''(\theta) + (\alpha-1)^2(\alpha+1)^2 f(\theta) \right]$$

$$= 0$$

Assume $r^{\alpha-3} \neq 0$ in the domain of the differential equation. Therefore

$$f^{IV}(\theta) + (\alpha+1)^2 f''(\theta) + (\alpha-1)^2 f''(\theta) + (\alpha^2-1)^2 f(\theta) = 0$$

This 4th order ordinary differential equation can be written as

---

*This type of solution was originally proposed by Klein and Wieghardt in 1905.

$$\left\{\frac{d^2}{d\theta^2}+(\alpha+1)^2\right\}\left\{\frac{d^2}{d\theta^2}+(\alpha-1)^2\right\}f(\theta)=0 \qquad (2.14)$$

The final solution depends upon the boundary conditions specified on both faces, i.e., the tangential and shear stresses are zero on both surfaces bounded by radii $\theta = \pm\ \theta_0$

$$\begin{aligned}
&\sigma_\theta\Big|_{\theta=\theta_0} = 0\\
&\sigma_\theta\Big|_{\theta=-\theta_0} = 0\\
&\tau_{r\theta}\Big|_{\theta=\theta_0} = 0\\
&\tau_{r\theta}\Big|_{\theta=-\theta_0} = 0
\end{aligned} \qquad (2.15)$$

Solutions

The solutions of the differential equation (2.14) depend upon the values of α. The physical meaning of the mathematical solutions for α equal to $1, 0, -1$ will first be examined.

Case 1 for $\alpha = 1$

The 4th order governing differential equation (2.14) becomes

$$f^{IV}(\theta) + 4f''(\theta) = 0$$

and its general solution is

$$f(\theta) = C_1\theta + C_2 + C_3\sin(2\theta) + C_4\cos(2\theta)$$

Therefore the stress function (2.13) takes the form

$$\varphi(r,\theta) = r^2 (C_1\theta + C_2 + C_3 \sin 2\theta + C_4 \cos 2\theta)$$

Obtain stress components by using equation (2.2) as follows

$$\sigma_r = 2 (C_1\theta + C_2 - C_3 \sin 2\theta - C_4 \cos 2\theta)$$

$$\sigma_\theta = 2 (C_1\theta + C_2 + C_3 \sin 2\theta + C_4 \cos 2\theta)$$

$$\tau_{r\theta} = -C_1 - 2C_3 \cos 2\theta + 2C_4 \sin 2\theta$$

In order to satisfy the boundary conditions (2.15),

$$\begin{aligned}
\sigma_\theta\Big|_{\theta=\theta_0} &= 2\left[C_1\theta_0 + C_2 + C_3 \sin(2\theta_0) + C_4 \cos(2\theta_0)\right] \\
&= 0 \\
\sigma_\theta\Big|_{\theta=-\theta_0} &= 2\left[-C_1\theta_0 + C_2 - C_3 \sin(2\theta_0) + C_4 \cos(2\theta_0)\right] \\
&= 0 \\
\tau_{r\theta}\Big|_{\theta=\theta_0} &= -C_1 - 2C_3 \cos(2\theta_0) + 2C_4 \sin(2\theta_0) = 0 \\
\tau_{r\theta}\Big|_{\theta=-\theta_0} &= -C_1 - 2C_3 \cos(2\theta_0) - 2C_4 \sin(2\theta_0) = 0
\end{aligned} \tag{2.16}$$

Perform operations of addition and subtraction on equation (2.16) to obtain the following two sets of simultaneous equations,

(i) Symmetric Solution;

$$C_2 + C_4 \cos(2\theta_0) = 0$$

$$C_4 \sin(2\theta_0) = 0$$

(ii) Antisymmetric Solution;

$$C_1\theta_0 + C_3 \sin(2\theta_0) = 0$$

$$C_1 + 2C_3 \cos(2\theta_0) = 0$$

In order to obtain nontrivial solutions for the symmetric case, θ_0 has to be equal to $\frac{\pi}{2}$ or π. Similarly, the condition for a nontrivial solution to the antisymmetric case is

$$\tan(2\theta_0) - 2\theta_0 = 0$$

which requires $\theta_0 = 128.725^\circ$

Obviously, if C_2 and C_4 are not zero, then C_1 and C_3 must vanish, and conversely. This means that the stresses do separate into purely symmetric or antisymmetric states, and the three sets of stress components corresponding to $\theta_0 = \frac{\pi}{2}, \pi$ and 128.725° are

(i) Symmetrical Case for $\theta_0 = \frac{\pi}{2}$

$$\sigma_r = 2\left[1 - \cos(2\theta)\right] C_4$$

$$\sigma_\theta = 2\left[1 + \cos(2\theta)\right] C_4$$

$$\tau_{r\theta} = 2\sin(2\theta)\, C_4$$

This can be shown to be equivalent to $\sigma_y = 4C_4$, $\sigma_x = \tau_{xy} = 0$, a uniform stress state which obviously satisfies the requirements on the elasticity solution.

(ii) Symmetric Case for $\theta_0 = \pi$

$$\sigma_r = -2\left[1 + \cos(2\theta)\right] C_4$$

$$\sigma_\theta = 2\left[-1 + \cos(2\theta)\right] C_4$$

$$\tau_{r\theta} = 2 \sin(2\theta)\, C_4$$

This is equivalent to the uniform stress state of

$$\sigma_x = -4\, C_4 \quad , \quad \sigma_y = \tau_{xy} = 0$$

(iii) Antisymmetric Case for $\theta_o = 128.725°$

$$\sigma_r = 2\left[0.4346\,\theta - \sin(2\theta)\right] C_3$$

$$\sigma_\theta = 2\left[0.4346\,\theta + \sin(2\theta)\right] C_3$$

$$\tau_{r\theta} = -(0.4346 + 2\cos 2\theta)\, C_3$$

This represents a nonuniform stress state.

Case 2 for $\alpha = 0$:

The 4th order governing differential equation (2.14) becomes

$$f^{IV}(\theta) + 2f''(\theta) + f(\theta) = 0$$

and its general solution is

$$f(\theta) = C_1 \sin\theta + C_2 \cos\theta + C_3\,\theta \sin\theta + C_4\,\theta \cos\theta$$

Therefore the stress function (2.13) takes the form

$$\varphi(r, \theta) = r\,(C_1 \sin\theta + C_2 \cos\theta + C_3\,\theta \sin\theta + C_4\,\theta \cos\theta)$$

and the stresses are

$$\sigma_r = \frac{2}{r}\left(C_3 \cos\theta - C_4 \sin\theta\right)$$

$$\sigma_\theta = 0 \qquad (2.17)$$

$$\tau_{r\theta} = 0$$

The boundary conditions (2.15) are identically satisfied. The stress field shown in equation (2.17) corresponds to the problem of a wedge subject to a concentrated force at its apex [14]; therefore the eigenvalue $\alpha = 0$ will not be considered as a possible solution in this investigation.

Case 3 for $\alpha = -1$:

The 4th order governing differential equation (2.14) becomes

$$f^{IV}(\theta) + 4 f''(\theta) = 0$$

and the stress function (2.13) takes the form

$$\varphi(r,\theta) = C_1\theta + C_2 + C_3 \sin(2\theta) + C_4 \cos(2\theta)$$

The stress components from equation (2.2) are found to be

$$\sigma_r = -4r^{-2}\left[C_3 \sin(2\theta) + C_4 \cos(2\theta)\right]$$

$$\sigma_\theta = 0$$

$$\tau_{r\theta} = r^{-2}\left[C_1 + 2C_3 \cos(2\theta) - 2C_4 \sin(2\theta)\right]$$

Since the stresses, and therefore the strains, are of order r^{-2},

it follows from the strain-displacement relations (2.3) through (2.5) that the displacements are of the order r^{-1}; therefore $\alpha = -1$ must be excluded on the basis that it will result in unbounded displacements at the sharp corner.

Now consider values of α not equal to 1, 0, -1. Then the general solution of the 4th order differential equation (2.14) can be expressed as follows:

$$f(\theta) = C_1 \sin(\alpha+1)\theta + C_2 \cos(\alpha+1)\theta + C_3 \sin(\alpha-1)\theta + C_4 \cos(\alpha-1)\theta \tag{2.18}$$

Therefore the solution of equation (2.12) is

$$\varphi(r,\theta) = r^{\alpha+1}\left[C_1 \sin(\alpha+1)\theta + C_2 \cos(\alpha+1)\theta + C_3 \sin(\alpha-1)\theta + C_4 \cos(\alpha-1)\theta \right] \tag{2.19}$$

From equation (2.2), the stresses corresponding to $\varphi(r,\theta)$ are given by the following expressions

$$\sigma_r = r^{\alpha-1}\{C_1[(\alpha+1)-(\alpha+1)^2]\sin(\alpha+1)\theta + C_2[(\alpha+1)-(\alpha+1)^2]\cos(\alpha+1)\theta + C_3[(\alpha+1)-(\alpha-1)^2]\sin(\alpha-1)\theta + C_4[(\alpha+1)-(\alpha-1)^2]\cos(\alpha-1)\theta$$

$$\sigma_\theta = (\alpha+1)\alpha\, r^{\alpha-1}\left[C_1 \sin(\alpha+1)\theta + C_2 \cos(\alpha+1)\theta + C_3 \sin(\alpha-1)\theta + C_4 \cos(\alpha-1)\theta \right]$$

$$\tau_{r\theta} = -\alpha\, r^{\alpha-1}\left[C_1(\alpha+1)\cos(\alpha+1)\theta - C_2(\alpha+1)\sin(\alpha+1)\theta + C_3(\alpha-1)\cos(\alpha-1)\theta - C_4(\alpha-1)\sin(\alpha-1)\theta \right]$$

and the corresponding equations that impose satisfaction of boundary conditions (2.15) are (recall that $\alpha \neq 1, 0, -1$)

$$C_1 \sin(\alpha+1)\theta_o + C_2 \cos(\alpha+1)\theta_o + C_3 \sin(\alpha-1)\theta_o + C_4 \cos(\alpha-1)\theta_o = 0$$

$$C_1 \sin(\alpha+1)\theta_o - C_2 \cos(\alpha+1)\theta_o + C_3 \sin(\alpha-1)\theta_o - C_4 \cos(\alpha-1)\theta_o = 0$$

$$C_1(\alpha+1)\cos(\alpha+1)\theta_o - C_2(\alpha+1)\sin(\alpha+1)\theta_o + C_3(\alpha-1)\cos(\alpha-1)\theta_o - C_4(\alpha-1)\sin(\alpha-1)\theta_o = 0$$

$$C_1(\alpha+1)\cos(\alpha+1)\theta_o + C_2(\alpha+1)\sin(\alpha+1)\theta_o + C_3(\alpha-1)\cos(\alpha-1)\theta_o + C_4(\alpha-1)\sin(\alpha-1)\theta_o = 0$$

Next, perform operations of addition and subtraction on these equations to obtain the following equivalent set of equations:

$$C_2(\alpha+1)\sin(\alpha+1)\theta_o + C_4(\alpha-1)\sin(\alpha-1)\theta_o = 0 \qquad (2.20)$$

$$C_2\cos(\alpha+1)\theta_o + C_4\cos(\alpha-1)\theta_o = 0 \qquad (2.21)$$

$$C_1\sin(\alpha+1)\theta_o + C_3\sin(\alpha-1)\theta_o = 0 \qquad (2.22)$$

$$C_1(\alpha+1)\cos(\alpha+1)\theta_o + C_3(\alpha-1)\cos(\alpha-1)\theta_o = 0 \qquad (2.23)$$

In order to obtain nontrivial solutions for C_2 and C_4 in equations (2.20) and (2.21), make the determinant of the coefficients vanish, which gives the following characteristic equation for α:

$$\alpha \sin(2\theta_o) + \sin(2\alpha\theta_o) = 0 \qquad (2.24)$$

From equation (2.20), C_2 can be expressed in terms of C_4, as

follows:

$$C_2 = -\frac{(\alpha-1)\sin(\alpha-1)\theta_o}{(\alpha+1)\sin(\alpha+1)\theta_o} C_4$$

Similarly from equations (2.22) and (2.23), C_1 and C_3 can be non-zero provided α satisfies the following characteristic equation

$$\alpha \sin(2\theta_o) - \sin(2\alpha\theta_o) = 0 \qquad (2.25)$$

According to equation (2.22), C_3 can be expressed in terms of C_1 as follows:

$$C_3 = -\frac{\sin(\alpha+1)\theta_o}{\sin(\alpha-1)\theta_o} C_1$$

Examining equations (2.24) and (2.25) together, it is evident that the only value of α which satisfies both is $\alpha = 0$, and this is excluded. Thus if one equation is satisfied, the other will not be. Consequently, if C_1 and C_3 are not zero, C_2 and C_4 must vanish and conversely. Moreover if C_2 and C_4 are nonzero, the stress function (2.19) becomes an even function of θ; this leads to symmetric stress distribution. If C_1 and C_3 are non-zero, the stress function $\varphi(r, \theta)$ becomes an odd function of θ, which leads to antisymmetric stress distribution.

Let α_{sn} and α_{an} denote the n-th roots of equations (2.24) and (2.25) respectively. Then the complete symmetric solution is

$$\varphi_s = \sum_{n=1}^{\infty} C_{sn} r^{\alpha_{sn}+1} \left[-\frac{(\alpha_{sn}-1)\sin(\alpha_{sn}-1)\theta_o}{(\alpha_{sn}+1)\sin(\alpha_{sn}+1)\theta_o} \cos(\alpha_{sn}+1)\theta + \cos(\alpha_{sn}-1)\theta \right]$$

and the complete antisymmetric solution is

$$\varphi_a = \sum_{n=1}^{\infty} C_{an} r^{\alpha_{an}+1}\left[\sin(\alpha_{an}+1)\theta - \frac{\sin(\alpha_{an}+1)\theta_o}{\sin(\alpha_{an}-1)\theta_o}\cdot\sin(\alpha_{an}-1)\theta\right]$$

Therefore the total stress function is given by

$$\begin{aligned}\varphi &= \varphi_s + \varphi_a \\ &= \sum_{n=1}^{\infty} C_{sn} r^{\alpha_{sn}+1}\left[-\frac{(\alpha_{sn}-1)\sin(\alpha_{sn}-1)\theta_o}{(\alpha_{sn}+1)\sin(\alpha_{sn}+1)\theta_o}\cdot\cos(\alpha_{sn}+1)\theta + \cos(\alpha_{sn}-1)\theta\right] \\ &+ \sum_{n=1}^{\infty} C_{an} r^{\alpha_{an}+1}\left[-\frac{\sin(\alpha_{an}+1)\theta_o}{\sin(\alpha_{an}-1)\theta_o}\cdot\sin(\alpha_{an}-1)\theta + \sin(\alpha_{an}+1)\theta\right]\end{aligned} \tag{2.26}$$

The complete expressions for the stresses from equation (2.2) are

$$\begin{aligned}\sigma_r &= \sum_{n=1}^{\infty} C_{sn} r^{\alpha_{sn}-1}\left[\alpha_{sn}(3-\alpha_{sn})\cos(\alpha_{sn}-1)\theta + \frac{\alpha_{sn}(\alpha_{sn}-1)\sin(\alpha_{sn}-1)\theta_o}{\sin(\alpha_{sn}+1)\theta_o}\cos(\alpha_{sn}+1)\theta\right] \\ &- \sum_{n=1}^{\infty} C_{an} r^{\alpha_{an}-1}\left[\alpha_{an}(\alpha_{an}+1)\sin(\alpha_{an}+1)\theta + \frac{\alpha_{an}(3-\alpha_{an})\sin(\alpha_{an}+1)\theta_o}{\sin(\alpha_{an}-1)\theta_o}\sin(\alpha_{an}-1)\theta\right]\end{aligned} \tag{2.27}$$

(2.27)
Cont'd

$$\sigma_\theta = \sum_{n=1}^{\infty} C_{sn}\, r^{\alpha_{sn}-1}\alpha_{sn}\,(\alpha_{sn}+1)\left[\cos(\alpha_{sn}-1)\theta - \frac{(\alpha_{sn}-1)\sin(\alpha_{sn}-1)\theta_o}{(\alpha_{sn}+1)\sin(\alpha_{sn}+1)\theta_o}\cos(\alpha_{sn}+1)\theta\right]$$

$$+\sum_{n=1}^{\infty} C_{an}\, r^{\alpha_{an}-1}\alpha_{an}\,(\alpha_{an}+1)\left[\sin(\alpha_{an}+1)\theta - \frac{\sin(\alpha_{an}+1)\theta_o}{\sin(\alpha_{an}-1)\theta_o}\sin(\alpha_{an}-1)\theta\right]$$

$$\tau_{r\theta} = -\sum_{n=1}^{\infty} C_{sn}\, r^{\alpha_{sn}-1}\alpha_{sn}\left[-(\alpha_{sn}-1)\sin(\alpha_{sn}-1)\theta + \frac{(\alpha_{sn}-1)\sin(\alpha_{sn}-1)\theta_o}{\sin(\alpha_{sn}+1)\theta_o}\sin(\alpha_{sn}+1)\theta\right]$$

$$-\sum_{n=1}^{\infty} C_{an}\, r^{\alpha_{an}-1}\alpha_{an}\left[(\alpha_{an}+1)\cos(\alpha_{an}+1)\theta - \frac{\sin(\alpha_{an}+1)\theta_o}{\sin(\alpha_{an}-1)\theta_o}(\alpha_{an}-1)\cos(\alpha_{an}-1)\theta\right]$$

Each independent term in stress expression (2.27) is a solution of the biharmonic governing differential equation (2.12) and satisfies the stress-free edge conditions (2.15). The stresses and strains are functions of $r^{\alpha-1}$ while displacements can be shown to depend on r^{α}. Therefore, physically meaningful values of α must have a nonnegative real part in order to avoid unbounded displacements in the region near the origin. Also note that singular stresses will be associated with values of α with real parts less than one, while values of α with real

parts greater than or equal to one will give bounded stresses in the neighborhood of the origin.

The equations given by (2.24) and (2.25) yield all the possible values of the root α. Their corresponding eigenvalues α_{sn} and α_{an} can be either real or complex numbers, and can be found numerically by simple computations. Combine (2.24) and (2.25) into the following form

$$\frac{\sin(2\alpha\theta_0)}{2\alpha\theta_0} = \pm \frac{\sin(2\theta_0)}{2\theta_0} \tag{2.28}$$

To determine all real roots, let α be x-axis and the quantities $\pm \frac{\sin(2\theta_0)}{2\theta_0}$ and $\frac{\sin(2\alpha\theta_0)}{2\alpha\theta_0}$ be y-axis. Roots with negative real parts are excluded since they lead to unbounded displacements at the tip. Then all positive real roots for any notch angles are given by the intersections of the lines $\pm \frac{\sin(2\cdot\theta_0)}{2\cdot\theta_0}$ with the curve $\frac{\sin(2\alpha\theta_0)}{2\alpha\theta_0}$. It is interesting to note that except for two special cases, there are a finite number of intersections and hence only a finite number of real roots. In the special case of a hairline crack, i.e., $\theta_0 = 180°$, equation (2.28) reduces to $\sin(2\pi\alpha) = 0$, which results in an infinite number of real roots given by $\alpha = n/2$, $n = 1,3,4,.....$as shown in Figure 3. Recall that $\alpha = 1$ is excluded; so that the apparent roots at $\alpha = 1$ in Figures 4 and 5 are not valid. In the special case of a half-space, i.e., $\theta_0 = 90°$, there are also an infinite number of real roots given by $\alpha = 2,3,4...$. For 60° and 90° notch angles, the graphic solutions indicate that there are only three intersections as shown in Figures 4 and 5. The upper and lower intersections correspond to the symmetric and antisymmetric roots respectively. The real roots for 20°, 60°, 90°, 120°, 140° and 160° notch angles as

determined from Newton's method with numerically evaluated derivatives are listed in Tables 1 through 6. It is interesting to note that the number of real roots first decrease from infinity to two then increase back to infinity as the notch angle continues increasing. It is of importance to note that there is at most one real symmetric and one real antisymmetric root with magnitudes less than 1. This can be shown to be true, in general, from consideration of graphs of the type shown in Figures 4 and 5; and these roots will give rise to the singularities.

It will be shown later that complex roots also exist for equation (2.28). Tables 1 through 6 indicate that the absolute values of real parts of complex roots are always greater than 1, and their magnitudes are also greater than any real roots.

Karp and Karal [13] have shown that the real part of each of the complex roots with positive real parts is always greater than the smallest positive real root. They also stated, without proof, that the complex root with the smallest real part does not give rise to any infinities in the physical quantities. England [12] has shown graphically that the positive real parts of complex roots are always greater than 1 for $\theta_0 < \pi/2$. Unfortunately this is not the region of interest in this study, and his graphic solution failed to apply to the important region (i.e., $\theta_0 > \pi/2$) where singularity occurs at sharp corners. In fact, there appears to be no proof that all complex roots have real parts greater than one for $\theta_0 > \pi/2$. However, this is suggested by the numerical results in Tables 1 through 6, which are believed to be typical for any notch angle, and confirmed by the numerical results in [13] for $\theta_0 = 165°$.

Since the smallest real roots dominate the behavior of the stress field in the vicinity of the sharp corners, it is important to study how the lowest roots vary with notch angles. Figure 6 obtained from solving the equation (2.28) by Newton's method indicates that the order of stress singularity decreases as notch angle increases; that is, as the notch angle increases, the smallest real eigenvalue increases toward 1, and the order of stress singularity given by $r^{\alpha-1}$ tends to decrease.

The eigenvalues of some critical notch angles for stress singularity are given in the following:

(a) For symmetric case

(i) For any angle $\theta_0 > \pi/2$, there is one and only one real eigenvalue which is less than 1; this eigenvalue will give rise to a singularity.

(ii) When θ_0 is any angle $\leq \pi/2$, the lowest real eigenvalue is ≥ 1, which means that there is no singularity.

(b) For antisymmetric case

(i) For any angle $\theta_0 > 128.7°$, there is one and only one real eigenvalue which is less than 1; this eigenvalue will give rise to a singularity.

(ii) When θ_0 is any angle $\leq 128.7°$, the lowest real eigenvalue is ≥ 1, which means that there is no singularity.

As mentioned previously, there are only a finite number of real eigenvalues with the exception of notch angles of 0° and 180°. However, there are always an infinite number of complex roots. In order to solve for the complex eigenvalues, assume α in complex form as (RP + IP $\bar{i}$). Substitution into equations (2.24) and (2.25) yields the following

complex function:

$$\left[\sin(2\theta_0 \cdot RP)\cosh(2\theta_0 \cdot IP) \pm RP \sin(2\theta_0)\right] +$$

$$+ \left[\cos(2\theta_0 \cdot RP) \cdot \sinh(2\theta_0 IP) \pm IP \sin(2\theta_0)\right] \bar{i} = 0$$

Two simultaneous equations are obtained from the requirement that the real and imaginary parts must each equal to zero.

$$\sin(2\theta_0 \cdot RP)\cosh(2\theta_0 IP) \pm RP \sin(2\theta_0) = 0$$

$$\cos(2\theta_0 \cdot RP)\sinh(2\theta_0 \cdot IP) \pm IP \sin(2\theta_0) = 0 \qquad (2.29)$$

Obviously, equations (2.29) remain unchanged if IP changes sign, which means that the complex roots always occur in complex conjugate pairs.

In order to solve the two sets of simultaneous equations for RP and IP, express RP in terms of IP from the second equation (2.29) as follows:

$$RP = \frac{1}{2\theta_0} \cos^{-1}\left[\frac{\mp IP \sin(2\theta_0)}{\sinh(2\theta_0 \cdot IP)}\right] \qquad (2.30)$$

where $2\theta_0 \neq 0$ and $IP \neq 0$.

Substitute into the first equation, and obtain the following expression with a single variable IP.

$$\sin\left\{\cos^{-1}\left[\frac{\mp IP\sin(2\theta_o)}{\sinh(2\theta_o \cdot IP)}\right]\right\}\cosh(2\theta_o \cdot IP)$$

$$\pm\frac{\sin(2\theta_o)}{2\theta_o}\cos^{-1}\left[\frac{\mp IP\sin(2\theta_o)}{\sinh(2\theta_o \cdot IP)}\right] = 0$$

Newton's iterative method, again with numerically evaluated derivatives, is used to solve for IP from this equation; and the corresponding RP can be found from equation (2.30). Some of the symmetric and antiymmetric complex roots along with real roots for 20°, 60°, 90°, 120°, 140° and 160° notch angles are listed in the Tables 1 through 6 which were previously discussed.

Since the complex eigenvalues occur as complex conjugate pairs, it can be shown that the stress function, φ, has the following form for each pair of eigenvalues:

$$\varphi = C_1(R\varphi + \bar{i}\, I\varphi) + C_2(R\varphi - \bar{i}\, I\varphi)$$

where $R\varphi$ and $I\varphi$ are the independent real and imaginary parts of φ for a given eigenvalue pair, and C_1, C_2 are constants. In this form, it appears that φ is complex which is meaningless since the stresses must be real. However, the constants C_1 and C_2 can themselves be complex conjugate so that φ can actually be written as

$$\varphi = b_1 R\varphi + b_2 I\varphi$$

where b_1 and b_2 are real constants. That is, each complex conjugate pair of eigenvalues leads to two independent real eigenfunctions for α and two independent real expressions for the stresses.

Actually it is not necessary to explicitly separate the complex stress function into real and imaginary parts. Computationally, it is much easier to directly use the complex eigenvalue in the stress expression (2.27) and utilize the computer to perform the complex arithmetic. Since the computer stores a complex number in two locations, it is very easy to obtain the real and imaginary parts of stress expressions for any complex eigenvalue. These two parts of the stress expressions are the two independent solutions for the stresses associated with the one complex eigenvalue.

As discussed earlier, for both symmetry and antisymmetry, there is at most one eigenvalue α with real part less than 1; and furthermore these roots are real. This means there are not more than two singular states; and based on one existing definition of the stress intensity factors for the crack tip singularity, K_s and K_a for the notch will be defined as follows:

$$K_s = \lim_{r\to 0} \sqrt{2\pi}\, r^{1-\alpha_{s1}}\, \sigma_\theta\,(r, \theta = 0)$$

$$= \sqrt{2\pi}\, \alpha_{s1}\,(\alpha_{s1}+1)\left[\,1 - \frac{(\alpha_{s1}-1)\,\sin(\alpha_{s1}-1)\,\theta_o}{(\alpha_{s1}+1)\,\sin(\alpha_{s1}+1)\,\theta_o}\right] C_{s1} \tag{2.31}$$

$$K_a = \lim_{r\to 0} \sqrt{2\pi}\, r^{1-\alpha_{a1}}\, \tau_{r\theta}\,(r, \theta = 0)$$

$$= -\sqrt{2\pi}\, \alpha_{a1}\left[\,(\alpha_{a1}+1) - \frac{\sin(\alpha_{a1}+1)\,\theta_o}{\sin(\alpha_{a1}-1)\,\theta_o}\,(\alpha_{a1}-1)\right] C_{a1} \tag{2.32}$$

where α_{sl} and α_{al} are the smallest real eigenvalues. Positive K_s and K_a are associated with the normal and shear stresses, respectively, shown in Figure 1 on the free body at $\theta = 0°$.

Table 1. The Real and Complex Roots of Characteristic Equation for 20° Notch Angle

	Symmetrical		Antisymmetrical	
No.	Real Part	Imaginary Part	Real Part	Imaginary Part
1	0.50043	0.0	0.56199	0.0
2	1.12537	0.0	1.69220	0.0
3	1.49762	0.0	1.99139	0.0
4	2.26710	0.0	2.88349	0.0
5	2.47679	0.0	3.96183	±0.13838
6	3.43195	±0.09837	5.02144	±0.19158

Table 2. The Real and Complex Roots of Characteristic Equation for 60° Notch Angle

	Symmetrical		Antisymmetrical	
No.	Real Part	Imaginary Part	Real Part	Imaginary Part
1	0.51222	0.0	0.73090	0.0
2	1.4702	±0.14185	2.07482	±0.22942
3	2.67761	±0.28490	3.27976	±0.32669
4	3.88148	±0.36049	4.48289	±0.38898
5	5.08407	±0.41364	5.68508	±0.43540

Table 3. The Real and Complex Roots of Characteristic Equation for 90° Notch Angle

	Symmetrical		Antisymmetrical	
No.	Real Part	Imaginary Part	Real Part	Imaginary Part
1	0.54448	0.0	0.90852	0.0
2	1.62925	±0.23125	2.30132	±0.31584
3	2.97184	±0.37393	3.64141	±0.41879
4	4.31037	±0.45549	4.97889	±0.48662
5	5.64710	±0.51368	6.31507	±0.53763

Table 4. The Real and Complex Roots of Characteristic Equation for 120° Notch Angle

	Symmetrical		Antisymmetrical	
No.	Real Part	Imaginary Part	Real Part	Imaginary Part
1	0.61573	0.0	1.15100	0.0
2	1.83354	±0.25225	2.58947	+0.34837
3	3.34371	±0.41404	4.09692	±0.46464
4	4.84945	±0.50601	5.60150	±0.54109
5	6.35321	±0.57156	7.10465	±0.59852

Table 5. The Real and Complex Roots of Characteristic Equation for 140° Notch Angle

	Symmetrical		Antisymmetrical	
No.	Real Part	Imaginary Part	Real Part	Imaginary Part
1	0.69714	0.0	1.35944	0.0
2	2.00561	±0.19840	2.82902	±0.31663
3	3.65103	±0.39199	4.47216	±0.44885
4	5.29269	±0.49489	6.11280	±0.53369
5	6.93260	±0.56730	7.75215	±0.59695

Table 6. The Real and Complex Roots of Characteristic Equation for 160° Notch Angle

	Symmetrical		Antisymmetrical	
No.	Real Part	Imaginary Part	Real Part	Imaginary Part
1	0.81872	0.0	1.63058	0.0
2	2.01825	0.0	3.12261	±0.10862
3	2.42068	0.0	4.92707	±0.31976
4	4.02507	±0.24296	6.73014	±0.42355
5	5.82873	±0.37709	8.53240	±0.49712

CHAPTER III

DERIVATION OF THE STIFFNESS MATRIX FOR A SINGULAR ELEMENT

Development of General Equations

The primary objective in this study is to determine the character of the singular stress state which exists at the sharp corners of arbitrary cutouts in finite plates subject to inplane external loading. This is accomplished through a finite element representation of a modified displacement formulation of the equations of elasticity.

A typical problem is shown in Figure 7. There is the possibility of a singular stress state at each of the sharp corners of the cutout, so a region around each corner is represented by singular finite elements (shaded in Figure 7) which contain the proper order of singularity according to the notch angle. Then the remainder of the plate domain, in which nonsingular stresses exist, is represented by nonsingular finite elements (in this study, either conventional constant strain triangles or special triangles with one stress-free edge).

In order to insure adjacent element displacement continuity, the displacements of points on the interelement boundaries are assumed to vary linearly between nodes. For the conventional constant strain triangles, this is achieved by the usual geometric assumption of linearly varying displacements in the interior of the finite element; these interior displacements, when taken continuously to the boundary, do indeed provide linear boundary displacements.

The situation is not so simple for the singular element. Essentially, the problem is that of a plate with two traction-free edges forming a notch of arbitrary angle, subject to imposed boundary displacements which are specified to be linear between nodes on the remainder of the boundary. In this thesis, this problem is solved approximately through an application of the principle of stationary complementary energy (or, equivalently in this case, the principle of complementary virtual work). This principle requires assumptions for the stress state, and the assumed stresses must satisfy equations of equilibrium in the interior and traction boundary conditions.

The stresses given in equation (2.27) are extremely appropriate for the assumption since those stresses not only satisfy equilibrium and the traction-free boundary conditions, but also, as a bonus, satisfy compatibility in the interior and provide the proper order of stress singularity.

Therefore, the principle of stationary complementary energy is used to express the stress coefficients in the stress series in terms of the nodal displacements on the boundary. The strain energy in the singular element can then be expressed in terms of the nodal displacements, which means that the stiffness matrix is available for the singular element. This stiffness matrix can be combined with the stiffness matrices of the nonsingular elements, and the solution proceeds as in a conventional displacement formulation. After the nodal displacements are determined, then the singular stress term coefficient can be determined; and the stress intensity factors can be evaluated according

to equations (2.31) and (2.32).

The complementary strain energy functional, π_c , for the singular element can be expressed in the following form

$$\pi_c = U_c + V_c \tag{3.1}$$

where

$$U_c = \frac{1}{2}\int_V \{\sigma\}^T [N] \{\sigma\}\, dV \tag{3.2}$$

$$V_c = -\int_{S_u} [S]^T [U^P]\, dS \tag{3.3}$$

where

U_c : complementary strain energy

V_c : potential of the traction

The elasticity matrix is defined as

$$[N] = \begin{bmatrix} \frac{1}{E} & -\frac{\mu}{E} & 0 \\ -\frac{\mu}{E} & \frac{1}{E} & 0 \\ 0 & 0 & \frac{1}{G} \end{bmatrix}$$

The stress series as given in equation (2.27) can be expressed in the following matrix form

$$\{\sigma\} = [L]\{C\} = [\, L_s \,\vdots\, L_a \,] \begin{Bmatrix} C_s \\ \cdots \\ C_a \end{Bmatrix} \tag{3.4}$$

where the symmetric and antisymmetric stress states are grouped separately.

Note that matrix [L] is a function of coordinates (r,θ) within the entire volume and $\{C\}$ are the stress coefficients. The matrix $[L_s]$ is composed of symmetric functions of θ, and the matrix $[L_a]$ is composed of antisymmetric functions of θ.

Substitution of equation (3.4) into equation (3.2) gives the following expression

$$U_c = \frac{1}{2}\{C\}^T \int [L]^T [N][L]\, dV \{C\}$$

$$= \frac{1}{2}\left[C_s^T \vdots C_a^T\right]\left[\int_V \left\{\begin{matrix} L_s^T \\ \hdashline L_a^T \end{matrix}\right\}[N]\left[L_s \vdots L_a\right] dV\right]\left\{\begin{matrix} C_s \\ \hdashline C_a \end{matrix}\right\}$$

Define

$$[H] = \int_V [L]^T [N][L]\, dV = \int_V \left\{\begin{matrix} L_s^T \\ \hdashline L_a^T \end{matrix}\right\}[N]\left[L_s \vdots L_a\right] dV$$

$$= \int_V \begin{bmatrix} L_s^T N L_s & L_s^T N L_a \\ L_a^T N L_s & L_a^T N L_a \end{bmatrix} dV \qquad (3.5)$$

$$= \begin{bmatrix} H_{ss} & 0 \\ 0 & H_{aa} \end{bmatrix}$$

where it is recognized that the integral of antisymmetric quantities over a symmetric domain will be zero. Also, $[H_{ss}]$ and $[H_{aa}]$ can be determined by integrating over one half the volume and doubling the results. Therefore,

$$U_c = \frac{1}{2} \cdot \{C_s\}^T [H_{ss}]\{C_s\} + \frac{1}{2}\{C_a\}^T [H_{aa}]\{C_a\} \qquad (3.6)$$

The surface tractions on the boundary in x- and y-directions can be found by the following boundary conditions

$$\{S\} = t \begin{bmatrix} \sigma_x^b & \tau_{xy}^b \\ \tau_{xy}^b & \sigma_y^b \end{bmatrix} \begin{Bmatrix} \ell_x \\ \ell_y \end{Bmatrix}$$

where ℓ_x and ℓ_y are the direction cosines of the unit normal drawn outwards on the boundary. The cartesian stress components σ_x^b, σ_y^b and τ_{xy}^b can be expressed in terms of the polar stress components σ_r^b, σ_θ^b and $\tau_{r\theta}^b$ by the transformation matrix [TS], i.e.,

$$\begin{Bmatrix} \sigma_x^b \\ \sigma_y^b \\ \tau_{xy}^b \end{Bmatrix} = [TS] \begin{Bmatrix} \sigma_r^b \\ \sigma_\theta^b \\ \tau_{r\theta}^b \end{Bmatrix} \tag{3.8}$$

where

$$[TS] = \begin{bmatrix} \cos^2\theta & \sin^2\theta & -2\sin\theta\cos\theta \\ \sin^2\theta & \cos^2\theta & 2\sin\theta\cos\theta \\ \sin\theta\cos\theta & -\sin\theta\cos\theta & \cos^2\theta - \sin^2\theta \end{bmatrix}$$

The polar stress components σ_r^b, σ_θ^b and $\tau_{r\theta}^b$ can be obtained from equation (2.27) by simply defining the radial coordinate along the boundary, i.e., $r = r_b = \sqrt{x_b^2 + y_b^2}$. Thus the surface traction can be written in matrix form as

$$\{S\} = [B]\{C\} = \left[\, B_s \,\vdots\, B_a \,\right] \left\{ \begin{array}{c} C_s \\ \hdashline C_a \end{array} \right\} \tag{3.9}$$

The displacement $\{ U^P \}$ along the boundary can be expressed in terms of nodal displacements $\{ q \}$ as

$$\{ U^P \} = [D]\{q\} \tag{3.10}$$

where the matrix [D] is a function of position along boundary, determined such that $\{ U^P \}$ are linear along boundary.

Substituting equations (3.9) and (3.10) into equation (3.3) gives the following expression

$$V_C = -\{C\}^T \int_{S_u} [B]^T [D]\, dS\, \{q\} = -\left[C_S^T \,\vdots\, C_a^T \right] \int_{S_u} \left\{ \begin{array}{c} B_S^T \\ \hdashline B_a^T \end{array} \right\} [D]\, dS\, \{q\} \tag{3.11}$$

Define

$$[T] = \int_{S_u} [B]^T [D]\, dS = \int_{S_u} \left\{ \begin{array}{c} B_S^T \\ \hdashline B_a^T \end{array} \right\} [D]\, dS = \left[\begin{array}{c} T_S \\ \hdashline T_a \end{array} \right] \tag{3.12}$$

Therefore,

$$V_C = -\{C_S\}^T [T_S]\{q\} - \{C_a\}^T [T_a]\{q\} \tag{3.13}$$

Each row of [T] can be interpreted as the generalized forces corresponding to boundary tractions associated with a specified stress state in the interior of the element. Since each stress state is in equilibrium, it follows that the boundary tractions will automatically be self-equilibrating. Therefore, the work done by those boundary tractions

will be zero for any set of boundary displacements which follow from rigid body motion of the singular element. That is,

$$[T_s]\{q_R\} = \{0\} \qquad \text{and} \qquad [T_a]\{q_R\} = \{0\}$$

where $\{q_R\}$ denotes any one of the three rigid body displacements. Also, due to symmetry and antisymmetry, it follows that

$$[T_s]\{q_a\} = \{0\} \qquad \text{and} \qquad [T_a]\{q_s\} = \{0\}$$

where $\{q_a\}$ and $\{q_s\}$ are antisymmetric and symmetric displacements, respectively.

Now substituting the equations (3.6) and (3.13) into equation (3.1), the complementary energy can be written as

$$\pi_c = \frac{1}{2}\{C_s\}^T[H_{ss}]\{C_s\} + \frac{1}{2}\{C_a\}^T[H_{aa}]\{C_a\} - \{C_s\}^T[T_s]\{q\} - \{C_a\}^T[T_a]\{q\} \tag{3.14}$$

The necessary conditions for π_c to be stationary are that the first derivatives of π_c with respect to C_s and C_a are equal to 0

i.e.,
$$\frac{\partial \pi_c}{\partial C_s} = 0 \qquad \therefore \quad \{C_s\} = [H_{ss}]^{-1}[T_s]\{q\} \tag{3.15}$$

and
$$\frac{\partial \pi_c}{\partial C_a} = 0 \qquad \therefore \quad \{C_a\} = [H_{aa}]^{-1}[T_a]\{q\} \tag{3.16}$$

The complementary strain energy U_c is a positive definite quadratic function of the stress coefficients, $\{C\}$. Therefore the matrix [H] is

guaranteed to be nonsingular, so that $[H_{SS}]^{-1}$ and $[H_{aa}]^{-1}$ always exist for use in equations (3.15) and (3.16).

Substitute equations (3.15) and (3.16) into equation (3.6) and obtain the expression for U_c;

$$U_c = \frac{1}{2}\{C_s\}^T [H_{ss}] \{C_s\} + \frac{1}{2}\{C_a\}^T [H_{aa}] \{C_a\}$$

$$= \frac{1}{2}\{q\}^T [T_s]^T [H_{ss}^{-1}]^T [H_{ss}] [H_{ss}]^{-1} [T_s] \{q\}$$

$$+ \frac{1}{2}\{q\}^T [T_a]^T [H_{aa}^{-1}]^T [H_{aa}] [H_{aa}]^{-1} [T_a] \{q\}$$

Since both $[H_{ss}]$ and $[H_{aa}]$ are symmetric, this can finally be written as

$$U_c = \frac{1}{2}\{q\}^T \left([T_s]^T [H_{ss}]^{-1} [T_s] + [T_a]^T [H_{aa}]^{-1} [T_a] \right) \{q\} \qquad (3.17)$$

The complementary strain energy can also be written in terms of displacements $\{q\}$;

$$U_c = \frac{1}{2}\{q\}^T [K] \{q\} \qquad (3.18)$$

where [K] is total stiffness matrix, which can be obtained by comparing equations (3.17) and (3.18);

$$[K] = [T_s]^T [H_{ss}]^{-1} [T_s] + [T_a]^T [H_{aa}]^{-1} [T_a] \qquad (3.19)$$

Obviously the total stiffness matrix is given by the sum of two matrices which are defined as follows:

$$[K_s] = [T_s]^T [H_{ss}]^{-1} [T_s]$$

$$[K_a] = [T_a]^T [H_{aa}]^{-1} [T_a]$$

where $[K_s]$ and $[K_a]$ are parts of the total stiffness matrix associated with symmetric and antisymmetric deformation, respectively.

With all of the equations now available for generating the stiffness matrix, a simple example with two singular terms in stress expressions and assumed linear displacements along the boundary will be utilized to demonstrate the procedure to obtain the total stiffness matrix of a singular element.

Two-Term Approximation

The assumed stresses in equations (2.27) are given as infinite series in which each term satisfies the interior equilibrium and stress-free boundary conditions. However, the leading terms of the stress expressions provide the stress singularity around the sharp corners. It is anticipated that the procedure to formulate the stiffness matrix will be simplified and that a reasonably accurate result might be possible by taking only symmetric and antisymmetric singular terms. In what follows, this two term approximation is used to illustrate the procedure to develop a stiffness matrix for a 9 node singular element. Let n = 1; then the stress expressions (2.27) become

$$\sigma_r = C_{s1} r^{\alpha_{s1}-1} \left\{ \left[(\alpha_{s1}+1) - (\alpha_{s1}-1)^2 \right] \cos(\alpha_{s1}-1)\theta + \frac{\alpha_{s1}(\alpha_{s1}-1)\sin(\alpha_{s1}-1)\theta_o}{\sin(\alpha_{s1}+1)\theta_o} \cdot \cos(\alpha_{s1} \quad 1)\theta \right]$$

$$- C_{a1} r^{\alpha_{a1}-1} \left[\alpha_{a1} (\alpha_{a1}+1) \sin(\alpha_{a1}+1)\theta + \frac{\alpha_{a1}(3-\alpha_{a1})\sin(\alpha_{a1}+1)\theta_o}{\sin(\alpha_{a1}-1)\theta_o} \cdot \sin(\alpha_{a1}-1)\theta \right]$$

$$= C_{s1} r^{\alpha_{s1}-1} RS(\theta) + C_{a1} r^{\alpha_{a1}-1} RA(\theta)$$

(3.20)

$$\sigma_\theta = C_{s1} r^{\alpha_{s1}-1} \alpha_{s1} (\alpha_{s1}+1) \left[\cos(\alpha_{s1}-1)\theta - \frac{(\alpha_{s1}-1)\sin(\alpha_{s1}-1)\theta_o}{(\alpha_{s1}+1)\sin(\alpha_{s1}+1)\theta_o} \cos(\alpha_{s1}+1)\theta \right]$$

$$+ C_{a1} r^{\alpha_{a1}-1} \alpha_{a1} (\alpha_{a1}+1) \left[\sin(\alpha_{a1}+1)\theta - \frac{\sin(\alpha_{a1}+1)\theta_o}{\sin(\alpha_{a1}-1)\theta_o} \sin(\alpha_{a1}-1)\theta \right]$$

$$= C_{s1} r^{\alpha_{s1}-1} \overline{TS}(\theta) + C_{a1} r^{\alpha_{a1}-1} \overline{TA}(\theta)$$

$$\tau_{r\theta} = -C_{s1} r^{\alpha_{s1}-1} \alpha_{s1} \left[-(\alpha_{s1}-1) \sin(\alpha_{s1}-1)\theta + \frac{(\alpha_{s1}-1)\sin(\alpha_{s1}-1)\theta_o}{\sin(\alpha_{s1}+1)\theta_o} \sin(\alpha_{s1}+1)\theta \right]$$

$$- C_{a1} r^{\alpha_{a1}-1} \alpha_{a1} \left[(\alpha_{a1}+1)\cos(\alpha_{a1}+1)\theta - \frac{\sin(\alpha_{a1}+1)\theta_o}{\sin(\alpha_{a1}-1)\theta_o} (\alpha_{a1}-1)\cos(\alpha_{a1}-1)\theta \right]$$

$$= C_{s1} r^{\alpha_{s1}-1} SS(\theta) + C_{a1} r^{\alpha_{a1}-1} SA(\theta) \qquad (3.20)\ \text{Cont'd}$$

where

$$RS(\theta) = \left[(\alpha_{s1}+1) - (\alpha_{s1}-1)^2 \right] \cos(\alpha_{s1}-1)\theta + \frac{\alpha_{s1}(\alpha_{s1}-1)\sin(\alpha_{s1}-1)\theta_o}{\sin(\alpha_{s1}+1)\theta_o} \cos(\alpha_{s1}+1)\theta$$

$$RA(\theta) = -\alpha_{a1}(\alpha_{a1}+1)\sin(\alpha_{a1}+1)\theta + \frac{\alpha_{a1}(3-\alpha_{a1})\sin(\alpha_{a1}+1)\theta_o}{\sin(\alpha_{a1}-1)\theta_o} \sin(\alpha_{a1}-1)\theta \qquad (3.21)$$

$$TS(\theta) = \alpha_{s1}(\alpha_{s1}+1)\left[\cos(\alpha_{s1}-1)\theta - \frac{(\alpha_{s1}-1)\sin(\alpha_{s1}-1)\theta_o \cos(\alpha_{s1}+1)\theta}{(\alpha_{s1}+1)\sin(\alpha_{s1}+1)\theta_o}\right]$$

$$TA(\theta) = \alpha_{a1}(\alpha_{a1}+1)\left[\sin(\alpha_{a1}+1)\theta - \frac{\sin(\alpha_{a1}+1)\theta_o}{\sin(\alpha_{a1}-1)\theta_o} \sin(\alpha_{a1}-1)\theta\right]$$

$$SS(\theta) = -\alpha_{s1}(\alpha_{s1}-1)\left[\frac{\sin(\alpha_{s1}-1)\theta_o \cdot \sin(\alpha_{s1}+1)\theta}{\sin(\alpha_{s1}+1)\theta_o} - \sin(\alpha_{s1}-1)\theta\right]$$

$$SA(\theta) = -\alpha_{a1}\left[(\alpha_{a1}+1)\cos(\alpha_{a1}+1)\theta - \frac{\sin(\alpha_{a1}+1)\theta_o}{\sin(\alpha_{a1}-1)\theta_o}(\alpha_{a1}-1)\cos(\alpha_{a1}-1)\theta\right]$$

Therefore σ_r, σ_θ and $\tau_{r\theta}$ can be written in the following simplified matrix form

$$\begin{Bmatrix} \sigma_r \\ \sigma_\theta \\ \tau_{r\theta} \end{Bmatrix} = \begin{bmatrix} \overline{RS} \cdot r^{\alpha_{s1}-1} & \overline{RA} \cdot r^{\alpha_{a1}-1} \\ \overline{TS} \cdot r^{\alpha_{s1}-1} & \overline{TA} \cdot r^{\alpha_{a1}-1} \\ \overline{SS} \cdot r^{\alpha_{s1}-1} & \overline{SA} \cdot r^{\alpha_{a1}-1} \end{bmatrix} \begin{Bmatrix} C_{s1} \\ \\ C_{a1} \end{Bmatrix} \tag{3.22}$$

Obtain the cartesian stress components σ_x^b, σ_y^b and τ_{xy}^b on the boundary from equation (3.8)

$$\begin{Bmatrix} \sigma_x^b \\ \sigma_y^b \\ \tau_{xy}^b \end{Bmatrix} = [TS] \begin{Bmatrix} \sigma_r^b \\ \sigma_\theta^b \\ \tau_{r\theta}^b \end{Bmatrix} = [TS] \begin{bmatrix} \overline{RS} \cdot r_b^{\alpha_{s1}-1} & \overline{RA} \cdot r_b^{\alpha_{a1}-1} \\ \overline{TS} \cdot r_b^{\alpha_{s1}-1} & \overline{TA} \cdot r_b^{\alpha_{a1}-1} \\ \overline{SS} \cdot r_b^{\alpha_{s1}-1} & \overline{SA} \cdot r_b^{\alpha_{a1}-1} \end{bmatrix} \begin{Bmatrix} C_{s1} \\ \\ C_{a1} \end{Bmatrix} \tag{3.23}$$

Let

$$[G] = [TS] \begin{bmatrix} \overline{RS}\, r_b^{\alpha_{s1}-1} & \overline{RA}\, r_b^{\alpha_{a1}-1} \\ \overline{TS}\, r_b^{\alpha_{s1}-1} & \overline{TA}\, r_b^{\alpha_{a1}-1} \\ \overline{SS}\, r_b^{\alpha_{s1}-1} & \overline{SA}\, r_b^{\alpha_{a1}-1} \end{bmatrix}$$

Then equation (3.23) becomes

$$\begin{Bmatrix} \sigma_x^b \\ \sigma_y^b \\ \tau_{xy}^b \end{Bmatrix} = \begin{bmatrix} G_s(1) & G_a(1) \\ G_s(2) & G_a(2) \\ G_s(3) & G_a(3) \end{bmatrix} \begin{Bmatrix} C_{s1} \\ \\ C_{a1} \end{Bmatrix} \tag{3.24}$$

Note that the surface tractions can be found easily by combining equations (3.7) and (3.24), and then [B] can be obtained from equation (3.9). Matrix [D] in equation (3.10) comes from the assumption of linear boundary displacements. Then matrix [T] follows from the boundary integration of equation (3.12).

(1) Along the boundary between nodes 1 and 2, with $0° \leq \theta \leq 45°$ (see Figure 2(a)), the coordinates of any points on the surface are

$$\begin{cases} x = \ell \\ \\ y = \ell \tan\theta \end{cases} \qquad r_b = (x^2 + y^2)^{1/2}$$

The surface traction is given by

$$\{S\} = t \begin{Bmatrix} \sigma_x^b \\ \\ \tau_{xy}^b \end{Bmatrix} = t \left[\begin{array}{c:c} G_s(1) & G_a(1) \\ \\ G_s(3) & G_a(3) \end{array}\right] \left[\begin{array}{c} C_{s1} \\ \hdashline \\ C_{a1} \end{array}\right]$$

According to equation (3.9)

$$[B] = t \left[\begin{array}{c:c} G_s(1) & G_a(1) \\ \\ G_s(3) & G_a(3) \end{array}\right]$$

For edge displacement, assume

$$\{U^P\} = \begin{Bmatrix} U_x^P \\ U_y^P \end{Bmatrix} = \begin{bmatrix} \frac{\ell-y}{\ell} & 0 & \frac{y}{\ell} & 0 \\ 0 & \frac{\ell-y}{\ell} & 0 & \frac{y}{\ell} \end{bmatrix} \begin{Bmatrix} q_x^1 \\ q_y^1 \\ q_x^2 \\ q_y^2 \end{Bmatrix}$$

According to equation (3.10)

$$[D] = \begin{bmatrix} \frac{\ell-y}{\ell} & 0 & \frac{y}{\ell} & 0 \\ 0 & \frac{\ell-y}{\ell} & 0 & \frac{y}{\ell} \end{bmatrix}$$

From equation (3.12) evaluate matrix [T] along the boundary

$$\therefore [T] = \int_{S_u} [B]^T [D]\, ds = \int_{y=0}^{y=\ell} t \begin{bmatrix} \frac{G_s(1)}{G_a(1)} & \frac{G_s(3)}{G_a(3)} \end{bmatrix} \begin{bmatrix} \frac{\ell-y}{\ell} & 0 & \frac{y}{\ell} & 0 \\ 0 & \frac{\ell-y}{\ell} & 0 & \frac{y}{\ell} \end{bmatrix} dy$$

(2) Along the boundary between nodes 2 and 3, with $45° \leq \theta \leq 90°$ and $x = \ell \cdot \cot(\theta)$, $y = \ell$, $r_b = (x^2 + y^2)^{1/2}$.

The surface traction is given by

$$\{S\} = t \begin{Bmatrix} \sigma_y^b \\ \tau_{xy}^b \end{Bmatrix} = t \left[\begin{array}{c:c} G_s(2) & G_a(2) \\ G_s(3) & G_a(3) \end{array}\right] \begin{Bmatrix} C_{s1} \\ C_{a1} \end{Bmatrix}$$

According to equation (3.9)

$$[B] = t \begin{bmatrix} G_s(2) & \vdots & G_a(2) \\ & & \\ G_s(3) & \vdots & G_a(3) \end{bmatrix}$$

For edge displacement, assume

$$\{U^P\} = \begin{Bmatrix} U_x^P \\ \\ U_y^P \end{Bmatrix} = \begin{bmatrix} \frac{x}{\ell} & 0 & \frac{\ell-x}{\ell} & 0 \\ & & & \\ 0 & \frac{x}{\ell} & 0 & \frac{\ell-x}{\ell} \end{bmatrix} \begin{Bmatrix} q_x^2 \\ q_y^2 \\ q_x^3 \\ q_y^3 \end{Bmatrix}$$

According to equation (3.10)

$$[D] = \begin{bmatrix} \frac{x}{\ell} & 0 & \frac{\ell-x}{\ell} & 0 \\ & & & \\ 0 & \frac{x}{\ell} & 0 & \frac{\ell-x}{\ell} \end{bmatrix}$$

From equation (3.12), evaluate matrix [T] along the boundary

$$[T] = \int_{x=\ell}^{x=0} t \begin{bmatrix} G_s(2) & G_s(3) \\ \cdots\cdots\cdots & \cdots\cdots\cdots \\ G_a(2) & G_a(3) \end{bmatrix} \begin{bmatrix} \frac{x}{\ell} & 0 & \frac{\ell-x}{\ell} & 0 \\ & & & \\ 0 & \frac{x}{\ell} & 0 & \frac{\ell-x}{\ell} \end{bmatrix} (-dx)$$

(3) Along the boundary between nodes 3 and 4, with $90° \leq \theta \leq 135°$ and $x = \ell \cot\theta$, $y = \ell$, $r_b = (x^2 + y^2)^{1/2}$

The surface traction is given by

$$\{S\} = \begin{Bmatrix} \sigma_y^b \\ \tau_{xy}^b \end{Bmatrix} = t \left[\begin{array}{c:c} G_s(2) & G_a(2) \\ G_s(3) & G_a(3) \end{array}\right] \begin{Bmatrix} C_{s1} \\ C_{a1} \end{Bmatrix}$$

According to equation (3.9)

$$[B] = t \left[\begin{array}{c:c} G_s(2) & G_a(3) \\ G_s(3) & G_a(3) \end{array}\right]$$

For edge displacement, assume

$$\{U^P\} = \begin{Bmatrix} U_x^P \\ U_y^P \end{Bmatrix} \begin{bmatrix} \frac{x+\ell}{\ell} & 0 & -\frac{x}{\ell} & 0 \\ 0 & \frac{x+\ell}{\ell} & 0 & -\frac{x}{\ell} \end{bmatrix} \begin{Bmatrix} q_x^3 \\ q_y^3 \\ q_x^4 \\ q_y^4 \end{Bmatrix}$$

According to equation (3.10)

$$[D] = \begin{bmatrix} \frac{x+\ell}{\ell} & 0 & -\frac{x}{\ell} & 0 \\ 0 & \frac{x+\ell}{\ell} & 0 & -\frac{x}{\ell} \end{bmatrix}$$

From equation (3.12), evaluate matrix [T] along the boundary

$$[T] = \int_{x=0}^{x=-\ell} t \begin{bmatrix} G_s(2) & G_s(3) \\ G_a(3) & G_a(3) \end{bmatrix} \begin{bmatrix} \frac{x+\ell}{\ell} & 0 & -\frac{x}{\ell} & 0 \\ 0 & \frac{x+\ell}{\ell} & 0 & -\frac{x}{\ell} \end{bmatrix} (-dx)$$

(4) Along the boundary between nodes 4 and 5, with $135° \leq \theta \leq \theta_0$ and $x = -\ell$, $y = -\ell \tan\theta$, $r_b = (x^2 + y^2)^{1/2}$.

The surface traction is given by

$$\{S\} = -t \begin{Bmatrix} \sigma_x^b \\ \tau_{xy}^b \end{Bmatrix} = -t \left[\begin{array}{c:c} G_s(1) & G_a(1) \\ G_s(3) & G_a(3) \end{array}\right] \begin{Bmatrix} C_{s1} \\ C_{a1} \end{Bmatrix}$$

According to equation (3.9)

$$[B] = -t \left[\begin{array}{c:c} G_s(1) & G_a(1) \\ G_s(3) & G_a(3) \end{array}\right]$$

For edge displacement, assume

$$\{U^P\} = \begin{Bmatrix} U_x^P \\ U_y^P \end{Bmatrix} = \begin{bmatrix} \frac{y-\ell}{\ell-h} + 1 & 0 & -\frac{y-\ell}{\ell-h} & 0 \\ 0 & \frac{y-\ell}{\ell-h} + 1 & 0 & \frac{y-\ell}{\ell-h} \end{bmatrix} \begin{Bmatrix} q_x^4 \\ q_y^4 \\ q_x^5 \\ q_y^5 \end{Bmatrix}$$

According to equation (3.10)

$$[D] = \begin{bmatrix} \frac{y-\ell}{\ell-h} + 1 & 0 & -\frac{y-\ell}{\ell-h} & 0 \\ 0 & \frac{y-\ell}{\ell-h} + 1 & 0 & -\frac{y-\ell}{\ell-h} \end{bmatrix}$$

From equation (3.12) evaluate matrix [T] along the boundary

$$[T] = \int_{y=\ell}^{y=-\ell \tan\theta_0} -t \begin{bmatrix} G_s(1) & G_s(3) \\ \hline G_a(1) & G_a(3) \end{bmatrix} \begin{bmatrix} \frac{y-\ell}{\ell-h} + 1 & 0 & -\frac{y-\ell}{\ell-h} & 0 \\ 0 & \frac{y-\ell}{\ell-h} + 1 & 0 & -\frac{y-\ell}{\ell-h} \end{bmatrix} (-dy)$$

Integration along the boundary from node 1 to node 5, or for $0 \leq \theta \leq \theta_0$, is always sufficient to provide all elements in the [T] matrix. First generate a partial matrix denoted by [T'] with elements T'_{ij}, by assembling the individual matrices as given above at common nodes. Then for each row of the final [T] matrix associated with a symmetric stress state, say the ith row of $[T_s]$ associated with the symmetric stress coefficient C_{si}, the elements T_{sij} are as follows:

$$T_{si1} = 2T'_{si1}, \quad T_{si2} = 0$$
$$T_{sij} = T'_{sij} \qquad j = 3,4, \ldots 10$$

$$T_{si11} = T_{si9} \qquad T_{si12} = -T_{si10}$$
$$T_{si13} = T_{si7} \qquad T_{si14} = -T_{si8}$$
$$T_{si15} = T_{si5} \qquad T_{si16} = -T_{si6}$$
$$T_{si17} = T_{si3} \qquad T_{si18} = -T_{si4}$$

These conditions on $[T_s]$ can be used to confirm that $[T_s]\{\varphi_a\} = 0$, as mentioned earlier; that is, symmetric forces do zero work during anti-symmetric displacements.

For the j^{th} row of $[T_a]$ associated with antisymmetric stress coefficient C_{aj}, the elements T_{ajk} are as follows:

$$T_{aj1} = 0$$

$$T_{aj2} = 2T'_{aj2}$$

$$T_{ajk} = T'_{ajk} \qquad k = 3,4. \ . \ . \ .10$$

$$T_{aj11} = -T_{aj9} \qquad T_{aj12} = T_{aj10}$$

$$T_{aj13} = -T_{aj7} \qquad T_{aj14} = T_{aj8}$$

$$T_{aj15} = -T_{aj5} \qquad T_{aj16} = T_{aj6}$$

$$T_{aj17} = -T_{aj3} \qquad T_{aj18} = T_{aj4}$$

It can be shown that $[T_a]\{q_s\} = 0$, as mentioned earlier, confirming that the antisymmetric forces do zero work during symmetric displacements.

Next, the matrix [H], obtained from integrating interior strain energy over the entire volume of the singular element is evaluated according to equation (3.5).

Define matrix [L] from equation (3.22), according to equation (3.4);

$$[L] = \left[\begin{array}{c|c} \overline{RS} \cdot r^{\alpha_{s1}-1} & \overline{RA} \cdot r^{\alpha_{a1}-1} \\ \overline{TS} \cdot r^{\alpha_{s1}-1} & \overline{TA} \cdot r^{\alpha_{a1}-1} \\ \overline{SS} \cdot r^{\alpha_{s1}-1} & \overline{SA} \cdot r^{\alpha_{a1}-1} \end{array}\right] = [L_S \mid L_a]$$

Substitution of the matrices [L] and elasticity matrix [N] into equation (3.5) gives the following expression

$$[H] = \int_V [L]^T [N][L]\, dV$$

$$= \iint_V \left[\begin{array}{ccc} \overline{RS}\, r^{\alpha_{s1}-1} & \overline{TS}\, r^{\alpha_{s1}-1} & \overline{SS}\, r^{\alpha_{s1}-1} \\ \hline \overline{RA}\, r^{\alpha_{a1}-1} & \overline{TA}\, r^{\alpha_{a1}-1} & \overline{SA}\, r^{\alpha_{a1}-1} \end{array}\right] \left[\begin{array}{ccc} \frac{1}{E} & -\frac{\mu}{E} & 0 \\ -\frac{\mu}{E} & \frac{1}{E} & 0 \\ 0 & 0 & \frac{1}{G} \end{array}\right]$$

$$\left[\begin{array}{c|c} \overline{RS} \cdot r^{\alpha_{s1}-1} & \overline{RA} \cdot r^{\alpha_{a1}-1} \\ \overline{TS} \cdot r^{\alpha_{s1}-1} & \overline{TA} \cdot r^{\alpha_{a1}-1} \\ \overline{SS} \cdot r^{\alpha_{s1}-1} & \overline{SA} \cdot r^{\alpha_{a1}-1} \end{array}\right] \cdot t r d\theta dr$$

Assume the thickness t is constant over the entire singular element and perform the integration with respect to r from the origin, r = 0, to the boundary r = r_b. Thus the volume integrand can be easily reduced to line integration along the boundary over the θ domain for $0 < \theta < \theta_0$, and the individual elements of the matrix [H] can be evaluated separately as follows.

$$H_{SS} = \int_{\theta=0.}^{\theta=\theta_0} \frac{t\, r_b^{2\alpha_{s1}}}{\alpha_{s1}} \left[\left(\frac{\overline{RS}}{E} - \frac{\mu}{E}\,\overline{TS}\right)\overline{RS} + \right.$$

$$\left. \left(-\frac{\mu}{E}\,\overline{RS} + \frac{\overline{TS}}{E}\right)\overline{TS} + \left(\frac{\overline{SS}}{G}\right)\overline{SS}\right] d\theta$$

$$H_{sa} = \int_{\theta=-\theta_0}^{\theta=\theta_0} \frac{t\, r_b^{\alpha_{s1}+\alpha_{a1}}}{\alpha_{s1}+\alpha_{a1}} \left[\left(\frac{\overline{RA}}{E} - \frac{\mu}{E}\,\overline{TA}\right)\overline{RS} + \right.$$

$$\left. \left(-\frac{\mu}{E}\,\overline{RA} + \frac{\overline{TA}}{E}\right)\overline{TS} + \left(\frac{\overline{SA}}{G}\right)\overline{SS}\right] d\theta = 0$$

$$H_{as} = \int_{\theta=-\theta_0}^{\theta=\theta_0} \frac{t\, r_b^{\alpha_{a1}+\alpha_{s1}}}{\alpha_{a1}+\alpha_{s1}} \left[\left(\frac{\overline{RS}}{E} - \frac{\mu}{E}\,\overline{TS}\right)\overline{RA} + \right.$$

$$\left. \left(-\frac{\mu}{E}\,\overline{RS} + \frac{\overline{TS}}{E}\right)\overline{TA} + \left(\frac{\overline{SS}}{G}\right)\overline{SA}\right] d\theta = 0$$

$$H_{aa} = \int_{\theta=0}^{\theta=\theta_0} \frac{t\, r_b^{2\alpha_{a1}}}{\alpha_{a1}} \left[\left(\frac{\overline{RA}}{E} - \frac{\mu}{E}\,\overline{TA}\right)\overline{RA} + \right.$$

$$\left. \left(-\frac{\mu}{E}\,\overline{RA} + \frac{\overline{TA}}{E}\right)\overline{TA} + \left(\frac{\overline{SA}}{G}\right)\overline{SA}\right] d\theta$$

As expected, H_{sa} and $H_{as} = 0$ due to antisymmetric integrands and a symmetric domain.

At this point, both [T] and [H] are expressed as line integrals along the boundary of the singular element. Unfortunately, the integrals can not be evaluated in closed form, so a numerical procedure must be used. The method selected is the simplest rectangular approximation in which the θ domain is divided into segments; the integrands

are assumed to be constant within each segment and equal to the midpoint value (see Figure 2(a)). It is expected that reasonable accuracy will be achieved by providing a sufficient number of segments along the boundary.

Check on the Accuracy of the Numerical Integration

The matrices [T] and [H] are evaluated numerically by dividing the boundary between two nodes into a number of segments of equal length. Therefore the stiffness matrix generated from the matrices [H] and [T] according to equation (3.19) is approximate, and the accuracy depends upon the number of segments on the boundary.

For a 90° notch angle and symmetric stresses, the elements of the [T] and [H[matrices are given in the following table for 5, 15, and 30 integration intervals between nodes. Since the assumed stress state contains only the symmetric singular term, [H] is a (1×1) matrix; since there are 14 displacement degrees of freedom for a 90° notch element, [T] is a (1×14) matrix but only 8 elements are recorded due to symmetry conditions of the type mentioned earlier. The results show that there is almost no difference between 5 and 30 segments; this strongly suggests that the simple rectangular integration is sufficiently accurate, and 30 segments should provide an excellent result.

Number of Segments = 5	Number of Segments = 15	Number of Segments = 30
$[H] = 9.29657 \times 10^{-7}$	$[H] = 9.29803 \times 10^{-7}$	$[H] = 9.29816 \times 10^{-7}$
$[T]^T$:	$[T]^T$:	$[T]^T$:
0.76148	0.76284	0.76297
0.0	0.0	0.0
0.27039	0.27016	0.27014

0.76365	0.76273	0.76265
-0.38953	-0.39035	-0.39043
1.23324	1.23468	1.23481
-0.26171	-0.26125	-0.26121
0.34721	0.34512	0.34493

Comments on the Determination of Stress Coefficients

As mentioned previously, the principle of stationary complementary strain energy is employed to establish the relationship between the stress coefficients and nodal displacements by equations (3.15) and (3.16) which can be rewritten as $[H_{ss}]\{C_s\} = [T_s]\{q\}$ and $[H_{aa}]\{C_a\} = [T_a]\{q\}$ in which $[H_{ss}]$ and $[H_{aa}]$ are nonsingular square matrices whose size are $(\frac{n}{2} \times \frac{n}{2})$; while $[T_s]$ and $[T_a]$ are rectangular matrices with sizes of $(\frac{n}{2} \times m)$ where n is the number of stress coefficients and m is the number of displacement degrees of freedom of the singular element.

It has already been noted that if a rigid body motion $\{q_R\}$ is applied to the singular element, then

$$[T_s]\{q_R\} = \{0\} \text{ and } [T_a]\{q_R\} = \{0\};$$

and since $[H_{ss}]$ and $[H_{aa}]$ are nonsingular, it follows that $\{C_s\} = \{0\}$ and $\{C_a\} = \{0\}$. That is, rigid body motions lead to zero stresses, as expected. The converse question is--does a zero stress state imply rigid body motion? This question can be answered by assuming $\{C_s\} = \{0\}$ and $\{C_a\} = \{0\}$ and determining the conditions under which

$$[T_s]\{q\} = \{0\} \quad \text{and} \quad [T_a]\{q\} = \{0\}$$

As an example, consider a singular element with symmetric boundary

displacements and the one singular stress state only. In this case, the equation $[T_s]\{q_s\} = \{0\}$ according to the numerical matrix [T] as given in the preceding section reduces to

$$0.38074\ q_1 + 0.27039\ q_3 + 0.76365\ q_4 - 0.38953\ q_5 +$$
$$1.23324\ q_6 - 0.26171\ q_7 + 0.34721\ q_8 = 0.$$

Obviously, there are six independent nodal displacements which satisfy the equation and thereby result in zero stresses. This means that even after eliminating three rigid body motions, the element stiffness matrix will still be singular. In this case, six displacements must be imposed before the stiffness matrix becomes nonsingular.

If one considers only the problem of determining stresses in the singular element due to imposed boundary displacements, then it is necessary to insure that there are exactly three independent displacements which lead to zero stresses. That is, there must be exactly three rigid body modes. This means that the rank of [T] must be (m-3) or $[T_s]$ must have rank $(\frac{m}{2} - 1)$ and $\{T_a\}$ must have rank $(\frac{m}{2} - 2)$. Therefore, as a necessary condition, there must be at least $(\frac{m}{2} - 1)$ symmetric stress coefficients and $(\frac{m}{2} - 2)$ antisymmetric stress coefficients. However, this is not a sufficient condition because it is possible to have the number of stress coefficients equal to or greater than (m-3) and still have a [T] matrix with rank less than (m-3).

These ideas can be clarified by considering the [T] matrix given in Appendix B, equation (B.3), for the special triangular element. First from equation (B.3) note that there are six stress coefficients, associated with six independent stress states, and there are six displacement degrees of freedom. There are obviously just three independent rows in

the [T] matrix--the rows associated with β_1, β_2 and β_5--so that there are exactly three independent stress-free displacements. Clearly, a reasonable approximate solution would be possible with β_1, β_2 and β_5 only. However, such a solution would not be possible with β_1, β_2 and β_6 only, or with β_1, β_2, β_3, β_4, and β_6 only, since in both cases the rank is only two. In fact one might have far more than six β's and still have a [T] matrix with rank less than three.

Satisfaction of Geometric Boundary Conditions

The stiffness matrix of a singular element is based on the solution to an elasticity problem with specified linear boundary displacements between nodes. Of course, the use of the principle of stationary complementary energy provides only an approximate solution to this elasticity problem. This means that the interior displacements derived from the stress state will not be exactly linear on the boundary, since satisfaction of geometric boundary conditions is the one requirement not satisfied exactly by the stress series of equation (2.27). Therefore, a measure of accuracy of any solution is provided by considering how well the geometric conditions are satisfied.

The interior displacement functions are first derived for a hairline crack problem based on the symmetric singular form of the stress series (2.27) for $\theta_0 = 180°$, and then the functions are generalized to include any number of terms. Thus, the deformed shape of a singular cracked element can be defined provided that the stress coefficients are given.

The singular symmetrical stress components taken from equation (3.20) for a hairline crack are

$$\sigma_r = 0.25\, C_1\, r^{-0.5}\left(5\cos\frac{\theta}{2} - \cos\frac{3\theta}{2}\right)$$

$$\sigma_\theta = 0.75\, C_1\, r^{-0.5}\left(\cos\frac{\theta}{2} + \frac{1}{3}\cos\frac{3\theta}{2}\right)$$

$$\tau_{r\theta} = 0.25\, C_1\, r^{-0.5}\left(\sin\frac{\theta}{2} + \sin\frac{3\theta}{2}\right)$$

Substituting the stress components in stress-strain relation (2.7) through (2.9) gives the strain components

$$\epsilon_r = \frac{\sigma_r - \mu\sigma_\theta}{E}$$

$$= \frac{C_1 r^{-0.5}}{4E}\left[\left(5\cos\frac{\theta}{2} - \cos\frac{3\theta}{2}\right) - 3\mu\left(\cos\frac{\theta}{2} + \frac{1}{3}\cos\frac{3\theta}{2}\right)\right]$$

$$\epsilon_\theta = \frac{\sigma_\theta - \mu\sigma_r}{E}$$

$$= \frac{C_1 r^{-0.5}}{4E}\left[3\left(\cos\frac{\theta}{2} + \frac{1}{3}\cos\frac{3\theta}{2}\right) - \mu\left(5\cos\frac{\theta}{2} - \cos\frac{3\theta}{2}\right)\right]$$

$$\gamma_{r\theta} = \frac{\tau_{r\theta}}{G} = \frac{C_1 r^{-0.5}}{4G}\left(\sin\frac{\theta}{2} + \sin\frac{3\theta}{2}\right)$$

Now find the displacements by strain-displacement relations (2.3) through (2.5) together with expressions for ε_r, ε_θ and $\gamma_{r\theta}$

$$\epsilon_r = \frac{\partial u_r}{\partial r}$$

$$= \frac{C_1 r^{-0.5}}{4E}\left[\left(5\cos\frac{\theta}{2} - \cos\frac{3\theta}{2}\right) - 3\mu\left(\cos\frac{\theta}{2} + \frac{1}{3}\cos\frac{3\theta}{2}\right)\right] \tag{3.25}$$

$$\epsilon_\theta = \frac{u_r}{r} + \frac{1}{r}\frac{\partial u_\theta}{\partial\theta}$$

$$= \frac{C_1 r^{-0.5}}{4E}\left[3\left(\cos\frac{\theta}{2} + \frac{1}{3}\cdot\cos\frac{3\theta}{2}\right) - \mu\left(5\cos\frac{\theta}{2} - \cos\frac{3\theta}{2}\right)\right] \tag{3.26}$$

$$\gamma_{r\theta} = \frac{1}{r}\frac{\partial u_r}{\partial\theta} + \frac{\partial u_\theta}{\partial r} - \frac{u_\theta}{r}$$

$$= \frac{C_1 r^{-0.5}}{4G}\left(\sin\frac{\theta}{2} + \sin\frac{3\theta}{2}\right) \tag{3.27}$$

Determine the displacement u_r from equation (3.25), i.e.,

$$u_r = \frac{C_1 r^{0.5}}{2E}\left[\left(5\cos\frac{\theta}{2} - \cos\frac{3\theta}{2}\right) - 3\mu\left(\cos\frac{\theta}{2} + \frac{1}{3}\cos\frac{3\theta}{2}\right)\right] + f(\theta)$$

Substitute the displacement u_r into equation (3.26) and solve for the displacement u_θ ;

$$u_\theta = -\int_0^\theta f(\theta)\,d\theta + \frac{C_1 r^{0.5}}{2E}\left[\left(\sin\frac{3\theta}{2} - 7\sin\frac{\theta}{2}\right) + \mu\left(\sin\frac{\theta}{2} + \sin\frac{3\theta}{2}\right)\right] + g(r)$$

The function g(r) can be identified as u_θ at $\theta = 0°$ and from symmetry requirements, $g(r) \equiv 0$. However, in order to indicate a procedure which applies for general displacement field, retain g(r) temporarily in what follows.

Substitute the displacements u_r and u_θ into equation (3.27) and obtain the following expression:

$$f'(\theta) + r\,g'(r) + \int_0^\theta f(\theta)\,d\theta - g(r) = 0$$

Since r and θ are independent variables, the necessary conditions for the equation to be identically zero are

$$f'(\theta) + \int_0^\theta f(\theta)d\theta = H$$

and

$$r g'(r) - g(r) = -H$$

The first equation can be written as

$$f''(\theta) + f(\theta) = 0$$

Obviously, the solution of this differential equation is

$$f(\theta) = K \cos\theta + A \sin\theta$$

Substitute into the integro-differential equation for $f(\theta)$ and conclude that $A = H$. Then $g(r)$ is given by

$$g(r) = Fr + H$$

Therefore the displacement function can be expressed as follows:

$$u_r = \frac{C_1}{2E} r^{0.5}\left[\left(5\cos\frac{\theta}{2} - \cos\frac{3\theta}{2}\right) - 3\mu\left(\cos\frac{\theta}{2} + \frac{1}{3}\cos\frac{3\theta}{2}\right)\right] + K\cos\theta + H\sin\theta$$

$$u_\theta = \frac{C_1}{2E} r^{0.5}\left[\left(\sin\frac{3\theta}{2} - 7\sin\frac{\theta}{2}\right) + \mu\left(\sin\frac{3\theta}{2} + \sin\frac{\theta}{2}\right)\right] + Fr + H\cos\theta - K\sin\theta$$

where F, H and K are rigid-body displacement parameters which can be defined by eliminating the rigid-body displacement. Of course, H and F are actually zero due to symmetry requirements.

The symmetric displacement functions have been derived based on

the singular term of the stress series. In fact the functions can be generalized to include any number of terms. The generalized symmetric functions according to Hardy [5] are listed in the following:

$$u_r = \sum_{n=1}^{\infty} \frac{C_n}{4G} r^{\frac{n}{2}} \left[h_n \cos\alpha_n\theta + (6 - 8\sigma' - n)\cos\beta_n\theta \right] + K\cos\theta$$

and

$$u_\theta = \sum_{n=1}^{\infty} \frac{C_n}{4G} r^{\frac{n}{2}} \left[-h_n \sin\alpha_n\theta + (6 - 8\sigma' + n)\sin\beta_n\theta \right] - K\sin\theta$$

where

$$\alpha_n = \frac{n+2}{2}$$

$$\beta_n = \frac{n-2}{2}$$

$$h_n = n + 2(-1)^n$$

The dimensionless elastic constant σ' is given by

$$\sigma' = \frac{\mu}{1+\mu}$$

As an example, consider the problem of a unit radial displacement at node 1, with all other nodes fixed; (see Figures 8 and 9 dashline). The symmetric stress coefficients are determined from equation (3.15) for both one and nine symmetric stress states; and the interior displacements are determined from the displacement functions with the rigid body constant, K, selected so that the displacement at node 1 is correct. The

implied boundary displacements are shown in Figures 8 and 9. There is obvious improvement in approximate solution when going from one to nine stress coefficients. The nine constant solution could be made to look even better by changing the rigid body constant so as to force a zero x-displacement at node 2.

Stiffness Matrices for Symmetric or Antisymmetric Problems

The complete stiffness matrix, as given by equation (3.19) can be used in all situations, including the most general case of both symmetric and antisymmetric stresses occurring simultaneously. However, many problems possess a structural symmetry with either symmetric loads or antisymmetric loads so that the structural response can be guaranteed to be either symmetric or antisymmetric respectively. In these cases, it is best to take advantage of the situation by considering a reduced domain with appropriate symmetry or antisymmetry conditions imposed on the interior boundaries along with the regular boundary conditions on the exterior boundaries. This reduces the size of the domain and permits either a reduction in the number of unknowns (for a fixed mesh size) or an increase in the number of finite elements (for a fixed number of unknowns).

For some problems, this use of symmetry will require just one-half of the singular element as shown for example in Figure 7a. The modified stiffness matrices for the singular element can be obtained by any one of the following methods.

The first procedure is to impose proper unit displacements (either symmetric or antisymmetric) at symmetrically located nodes and determine the generalized nodal forces which result. These nodal forces, when properly arranged, constitute the columns of the stiffness matrix for

one-half the singular element experiencing either symmetric or antisymmetric distortions.

An alternative procedure is to define transformation matrices $[\bar{T}]$ which serve to impose either symmetric or antisymmetric nodal displacements. That is,

$$\{q_{total}\} = [\bar{T}]\{q_{red}\}$$

will relate the total vector of generalized displacements, $\{q_{total}\}$, to a reduced vector, $\{q_{red}\}$, consisting of just one-half the total, with the remaining displacements given by either symmetry or antisymmetry conditions. This transformation can be applied to the strain energy U , as follows:

$$\begin{aligned} U &= \frac{1}{2}\{q_{total}\}^T [K]\{q_{total}\} \\ &= \frac{1}{2}\{q_{red}\}^T [\bar{T}]^T [K][\bar{T}]\{q_{red}\} \\ &= \frac{1}{2}\{q_{red}\}^T [K_{red}]\{q_{red}\} \end{aligned} \tag{3.28}$$

where the appropriately transformed stiffness matrix is

$$[K_{red}] = [\bar{T}]^T [K][\bar{T}]$$

Now, the strain U in equation (3.28) is the energy in the complete singular element. For one-half the element, there is just one-half the energy, so that the final reduced stiffness matrix suitable for use with one-half the element is

$$[K_{red}] = \frac{1}{2}[\bar{T}]^T [K][\bar{T}]$$

CHAPTER IV

RESULTS

Effect of the Stress Approximation

The singular stiffness matrix is generated first by adopting only singular terms in the stress series and secondly by taking a number of terms from the series equal to the total displacement degrees of freedom of the singular element. In order to study the effect of the stress approximation on the stress intensity factors, a number of finite element models are constructed for double-edge notched (see Figures 10, 12, and 14) and single-edge notched (see Figure 16, 18 and 20) finite plates with notch angles of 0°, 60° and 90°. One quarter of the finite element model of the doubly notched plates and one half of the finite element model of single notched plates are shown in Figures 11 through 15 and Figures 17 through 21, respectively. Note that the finite element detail models 11 and 17, 13 and 19, 15 and 21 are identical. Thus a finite element detailed model can be used to represent both double- and single-edge notched plates by simply imposing the appropriate set of constraint conditions along the symmetric boundary (see the difference in constraint conditions between Figures 11 and 17, Figures 13 and 19, and Figures 15 and 21).

The uniformly distributed loads are converted into a set of work equivalent concentrated nodal loads. Since the boundary displacements of the conventional triangular elements are assumed to have a linear variation between nodes, it follows that the concentrated forces on a

node are equal to total uniformly distributed loads acting on half of the area between two adjacent nodes.

The finite element solutions obtained from singular terms and multiple terms approximations for the double- and single-edge notched plates are given in Tables 7 and 8. The tables indicate that the differences in stress intensity factors are between 1.7% and 8.2%. It appears that the singular term only solutions provide sufficiently accurate results for practical purposes except for crack propagation studies, and this approximation is used for most of the study which follow.

As mentioned in Chapter III, "Comments on the Determination of Stress Coefficients," if the selected number of stress coefficients are less than (m -3), when m is the total number of degrees of freedom of a singular element, then there will be more than three zero-stress displacements. This means that the singular element stiffness matrix generated by the matrices [T] and [H] remains singular even after the three rigid body displacement modes are eliminated. However, in the finite element solution for a plate problem, the stiffness matrix of the singular element is merged into the overall stiffness matrix of a structural model by the customary direct stiffness method. This means that the overall stiffness matrix will usually be nonsingular after eliminating three rigid body displacements since conventional finite elements will generate strain energy even though, for certain displacements, the singular element might not generate energy. This explains why the one or two term stress approximations can be used to give results for K_s and K_a even though the singular element has more than three zero-stress states. The exception will occur if every node of the singular element

is not connected to a conventional element. In this case, even after eliminating three rigid body modes, the over-all stiffness matrix will still be singular, due to the fact that a zero-stress state exists which does not strain any conventional elements. This situation can be avoided easily by proper modeling.

Effect of Numerical Integration Accuracy

The numerical values of $[T_s]$ and $[H_{ss}]$ of a singular element with 90° notch angle for various number of segments, i.e., 5, 15 and 30, are given in Chapter III; and the stiffness matrix can then be generated according to equation (3.19). A double-edge 90° notched plate (see Figures 14 and 15) is selected for further investigation of the effect of the number of segments on the determination of the stress intensity factors. The results in Table 9 merely confirm what was shown in Chapter III; that is, rectangular numerical integration is sufficiently accurate. Thirty intervals between nodes are used in the studies which follow.

Effect of Mesh Refinement

The accuracy of stress intensity factors obtained depends upon mesh sizes. A square plate with 90° notch cutout (see Figure 22) is idealized as three distinct finite element models with the ratio of the size of singular element and notched plate being 1/2, 1/3, 1/4 (see Figures 23, 24, and 25); the size of the conventional right triangular elements are also selected to match the size of singular element. Table 10 indicates that for the example problem, the stress intensity factor converged from below with mesh refinement. The worst result appears to

be about 25% in error, but this large error may be partially due to the concentrated external loading.

For another example with uniform loading, consider the plate shown in Figure 26, idealized as three distinct finite element models with the ratio of the size of singular element and notched plate being 1/3, 1/6 and 1/12 (see Figures 27, 28 and 29). Note that the detail which falls outside the region of the dark lines is unchanged, while the conventional elements are sized as required by the singular element within the dark line. The first run of Table 11 shows rapid convergence from below, with a maximum difference of just 3%.

Effect of Strain Energy Approximation in the Neighborhood of the Notch Tip

For each distinct finite element model, the stress intensity factors can also be determined from the following idealizations: (1) the singular element is completely removed from the model; this is based on assumption that strain energy stored in the singular element may be small compared to total strain energy (2) the singular element is replaced by a number of conventional triangular elements (see dashed lines in Figures 27, 28 and 29). In this idealization, the stress intensity factors are calculated by imposing the nodal displacements obtained from the overall model to the singular element. The numerical results obtained from the various methods for the three sizes of singular element are given in Table 11.

The third row of Table 11 shows that the stress intensity factors calculated by completely neglecting the strain energy in the singular element are unacceptably high even for the finest mesh. It would be

expected that the results would be high since neglecting the energy is physically equivalent to eliminating a portion of the plate, which would lead to increased nodal displacements and thereby increased stress intensity factors.

Next, conventional triangular elements are used in the area of the singular element in order to provide an approximation for strain energy in that region. The results, shown in the next-to-last row of Table 11, are smaller than those obtained with the singular element, indicating that a collection of conventional triangles is stiffer than a singular element of the same size.

Comparison with Existing Solutions

The typical cracked plates are analyzed with the singular element whose stiffness matrix is based on a 1 term symmetric stress approximation. These cracked plates, which have existing solutions, are centrally cracked plates and single-edge cracked plate. A typical centrally cracked square plate with the crack line perpendicular to the direction of applied loads as shown in Figure 30, with crack length/width ratio being 0.4, is idealized with a coarse model (see Figure 31) and fine model (see Figure 32). Also, in order to satisfy the free boundary conditions exactly, the special triangular elements are used to replace conventional triangular elements along the free edges (see Figure 33). The numerical results of the coarse model and fine models with and without the special triangular elements are given in Table 12. The existing solution [8] is a finite element solution based on the assumed displacement hybrid model and the theoretical basis is a modified principle of minimum potential energy.

The coarse model, 9 term solution is within approximately 0.5%; and the fine model, 1 term solution agrees exactly with the existing solution. The introduction of the special triangular element leads to a 3% reduction in predicted K_s.

The second centrally cracked plate has the crack line parallel to the direction of applied load (see Figure 34); the finite element model of one quarter plate is given in Figure 35. The numerical result for K_s, using a singular element with 1 term symmetric stress approximation, is given in Table 13, which indicates that the finite element solution is the exact solution. Note that there is no need to utilize the special triangular elements along the upper edge of the finite element model, since the conventional triangular elements contain the exact solution.

In order to compare results with an existing solution [8] for a square plate with single-edge crack, a finite element model of one half the cracked plate is established in such a way that the total number of elements is as close as possible to Atluri's model, which contains 24 elements including 2 singular elements. The numerical results are given in Table 13, which shows an excellent agreement with the existing solution. Additional comparison can be made between the finite element solutions for single-edge cracked plates with different aspect ratios (see Figures 16 and 36). Table 13 indicates that the finite element solutions have the right trend in that the stress intensity factor for a square plate is indeed higher than the one for a rectangular plate.

Solution of Some Typical Plates with Right Angle Re-entry Corners

The results presented to this point have been directed primarily toward evaluating the accuracy of the approximate solution. The remainder of this chapter presents results for a number of finite width plates with re-entry corners. The intention is to show the types of problems which can be solved with the notched singular element. Extremely accurate results are not presented because economics has dictated the use of relatively coarse meshes. Since there are no existing solutions which can be used to measure accuracy, the best that can be done it to compare relative magnitudes of K_s and K_a for various geometries of plates and confirm expected trends.

A 90° singular element is applied to solve a square plate with a central square cutout subject to both uniaxial and biaxial tensile stress (see Figure 38). A set of appropriate symmetric constraint conditions are imposed on a finite element model of the quarter plate (see Figure 39). The symmetric and antisymmetric stress intensity factors obtained from the finite element solution are given in Table 14. Note that K_a changes sign in going from condition a to condition b; this occurs because the shear stress changes sign in the neighborhood of the notch tip. The values given in Table 14 do satisfy the principle of superposition; that is, the values for condition c are the sum of values for conditions a and b.

In the case of biaxial loading, it is possible to take further advantage of symmetry, since the loading and the geometry of the model (see Figure 39) are symmetric about the diagonal. Therefore, the size of model can be further reduced to 1/8 of the entire plate by imposing

symmetric constraint conditions along the diagonal.

The finite element model as given in Figure 39 can also be used to represent a single-edge rectangular cutout plate (see Figure 40) by simply changing the boundary conditions (see Figure 41). The opening and sliding modes of deformation under the uniaxial and biaxial tensile stresses are listed in Table 15. Comparison can be made between the results in Tables 14 and 15. It appears that sliding mode values of K_a are almost the same while the opening mode values of K_s are substantially increased in the case of single-edge rectangular cutout plate. The solutions are reasonable since the single-edge rectangular cutout plate is more flexible than the square cutout plate as far as the opening deformation of the corner is concerned. As the result, the K_s should be higher for the single-edge rectangular cutout case.

Next the square cutout is rotated 45° to be a diamond-shape cutout in the square plate (see Figure 42), with the finite element representation of a quarter plate given in Figure 43. The finite element solutions for opening modes, K_s, occurring at corners under the uniaxial and biaxial loads are given in Table 16. Note that the ratio of stress intensity factors at points 1 and 2 under the uniaxial stress is -3, and the ratio becomes 1 when the biaxial stress is applied. Incidentally, the numerical ratio of stress intensity factors of the diamond-shape cutout is equal to the ratio of the stresses in corresponding locations in a plate with a circular cutout under the two sets of loads. Once again the solution for the biaxial tensile stress demonstrates the principle of superposition for the problem of linear elasticity. Further advantage of symmetry can be taken in the case of biaxial tensile load

by imposing the symmetric constraint conditions along the diagonal.

Singular points are frequently found in the members of building construction. The 90° singular element is used to determine the stress intensity factors at the sharp corners of those members such as single stepped plate, footing plate, doubly stepped plate and footing plate with free ends. The geometry of the plates and applied loads are shown in Figures 44, 46, 48, and 50 and their finite element representations are shown in Figures 45, 47, 49 and 51. Note that an identical finite element model is used to represent various geometries of the plates by simply imposing appropriate symmetrical constraint conditions along the symmetrical axis.

It is of interest to note that in addition to free-free corners, a different type of singularity also occurs at fixed-free corners, 1 and 2, as shown in Figures 44 and 46. The fixed-free corner element was developed by Hardy [5] to calculate the stress for a semi-infinite strip. However, the two types of singular points are separated far enough in the particular problems considered here, so that the interaction between the singular points can be ignored. Therefore the singularity at the fixed-free corner is not considered in the determination of stress intensity factors at the free-free corners.

The results of finite element solutions for the stepped plates are given in Table 17 which indicates that the stress intensity values for single stepped plate are smaller than those for a footing plate. This is an acceptable solution since the single stepped plate has a tendency to deform upward due to the eccentricity of the external applied loads. As the result, at the sharp corner, the opening deformation due

to axial load is reduced. Table 17 further indicates that the stress intensity values are increased from footing plate to doubly stepped plate to footing plate with free ends. These results suggest that the softer the structures, the more the deformation; and therefore the softest plate should have the highest stress intensity factors.

Effect of Length of the Plate

The stress intensity factors will be functions of plate length as well as the crack length, width of the plate and loading. To investigate this length effect, three different geometries of single-edge cracked plates with length-width ratios of 1, 2 and 3 are considered.

The finite element models of the typical cracked plate as shown in Figure 53 are given in Figures 54, 55 and 56. Table 18 indicates that the stress intensity factors decrease by 8.5% as the length-width ratio increases from 1 to 2. The table further indicates almost no change in the stress intensity factor as the length-width ratio increases from 2 to 3. Therefore the solution for a plate with length-width ratio greater than 2 can be used as the solution for an infinite strip.

The data for K_s versus length-width ratio as given in Table 18 are shown in Figure 57. Also the value of K_s calculated from Tada's empirical formula [15] shows 5.26 for the infinite single-edge cracked strip with crack length-width ratio being 0.4; this result is 7.5% in error compared to the finite element result for length-width ratio of 3. The discrepancy may be due to the fact that Poisson's ratio μ used in this study is different from the test material (Young's modulus does not affect the result), or the empirical formula is constructed based on plane strain problem while the plane stress problem is assumed in this study.

Effect of the Size of Interior Cutout

The stress intensity factors depend also upon the flexibility of the plate. This effect is investigated by considering the square plate with central square cutout and varying the size of the cutout. The width ratios considered are $\frac{1}{3}$, $\frac{1}{2}$, and $\frac{2}{3}$.

The finite element models of the typical square plates as shown in Figure 58 are given in Figures 59, 60 and 61. Table 19 indicates that both K_s and K_a increase sharply as the material is removed from the square plate.

Table 7. Effect of Stress Approximation on the Stress Intensity Factors, K_s, for Double-Edge Notch Plates*

	NOTCHED ANGLES		
Various Approximations	(a) $\theta = 0°$	(b) $\theta = 60°$	(c) $\theta = 90°$
9 term solution for θ=0° and 60° 7 term solution for θ=90°	3.046	3.087	3.343
1 term solution	2.947	3.139	3.426
Difference	-3.2%	1.7%	2.5%
Existing Solution [15]	2.864	-	-

*Based on 30 integration intervals (segments) between nodes on the singular element.

(a) The cracked plate and the finite element model are given in Figures 10 and 11; the existing solution is based on infinite strip.

(b) The notched plate and the finite element model are given in Figures 12 and 13.

(c) The notched plate and the finite element model are given in Figures 14 and 15.

Table 8. Effect of Stress Approximation on the Stress Intensity Factors, K_s, for Single-Edge Notched Plates*

Various Approximations	NOTCHED ANGLES (a) $\theta = 0°$	(b) $\theta = 60°$	(c) $\theta = 90°$
9 term solution for θ=0° and 60° 7 term solution for θ=90°	4.446	4.538	4.948
1 term solution	4.083	4.307	4.710
Difference	-8.2%	-5.1%	-4.8%
Existing Solution [15]	5.26	-	-

*Based on 30 integration intervals (segments) between nodes on the singular element.

(a) The cracked plate and the finite element model are given in Figures 16 and 17; the existing solution is based on infinite strip.

(b) The notched plate and the finite element model are given in Figures 18 and 19.

(c) The notched plate and the finite element model are given in Figures 20 and 21.

Table 9. Effect of Numerical Integration Accuracy on the Stress Intensity Factors, K_s, for a Double-Edge 90° Notched Plate*

Number of Integration Intervals (Segments) between Nodes on the Singular Element	5	15	30
K_s	3.432	3.432	3.426

*The notched plate and the finite element model are given in Figures 14 and 15; based on singular stress term only (the 1 term stress approximation)

Table 10. Effect of Mesh Refinement on the Stress Intensity Factor, K_s, for a Square Plate with Single-Edge 90° Notch*

	Size 1[a]	Size 2[b]	Size 3[c]
K_s	2.433	2.944	3.229

*See Figure 22; based on 1 term stress approximation and 30 segments between nodes on the singular element.

[a]See Figure 23.

[b]See Figure 24.

[c]See Figure 25.

Table 11. Effect of Mesh Refinement on the Stress Intensity Factors, K_s, for a Square Plate with Single-edge 90° Notch

Methods of Solution	Model I[a]	Model II[b]	Model III[c]
Singular element with conventional triangles	7.901	8.141	8.152
Singular element, conventional triangles, and special triangles along the notch face	7.904	8.130	8.108
Neglect energy in singular element; conventional triangles	42.573	26.924	21.992
Replace singular element with conventional triangles	6.366	7.059	7.304
Replace singular element with conventional and special triangles	6.498	7.191	7.430

*See Figure 26; based on 1 term stress approximation and 5 segments between nodes on the singular element.

(a) See Figure 27.

(b) See Figure 28.

(c) See Figure 29.

Table 12. Stress Intensity Factors, K_s, for a Centrally Cracked Plate*

	Methods of Solution			
	Coarse Model[a] 1 Term Solution	Coarse Model[a] 9 Term Solution	Fine Model[b] 1 Term Solution	Fine Model[b] 1 Term Solution with Special Triangular Elements
K_s	2.942	3.037	3.057	2.913
Existing Solution [8]	3.058	3.058	3.058	3.058

*See Figure 30; based on 30 segments between nodes on the singular element.

[a]The cracked plate and the finite element coarse model are given in Figures 30 and 31.

[b]The cracked plate and the finite element fine model are given in Figures 30 and 32.

Table 13. Stress Intensity Factors for a Plate with Longitudinal Crack and Plates with Single-Edge Crack*

	Geometries		
	Longitudinal Crack[a]	Square Plate with Single Edge Crack[b]	Rectangular Plate with Single-Edge Crack[c]
K_s	0.0	5.27	4.083
Existing Solution	0.0	5.26 [7]	4.018 [15]

*Based on 1 term stress approximation and 30 segments between nodes on the singular element.

[a]The cracked plate and the finite element model are given in Figures 34 and 35.

[b]The cracked plate and the finite element model are given in Figures 36 and 37.

[c]The cracked plate and the finite element model are given in Figures 16 and 17. The existing solution is based on infinite strip.

Table 14. Stress Intensity Factors for a Square Plate with a Square Cutout*

	Loading Conditions		
	(a)	(b)	(c)
K_s at Location 1	1.382	1.382	2.764
K_a at Location 1	2.346	-2.346	0

*The cutout plate and the finite element model are shown in Figures 38 and 39; based on 2 term stress approximation and 30 segments between nodes on the singular element.

(a) Loads are applied in x-direction only.

(b) Loads are applied in y-direction only.

(c) Equal loads are applied in x- and y-directions.

Table 15. Stress Intensity Factors for a Rectangular Plate with a Single-Edge Rectangular Cutout*

	Loading Conditions	
	(a)	(b)
K_s	2.917	3.104
K_a - Location 1	2.309	0.002
K_a - Location 2	-2.309	-0.002

*The cutout plate and the finite element model are shown in Figure 40 and 41; based on 14 terms stress approximation and 30 segments between nodes on the singular element.

(a) Loads are applied in y-direction only.

(b) Loads are applid in x- and y-directions.

Table 16. Stress Intensity Factors, K_s, for a Square Plate with a Central Diamond-Shape Cutout*

	Loading Conditions		
	(a)	(b)	(c)
K_s at Location 1	+3.847	-1.295	2.553
K_s at Location 2	-1.295	+3.847	2.553

*The cutout plate and the finite element model are shown in Figures 42 and 43; based on 14 term stress approximation and 30 segments between nodes on the singular element.

(a) Loads are applied in x-direction only.

(b) Loads are applied in y-direction only.

(c) Equal loads are applied in x- and y-directions.

Table 17. Stress-Intensity Factors of Some Typical Stepped Plates*

Geometries	K_s	K_a
Singly Stepped Plate[a]	0.929	1.437
Footing Plate[b]	1.466	1.494
Doubly Stepped Plate[c]	1.506	1.568
Footing Plate with Free Ends[d]	2.245	1.627

*Based on 14 term stress approximation and 30 segments between nodes on the singular element.

[a]The singly stepped plate and the finite element model are shown in Figures 44 and 45.

[b]The footing plate and the finite element model are shown in Figures 46 and 47.

[c]The doubly stepped plate and the finite element model are shown in Figures 48 and 49.

[d]The footing plate with free ends and the finite element model are shown in Figures 50 and 51.

Table 18. Effect of Length on the Stress Intensity Factors, K_s, for a Single-edge Cracked Plate*

	Model I(a) $\frac{H}{W} = 1$	Model II(b) $\frac{H}{W} = 2$	Model III(c) $\frac{H}{W} = 3$
K_s	5.325	4.875	4.863

*See Figure 53; based on 9 term stress approximation and 30 segments between nodes on the singular element.

(a) See Figure 54.

(b) See Figure 55.

(c) See Figure 56.

Table 19. Effect of the Size of Interior Cutout on the Stress Intensity Factors for a Square Plate*

	Model I[a] $\frac{d}{W} = \frac{1}{3}$	Model II[b] $\frac{d}{W} = \frac{1}{2}$	Model III[c] $\frac{d}{W} = \frac{2}{3}$
K_s	2.342	3.638	6.748
K_a	-2.988	-3.981	-5.855

*See Figure 58; based on 2 term stress approximation and 30 segments between nodes on the singular element.

(a) See Figure 59

(b) See Figure 60

(c) See Figure 61

CHAPTER V

CONCLUSIONS AND RECOMMENDATIONS

Conclusions

The stiffness matrix of a singular element as shown in Figure 2 has been developed to investigate the effect of notch angle on stress intensity factors at sharp corners of finite plates with arbitrary cut-outs. The singular element is utilized to replace highly detailed conventional finite element models around the sharp corners with resulting economies in both data preparation and computer time. A number of two dimensional elasticity problems have been solved by addition of the stiffness matrix of the singular element to the overall stiffness matrix of a structural model by the customary direct stiffness method. The accuracy and efficiency of the singular element is demonstrated by determining the stress intensity factors of simple crack configurations for which there are analytical solutions.

Several conclusions are reached in this study and discussed in the following.

(1) Stiffness matrices of singular elements have been derived based on assumed stresses which contain either singular terms only or singular plus nonsingular terms in the stress series. Numerical results given in Tables 7 and 8 indicate that the differences between solutions for the two approximations are between 1.7% and 8.2%. The study is extended to use the singular-term only approximation to predict stress intensity factors for some simple cracked plates

for which there are existing solutions; it is concluded from the numerical results shown in Tables 12 and 13 that the singular term approximation can provide excellent means to obtain accurate solutions.

(2) In Chapter III, "Check on the Accuracy of the Stiffness Matrix Obtained from Numerical Integration," matrices [T] and [H] of a singular element with 90° notch angle are evaluated numerically with the number of integration intervals between nodes being 5, 15, and 30. The stress intensity factors of a double-edge 90° notched plate with the various integration intervals are also tabulated in Table 9. It is concluded that the simple rectangular integration with 30 integration intervals is sufficiently accurate.

(3) The effect of mesh refinement on the solution has been studied. As an example, a square 90° notched plate with various sizes of singular element is used to illustrate the sensitivity of the stress intensity value to the selected size of singular element. Table 10 shows that the larger the singular and conventional elements, the lower the stress intensity values. The biggest error is 25%, a large error due primarily to the coarse mesh but also possibly caused by the type of external loads. Another example with uniform loading shows rapid convergence of values for K_s (see Table 11).

(4) Nonsingular elements can be used to determine nodal displacement in the neighborhood of the notch tip. These displacements can then be imposed on the singular element to determine stress intensity factors. Table 11 shows that such results are still 10% in error even for the finest mesh considered, which indicates that the singular element

provides a more accurate estimate of strain energy as well as providing the proper stress singularity. Table 11 also shows that it is unacceptable to completely ignore the strain energy in the region of the notch tip.

(5) Central and edge cracked plates have been analyzed in order to compare with the existing solutions; Tables 12 and 13 show excellent agreement.

(6) The singular element has been utilized to predict stress intensity factors at sharp corners of interior square cutouts, diamond-shape cutouts and a number of other plates with 90° re-entry corners. Although there are no existing solutions that can be used to compare with the finite element solutions, the numerical results as given in Tables 14 through 17 have been checked for consistency and reasonableness through judgment.

(7) A single-edge cracked square plate has been analyzed by two different finite element models; namely coarse model in Figure 32 and fine model in Figure 54. The values of computed K_s for the coarse and fine models are 5.27 and 5.325 respectively. Note that the difference between two solutions is within 1.0%. It appears that the relatively coarse model provides accurate result for stress intensity factors.

(8) The square plate with central square cutout with width ratios being 1/3, 1/2 and 2/3 has been analyzed by fine finite element models. It appears that stress intensity factors depend upon the flexibility of the plate.

Recommendations

No attempt is made to assess the effect of changes in accuracy with singular element aspect ratio, the imposed boundary displacement and the number of element nodal points. The selected square shape of the element is arbitrary, and some other shape might provide more accurate results. The imposed linear boundary displacement is chosen to fit conveniently with the most common constant strain triangular element. If a more refined triangular element is utilized, then the imposed boundary displacements on the singular element might be correspondingly refined; this should result in improved accuracy. Hence the effects of the element shapes and the assumed boundary displacements on the prediction of stress intensity factors might prove to be worthy of further study. Furthermore it is expected to extend this study to calculate stress intensity factors for orthotropic material [18].

Several possibilities exist for such refinement, one of which is to define an 11-node singular element for notch angles less than 90° (7 nodes would still be sufficient for notch angles greater than or equal to 90°). This element would be joined to conventional linear strain triangles, so that the imposed boundary displacements on the singular element would be quadratic.

One application of the stress intensity factors at notches might be in crack initiation at re-entry corners. Even though the actual corner will not be perfectly sharp, it is possible that the time to crack initiation might be related to the ideal stress intensity factors which are developed in this dissertation. Further research is needed to establish such a relation, if it exists. Of course, after the crack

initiates, then it is necessary to introduce the hairline crack singular element for further study of crack propagation.

APPENDICES

APPENDIX A

ILLUSTRATIONS

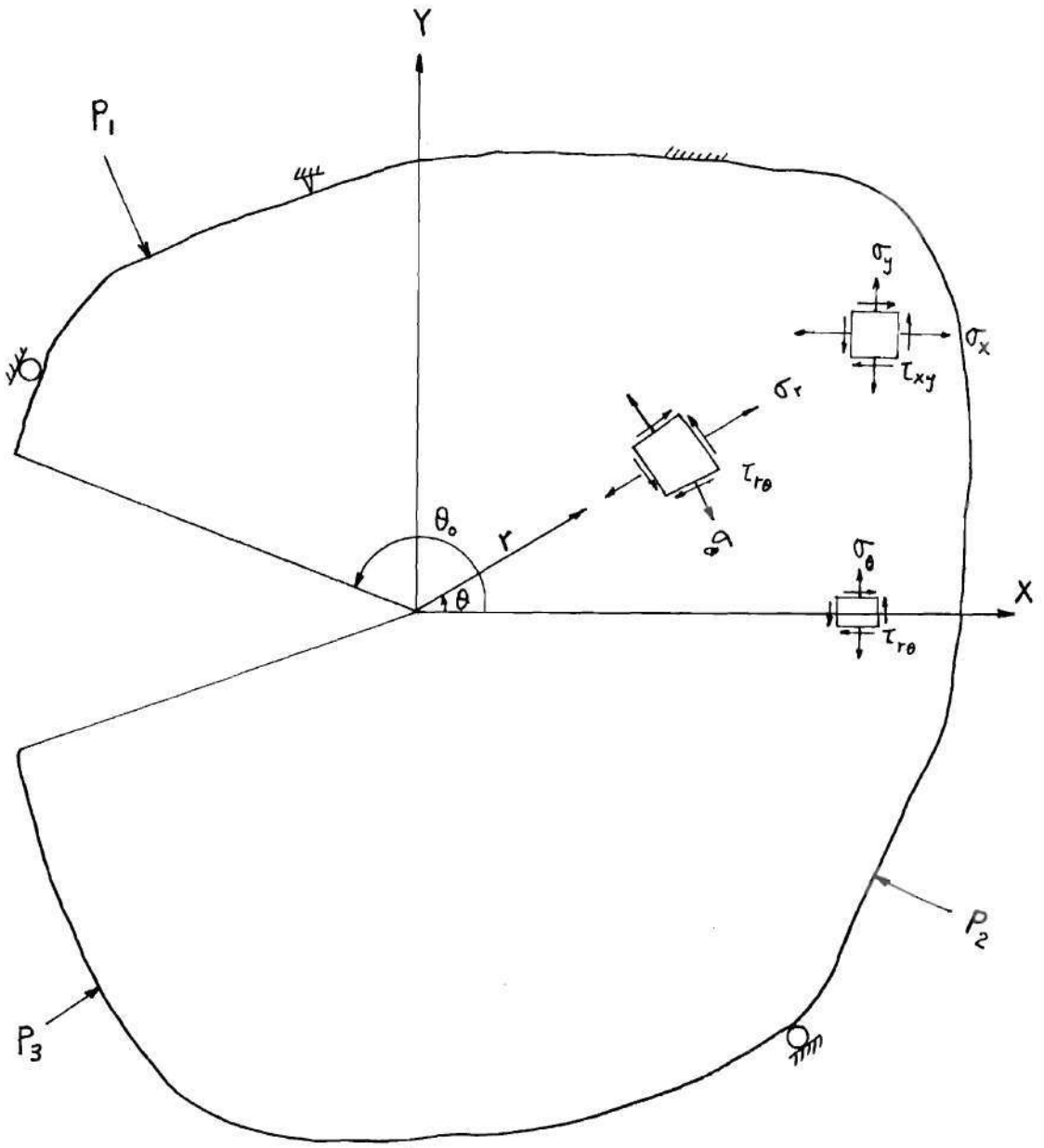

Figure 1. Coordinates in the Neighborhood of the Sharp Corner of Arbitrary Notch Angle in Elastic Medium.

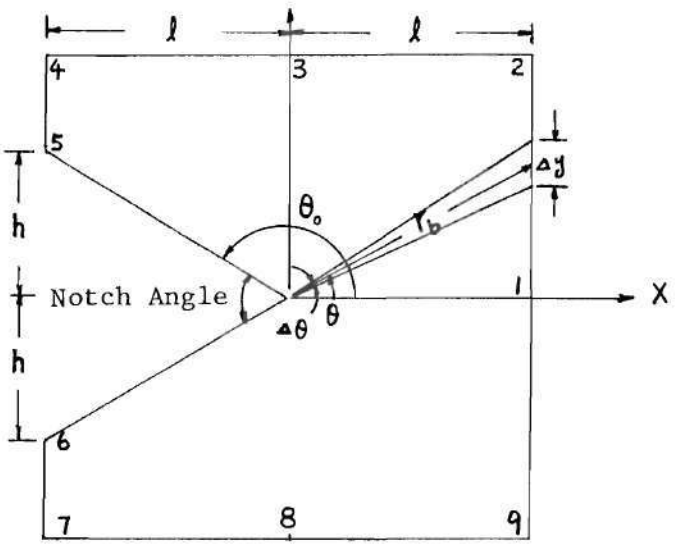

(a) $0° \leq$ notch angle $< 90°$

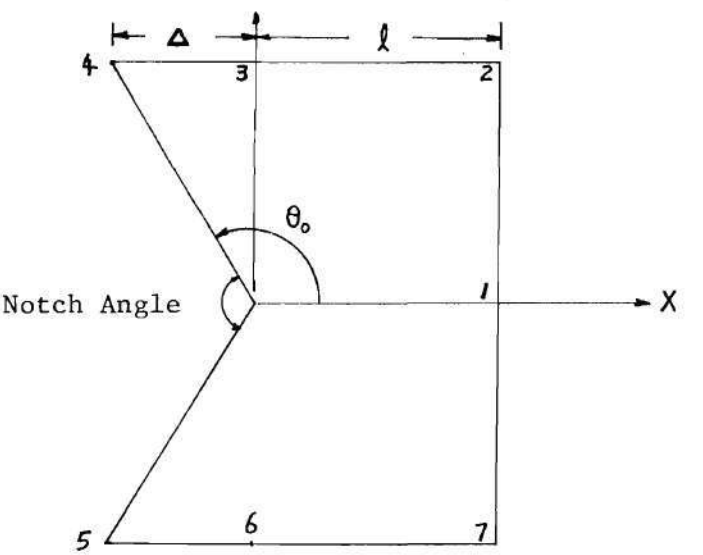

(b) $90° \leq$ notch angle $< 180°$

Figure 2. Typical Singular Elements.

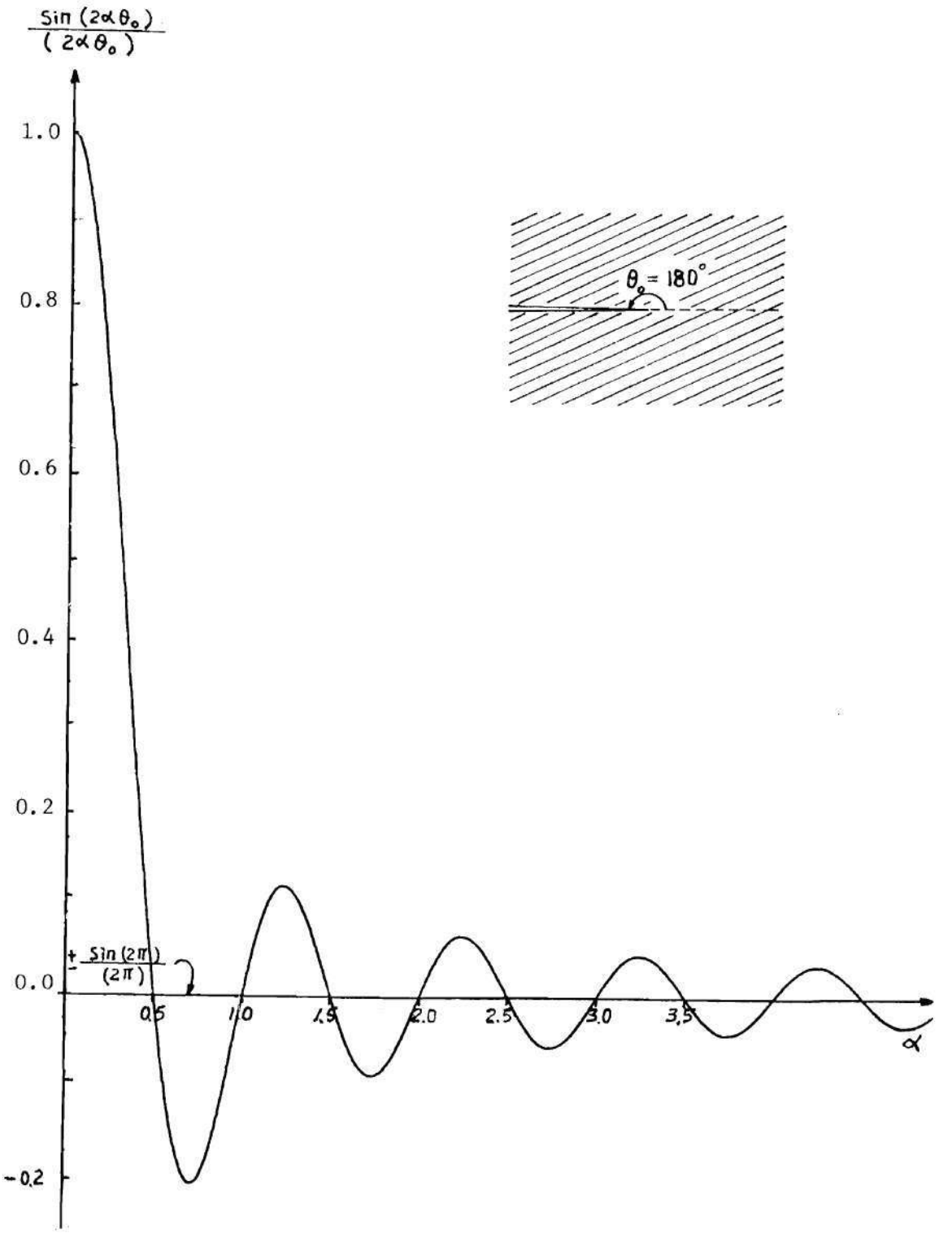

Figure 3. Graphical Solution of Real Roots for 0° Notch Angle.

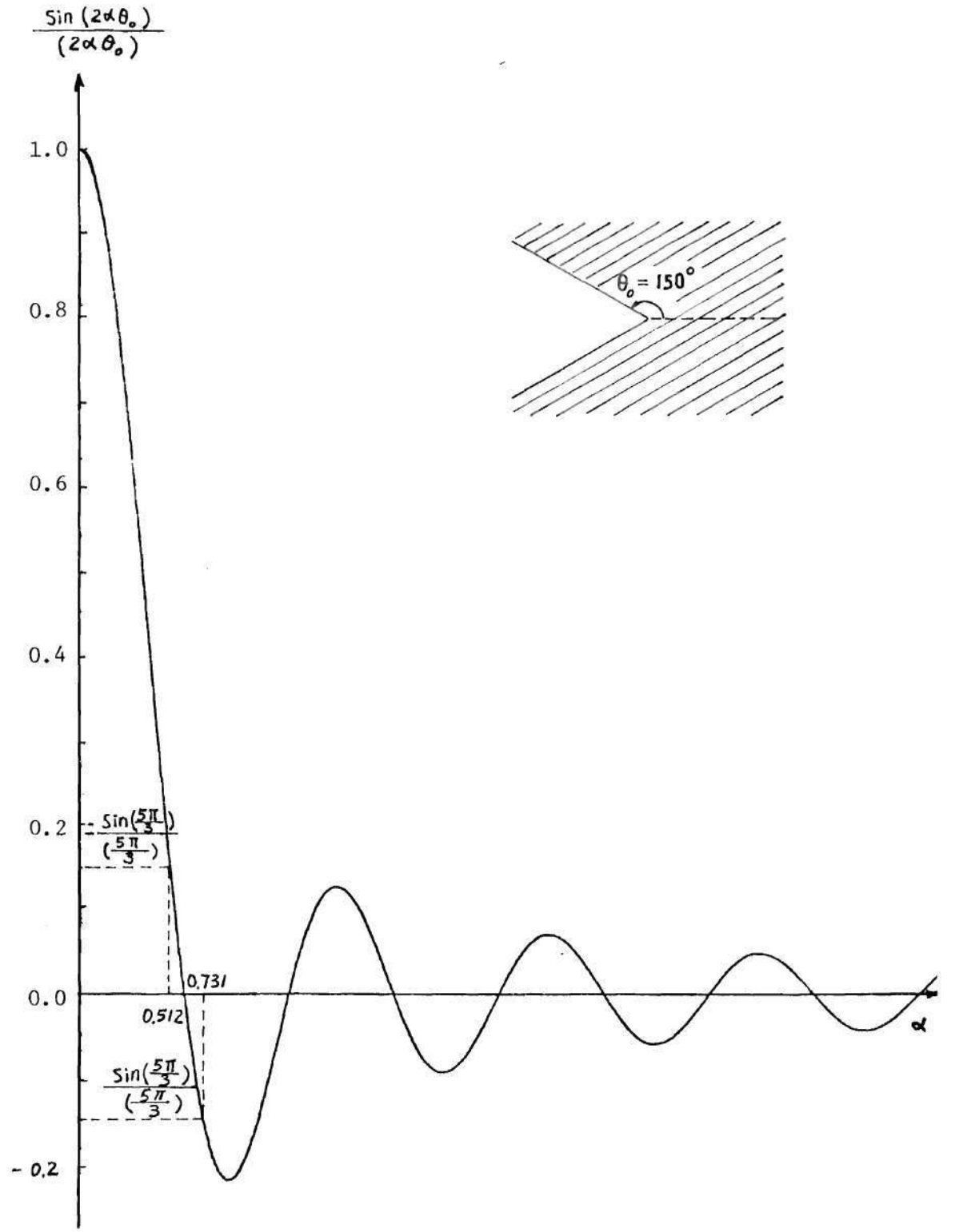

Figure 4. Graphical Solution of Real Roots for 60° Notch Angle.

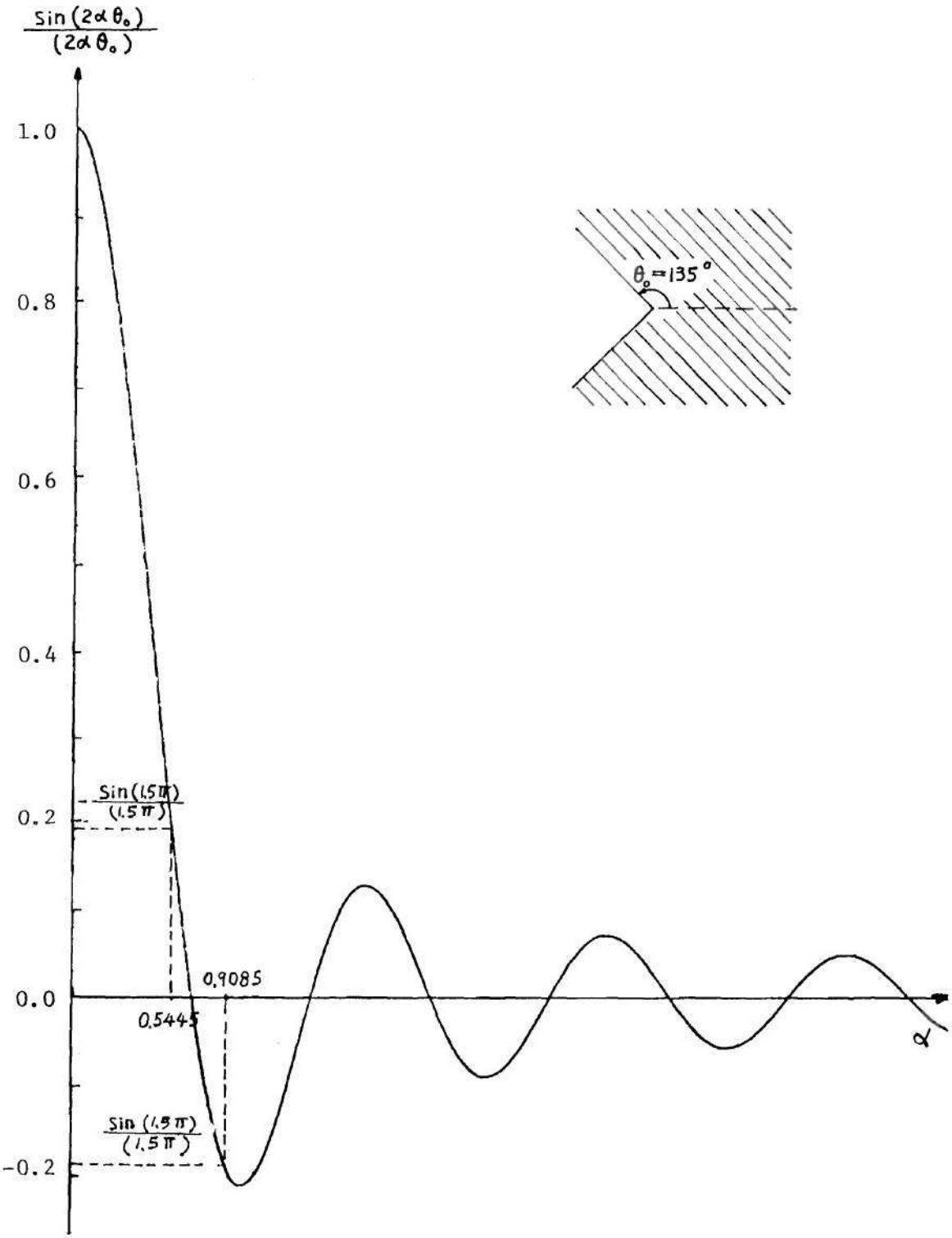

Figure 5. Graphical Solution of Real Roots for 90° Notch Angle.

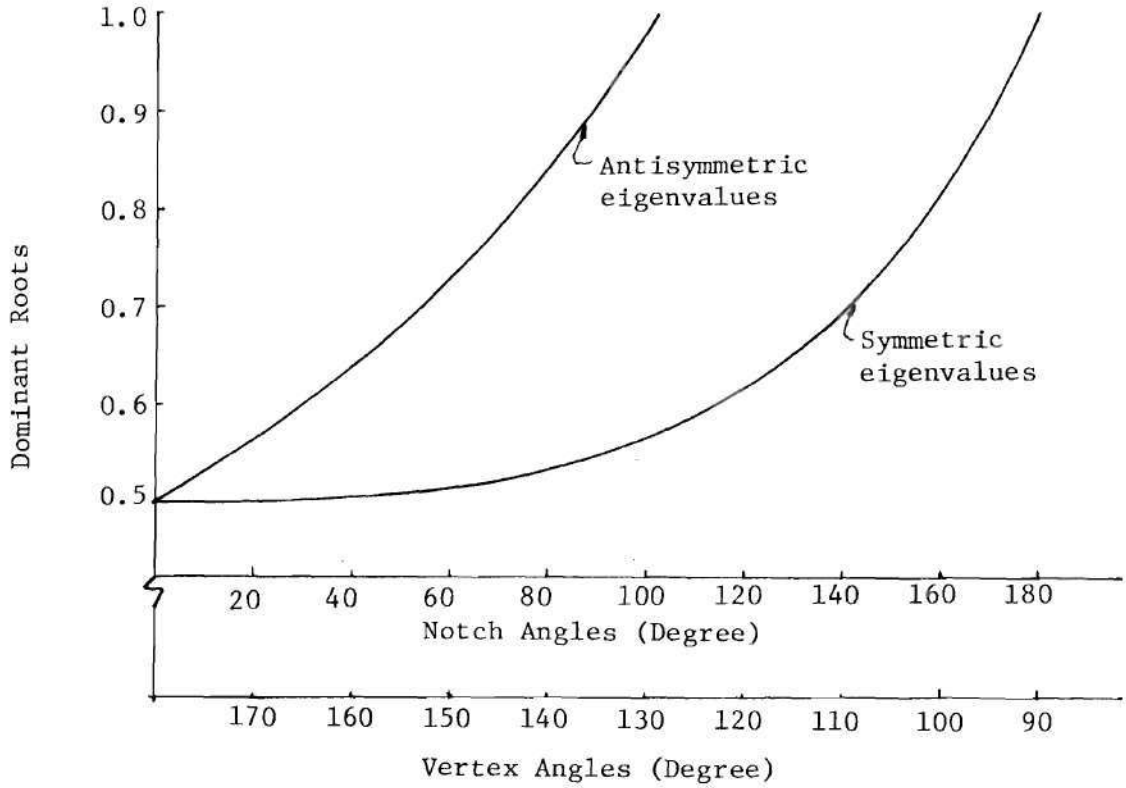

Figure 6. Effect of Notch Angles on Dominant Roots of Eigenfunctions.

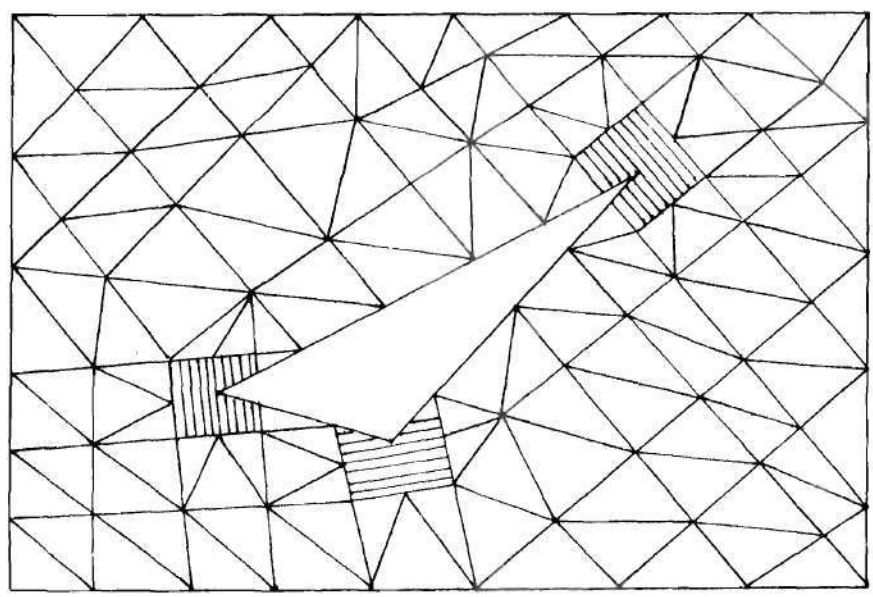

Figure 7. A Typical Finite Element Model for Arbitrary Cutouts.

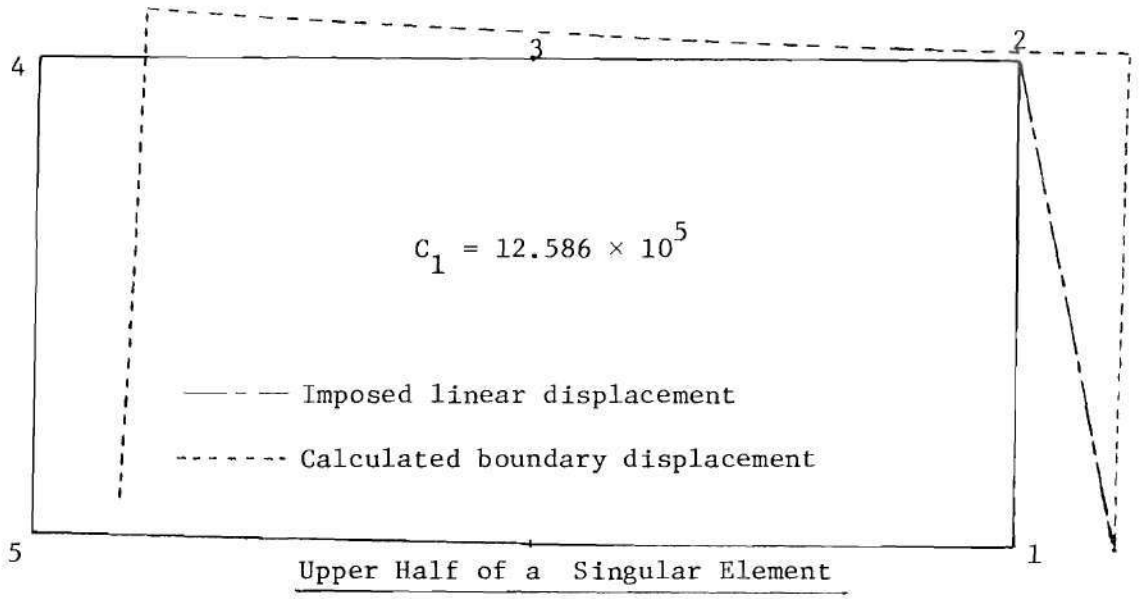

Figure 8. Comparison of the Specified Linear Displacement and the Boundary Displacement Calculated Based on 1 Term Approximation.

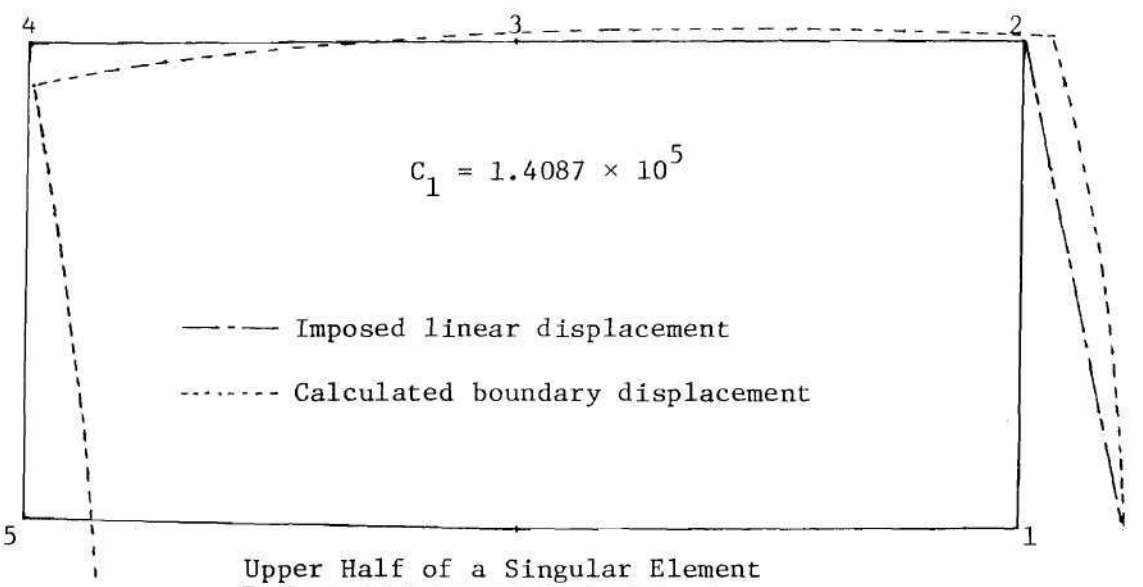

Figure 9. Comparison of the Specified Linear Displacement and the Boundary Displacement Calculated Based on 9 Term Approximation.

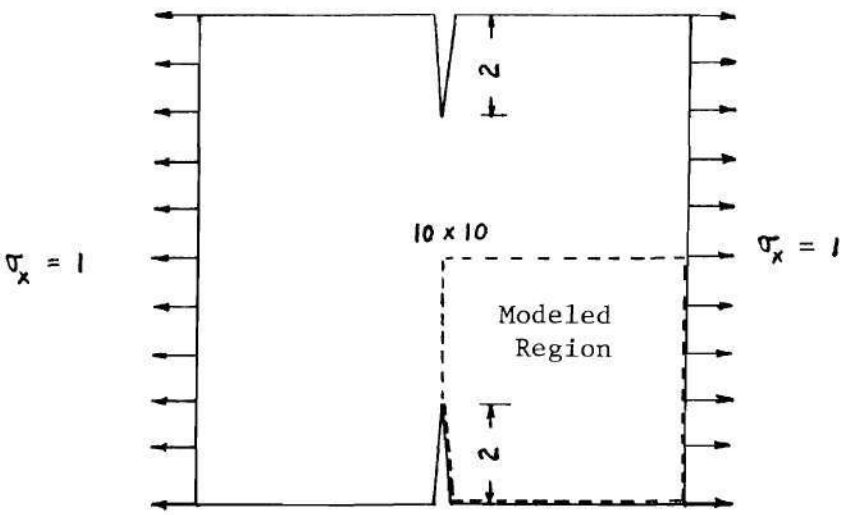

Figure 10. Double-Edge Notched Plate with $\theta = 0°$

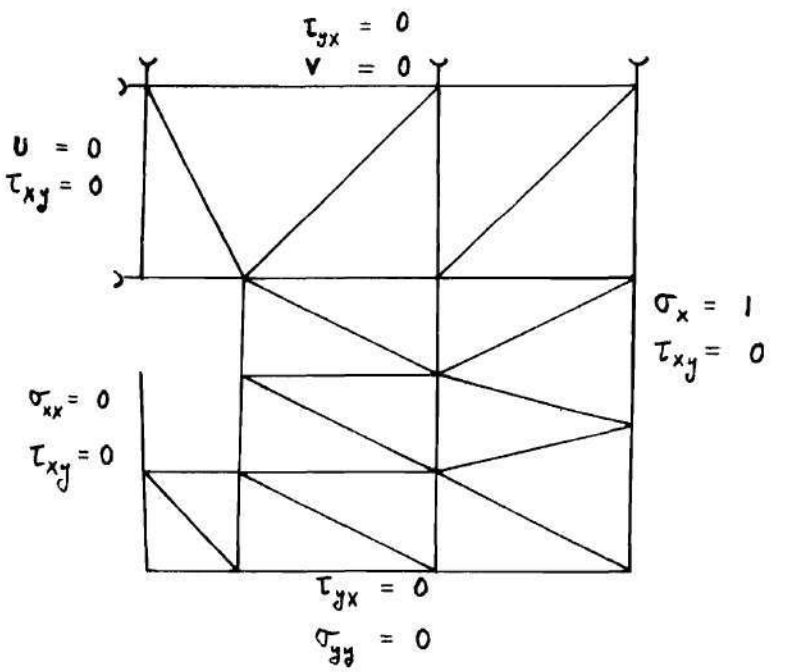

Figure 11. Finite Element Model of One Quarter of the Plate in Figure 10.

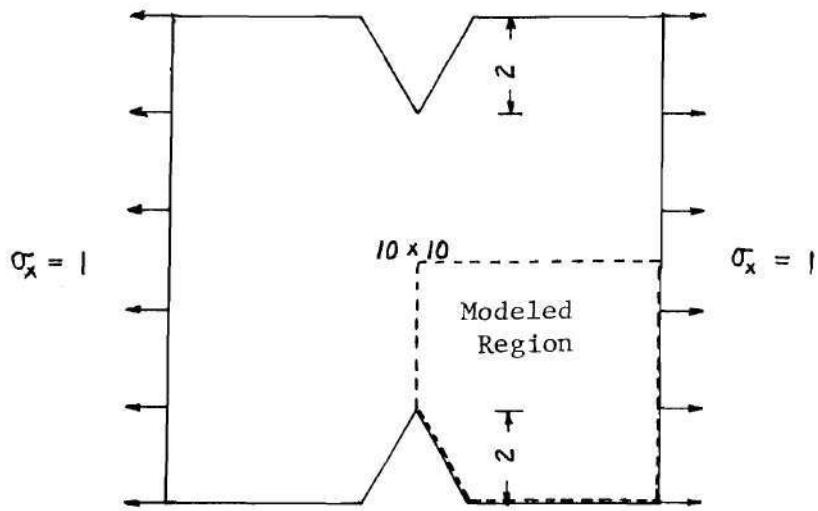

Figure 12. Double-Edge Notched Plate with $\theta = 60°$.

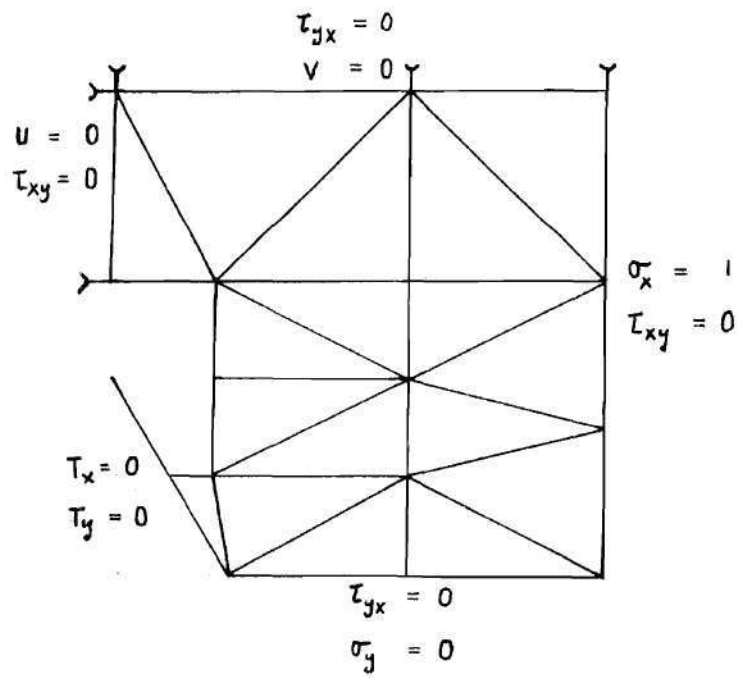

Figure 13. Finite Element Model of One Quarter of the Plate in Figure 12.

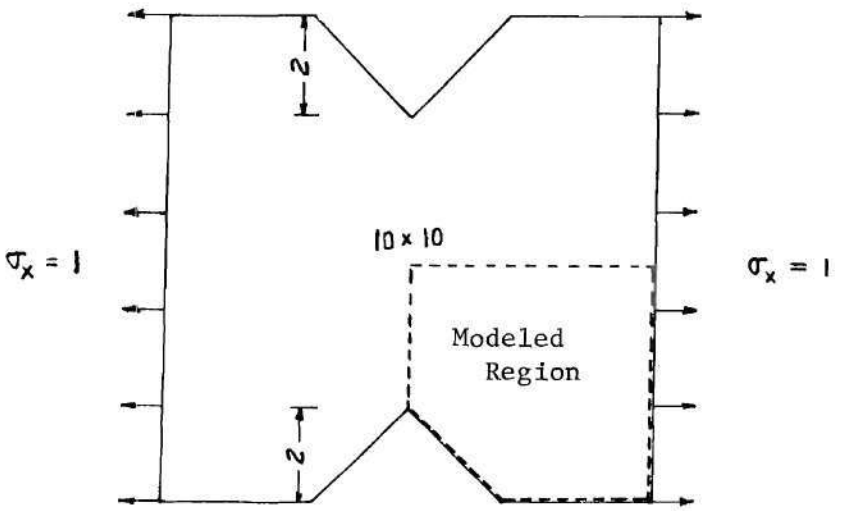

Figure 14. Double-Edge Notched Plate with $\theta = 90°$.

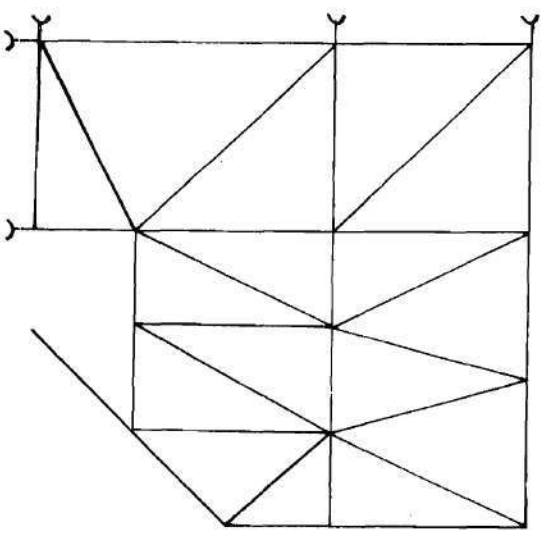

Figure 15. Finite Element Model of One Quarter of the Plate in Figure 14

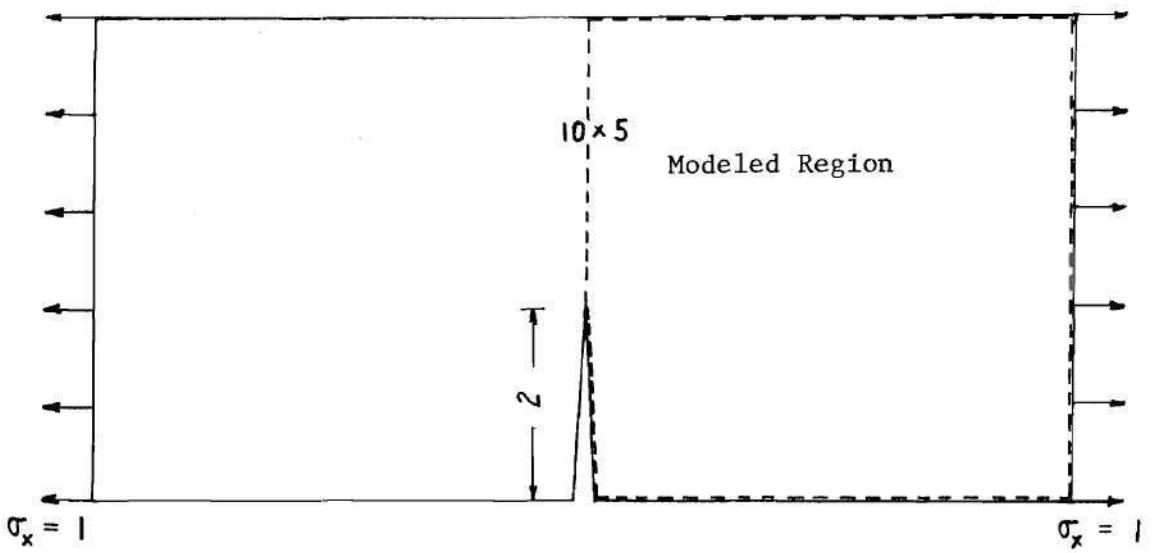

Figure 16. Single-Edge Notched Plate with $\theta = 0°$.

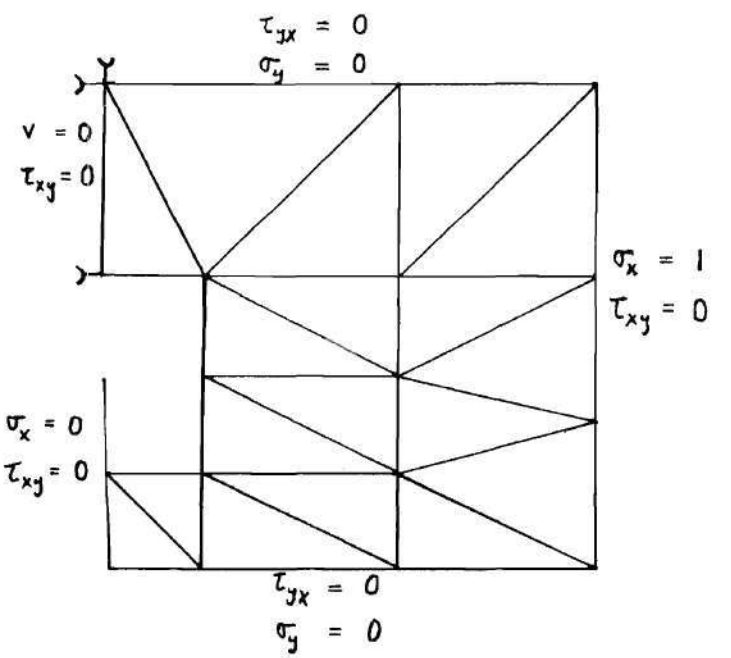

Figure 17. Finite Element Model of One Half of the Plate in Figure 16.

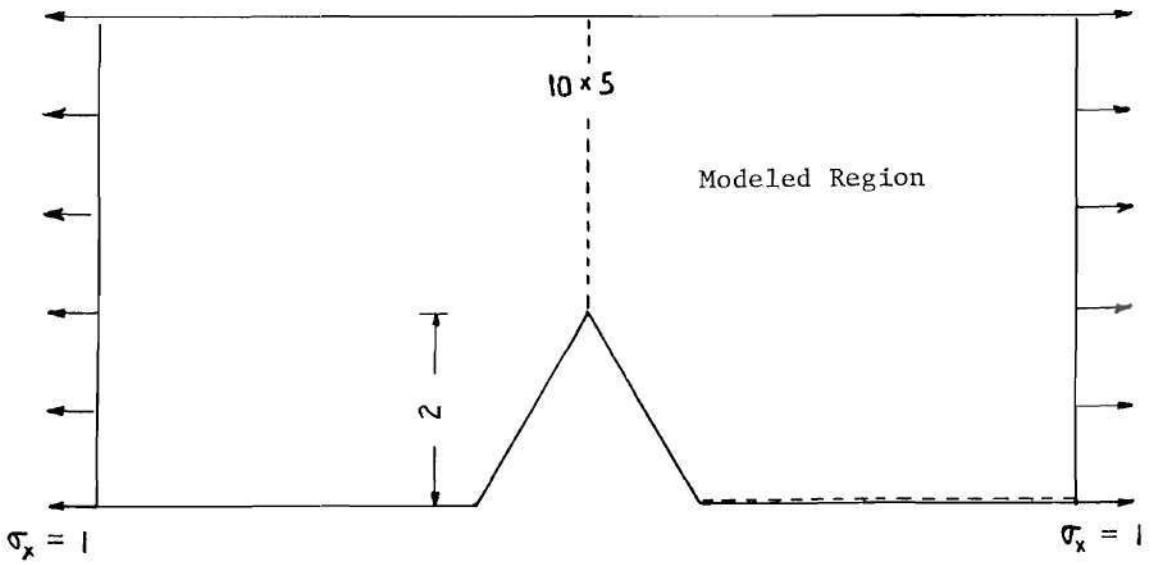

Figure 18. Single-Edge Notched Plate with $\theta = 60°$.

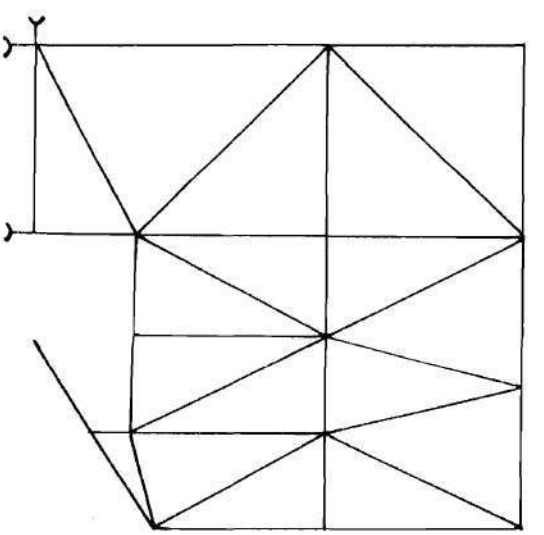

Figure 19. Finite Element Model of One Half of the Plate in Figure 18.

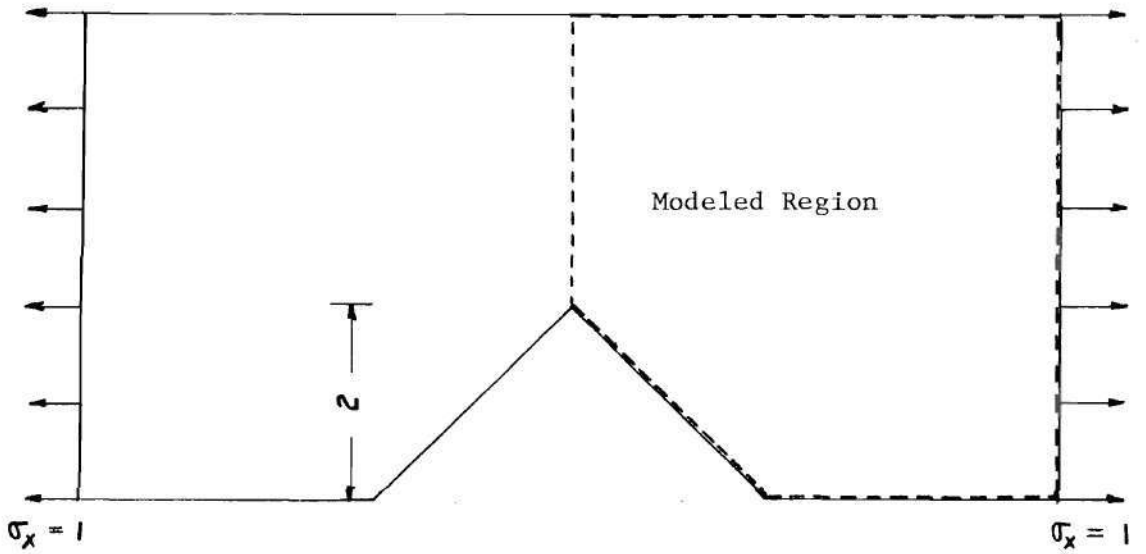

Figure 20. Single-Edge Notched Plate with $\theta = 90°$.

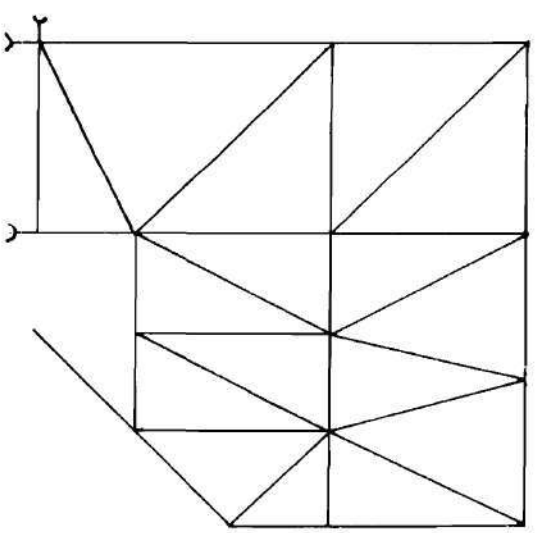

Figure 21. Finite Element Model of One Half of the Plate in Figure 20.

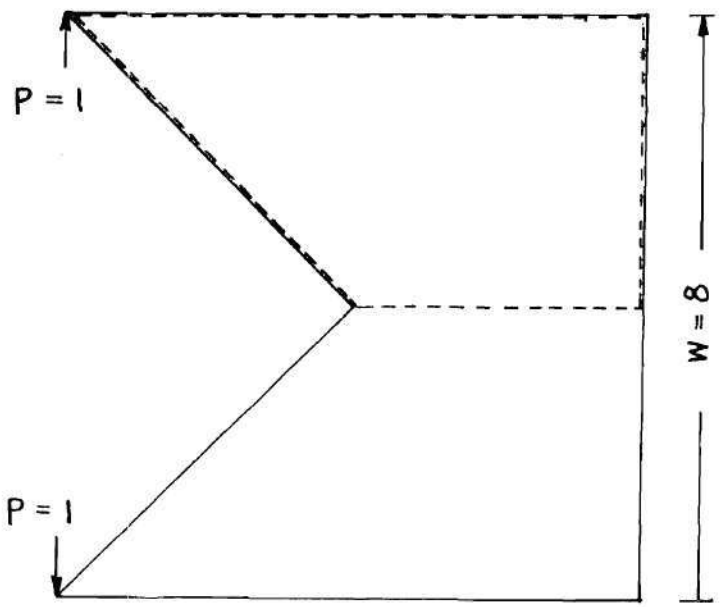

Figure 22. Square Plate with 90° Notch Cutout

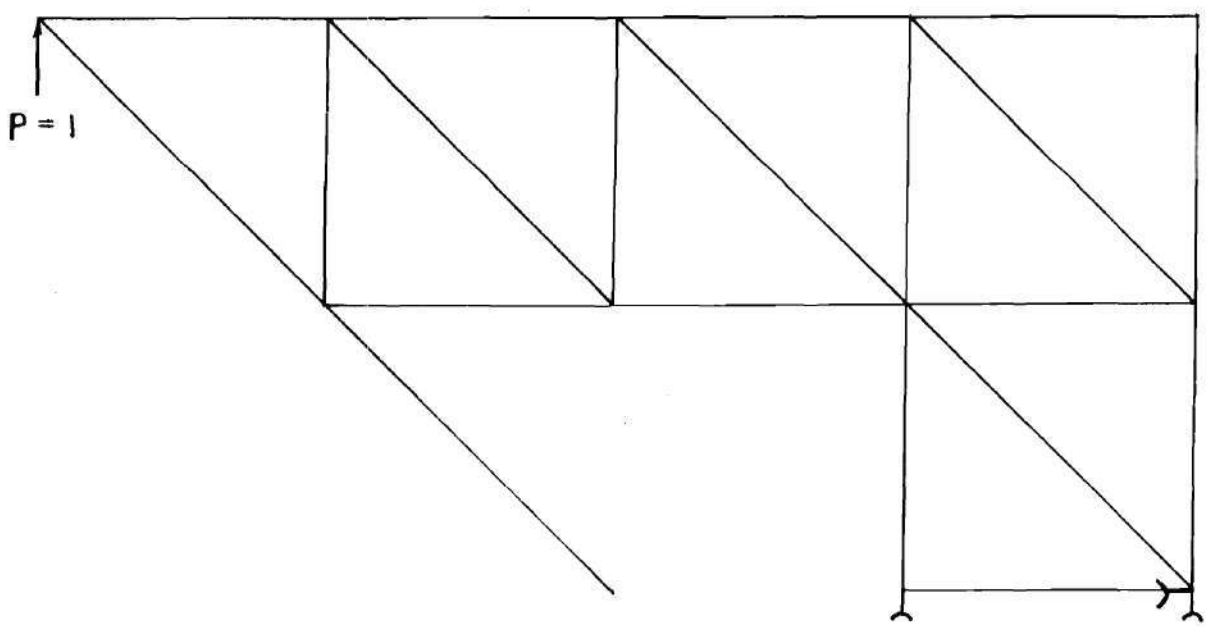

Figure 23. Finite Element Model I($\frac{2\ell}{w}$ = 0.5) of Upper Half Square Plate with 90° Notch Cutout.

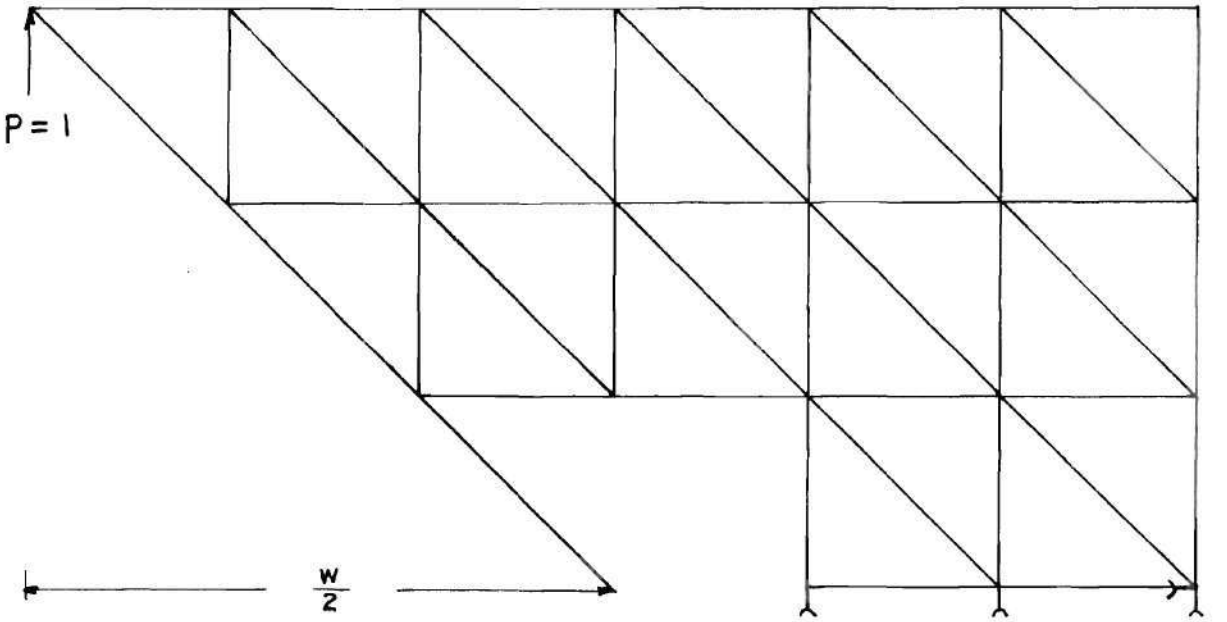

Figure 24. Finite Element Model II ($\frac{2\ell}{w} = \frac{1}{3}$) of Upper Half Square Plate with 90° Notch Cutout.

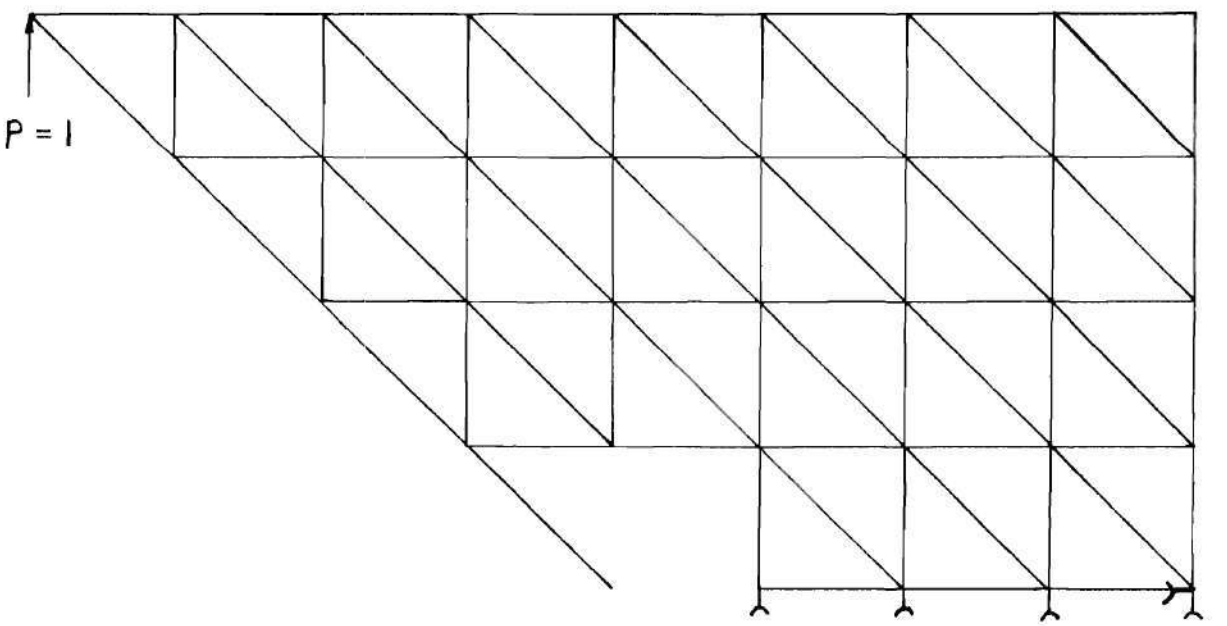

Figure 25. Finite Element Model III ($\frac{2\ell}{w} = 0.25$) of Upper Half Square Plate with 90° Notch Cutout.

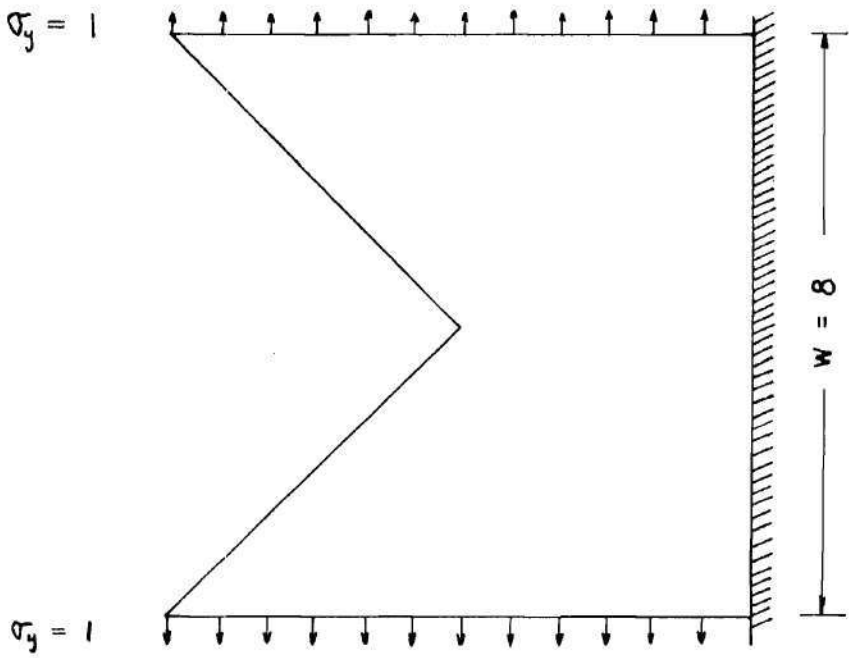

Figure 26. Square Plate with 90° Notch Cutout.

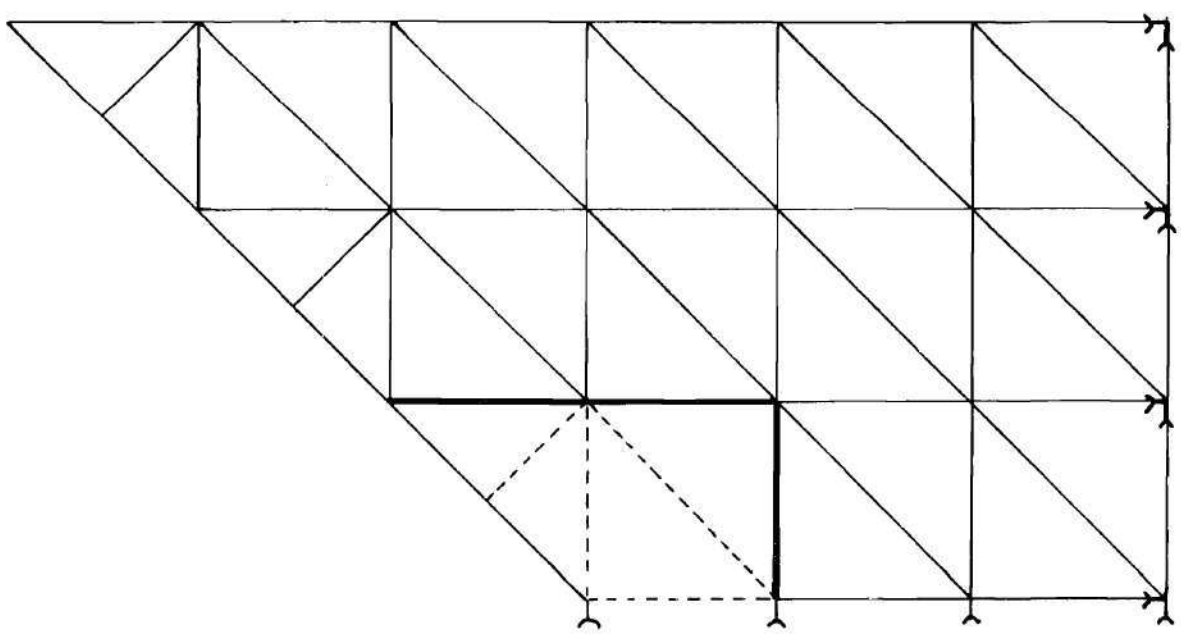

Figure 27. Finite Element Model I ($\ell/w/2 = 1/3$) of Upper Half Square Plate with 90° Notch Cutout.

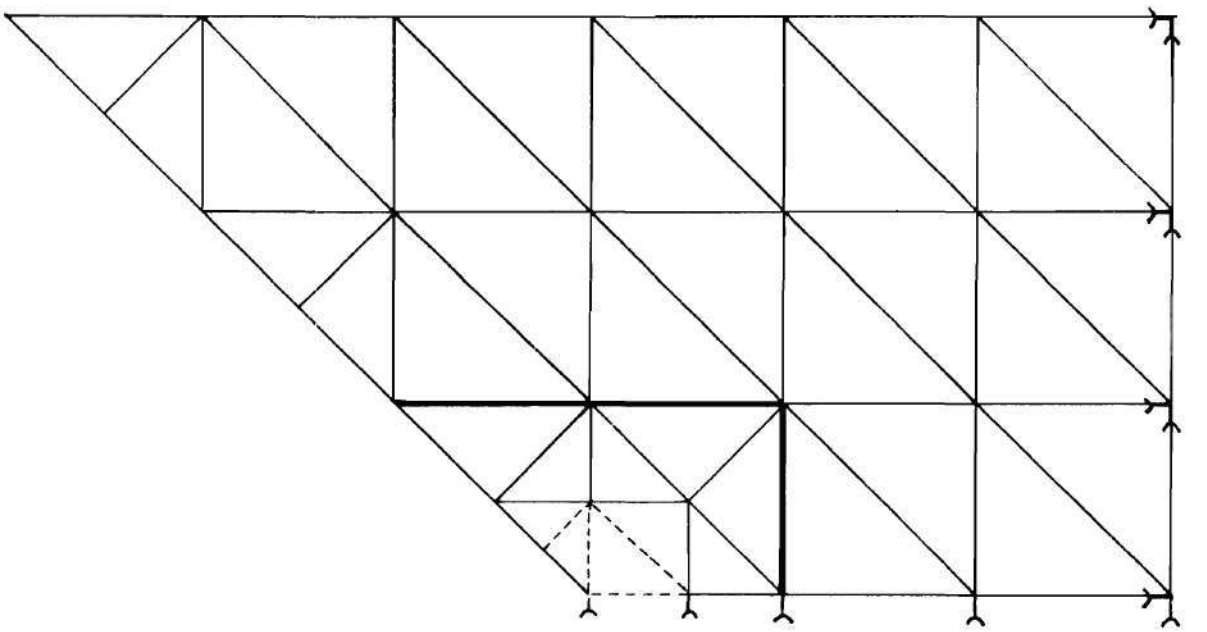

Figure 28. Finite Element Model II ($\ell/w/2 = 1/6$) of Upper Half Square Plate with 90° Notch Cutout.

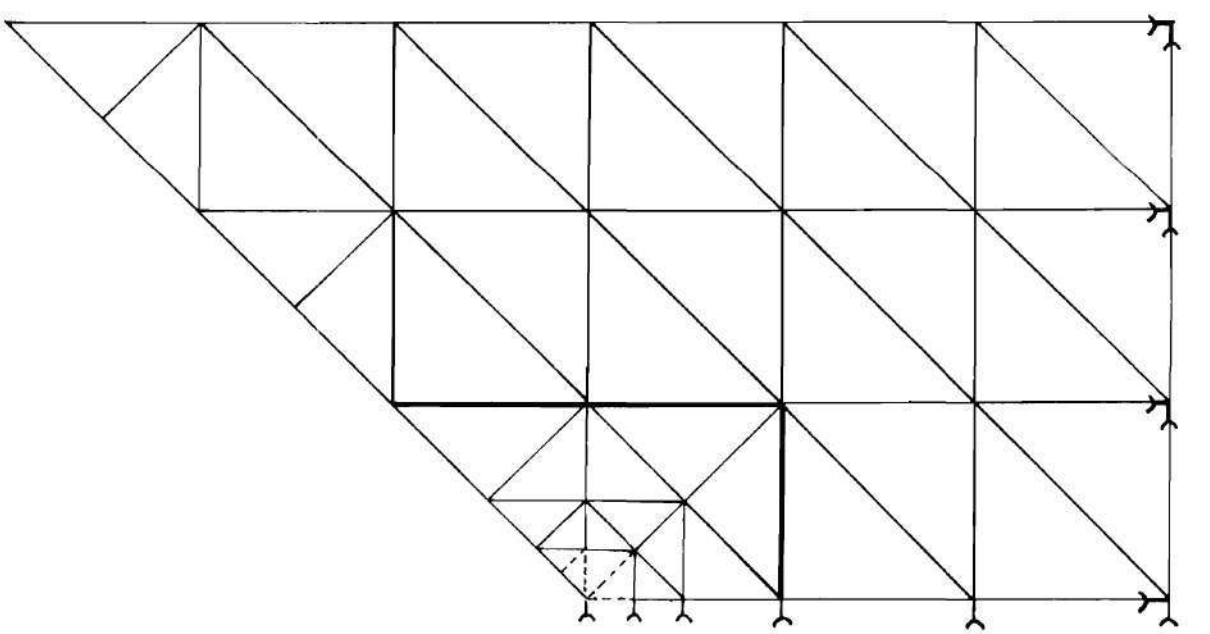

Figure 29. Finite Element Model III ($\ell/w/2 = 1/12$) of Upper Half Square Plate with 90° Notch Cutout.

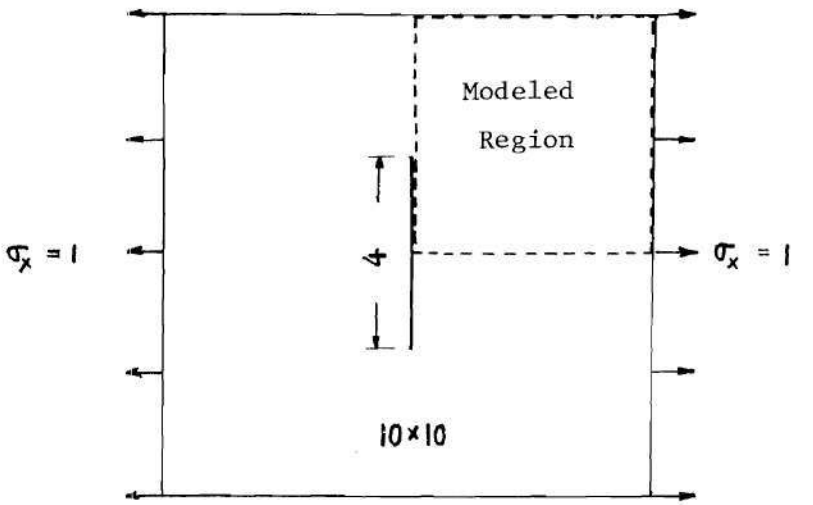

Figure 30. Centrally Cracked Plate with Cracked Line Perpendicular to the Direction of Applied Load.

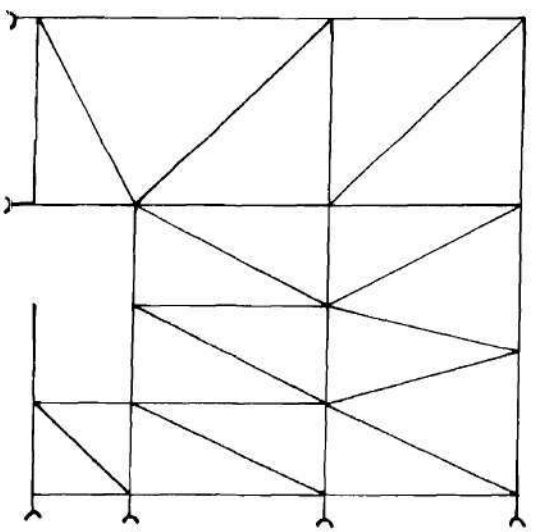

Figure 31. Finite Element Coarse Model of One Quarter of the Plate in Figure 30.

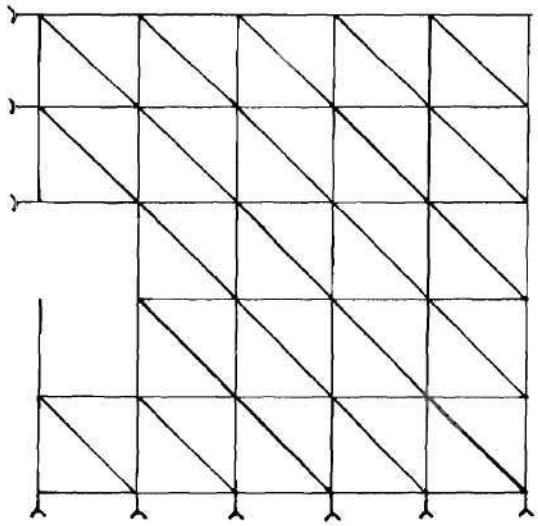

Figure 32. Finite Element Fine Model of One Quarter of the Plate in Figure 30.

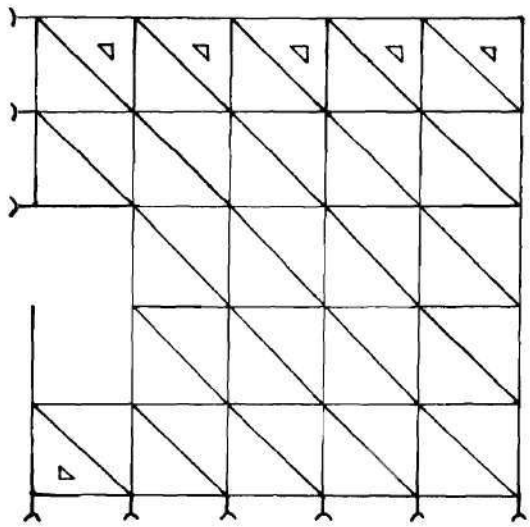

Figure 33. Finite Element Fine Model (with Special Triangular Elements) of One Quarter of the Plate in Figure 30.

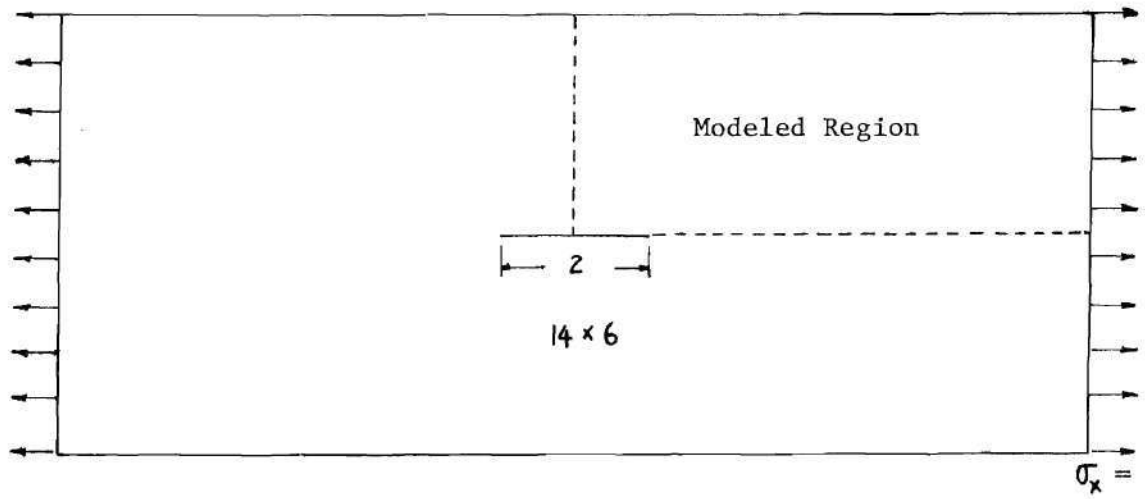

Figure 34. Centrally Cracked Plate with the Crack Line Parallel to the Direction of Applied Load.

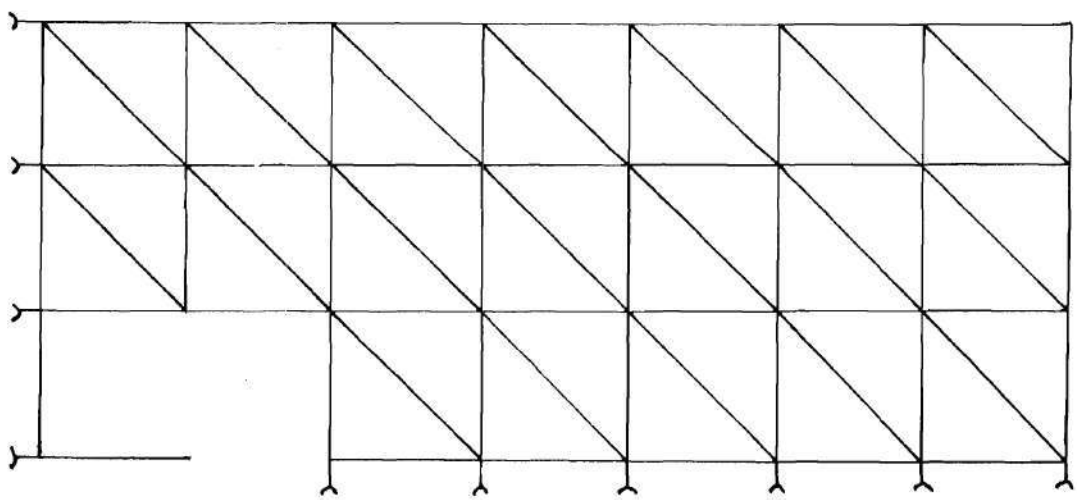

Figure 35. Finite Element Model of One Quarter of the Plate in Figure 34.

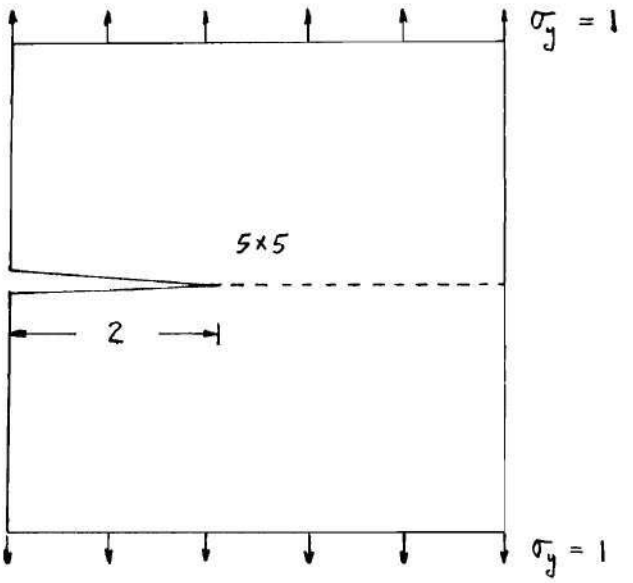

Figure 36. Square Plate with Single-Edge Crack.

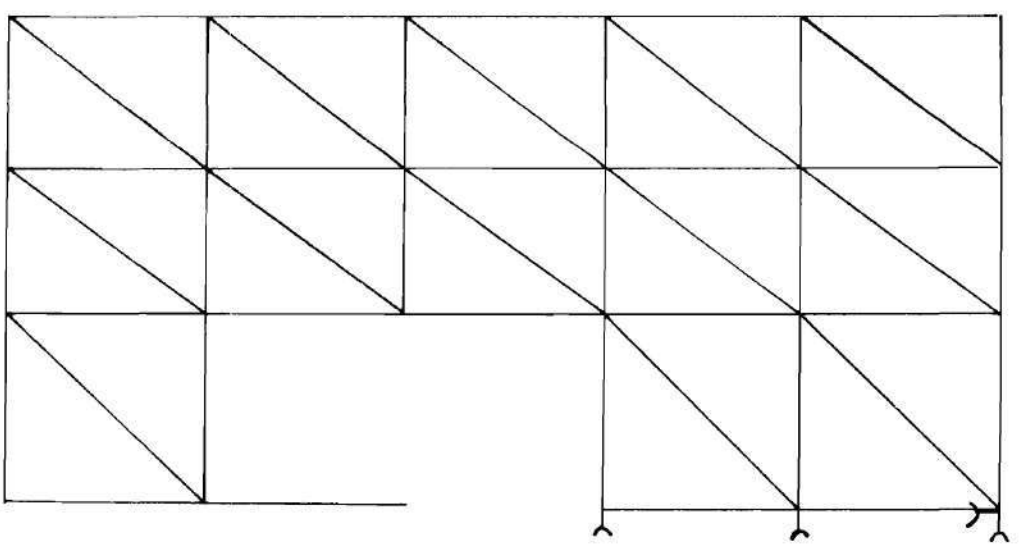

Figure 37. Finite Element Model of One Half of the Plate in Figure 36.

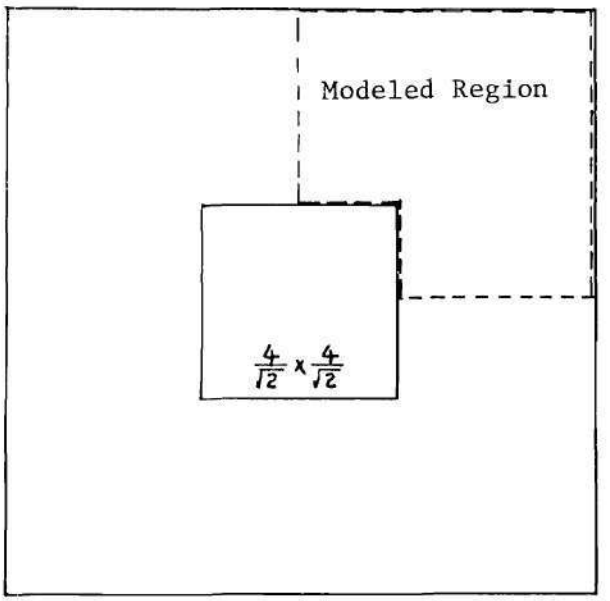

Figure 38. Plate with a Central Square Cutout.

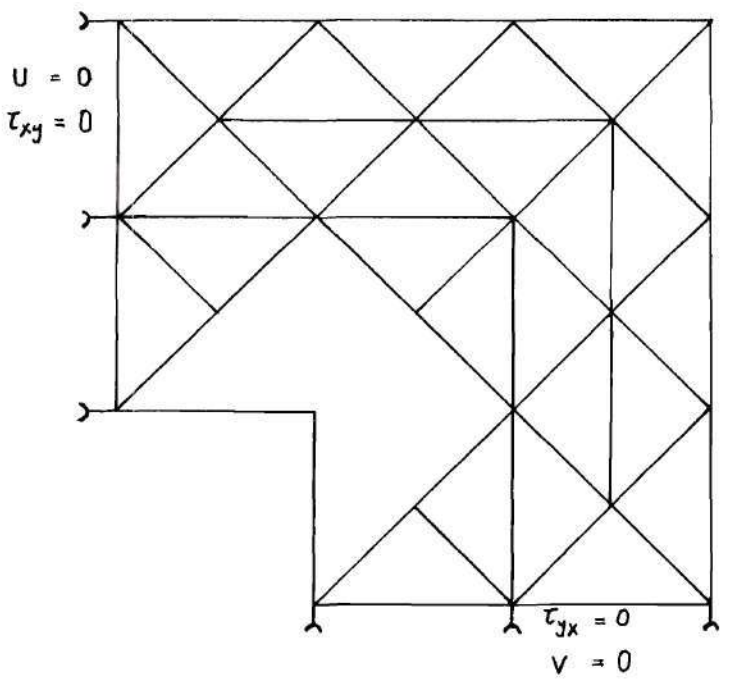

Figure 39. Finite Element Model of One Quarter of the Plate in Figure 38.

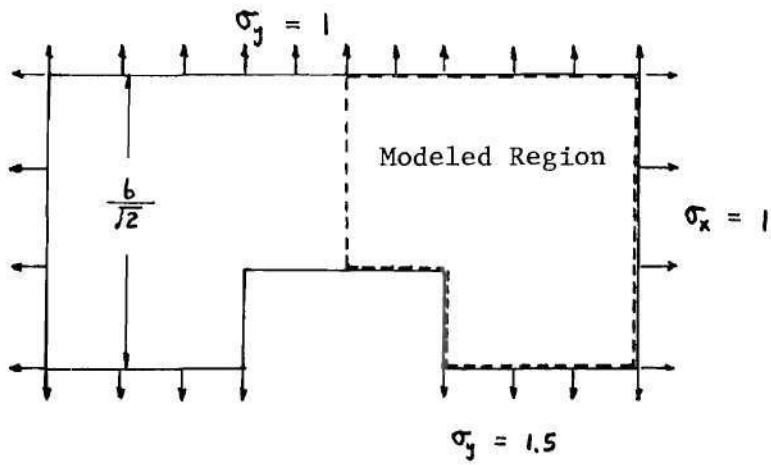

Figure 40. Plate with a Single-Edge Rectangular Cutout.

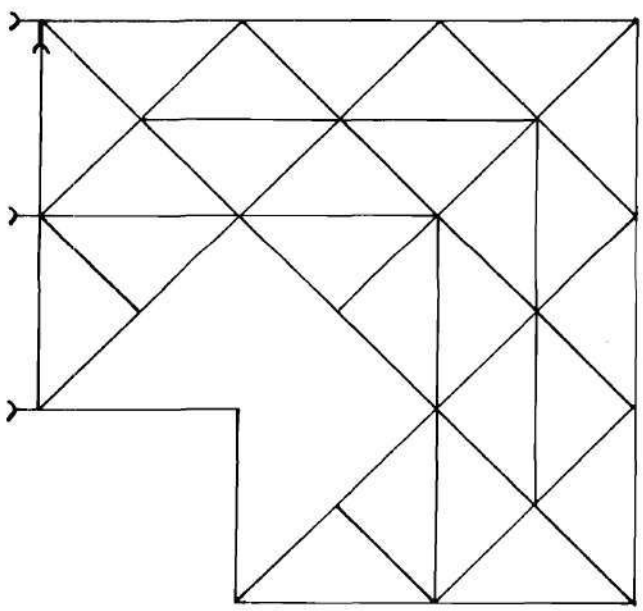

Figure 41. Finite Element Model of One Quarter of the Plate in Figure 40.

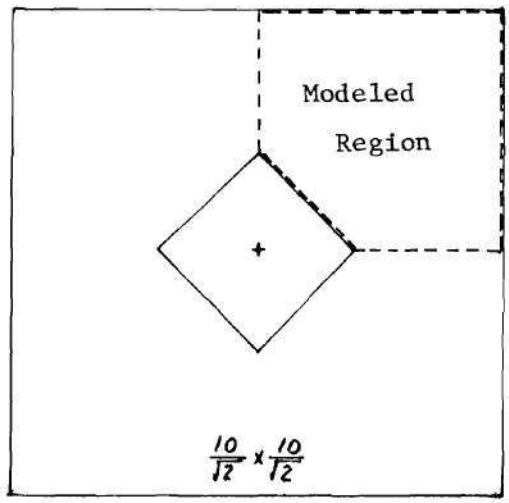

Figure 42. Plate with a Central Diamond-Shape Cutout.

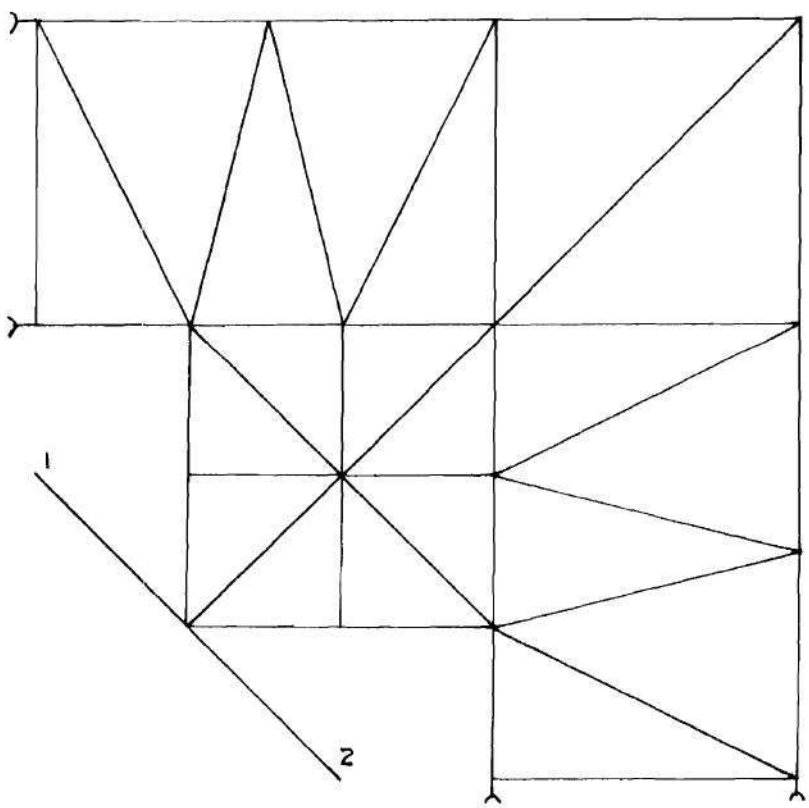

Figure 43. Finite Element Model of One Quarter of the Plate in Figure 42.

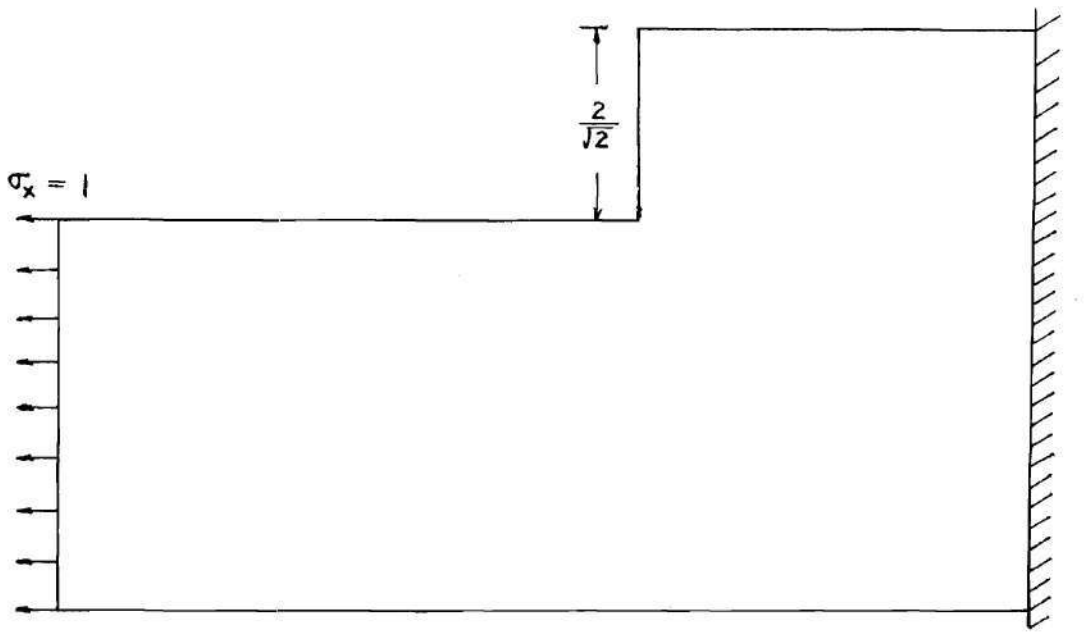

Figure 44. A Singly Stepped Plate.

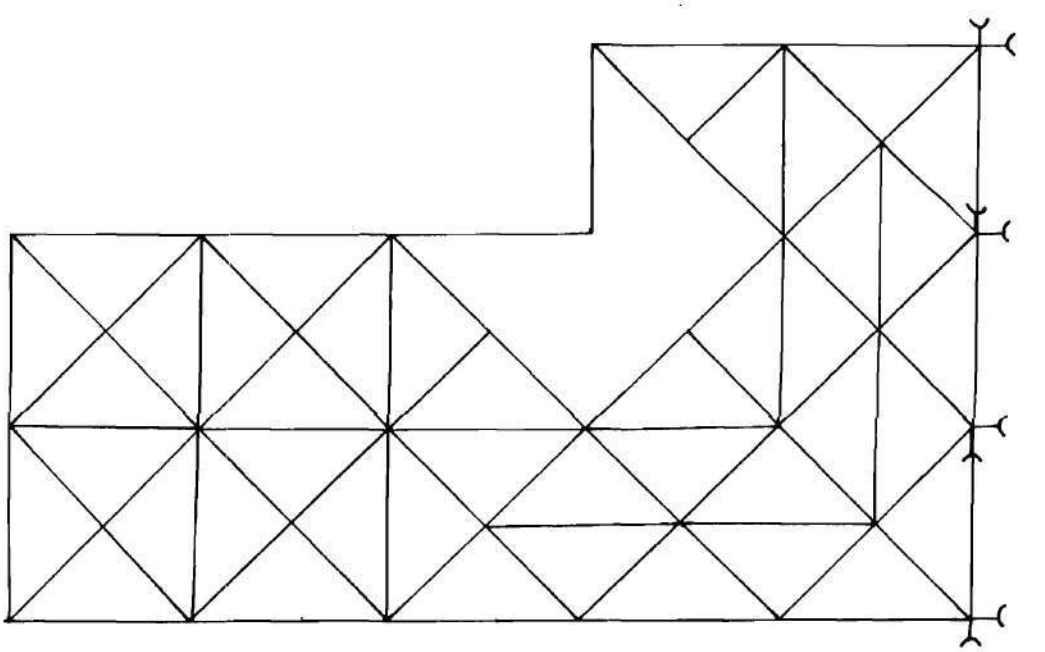

Figure 45. Finite Element Model of the Singly Stepped Plate.

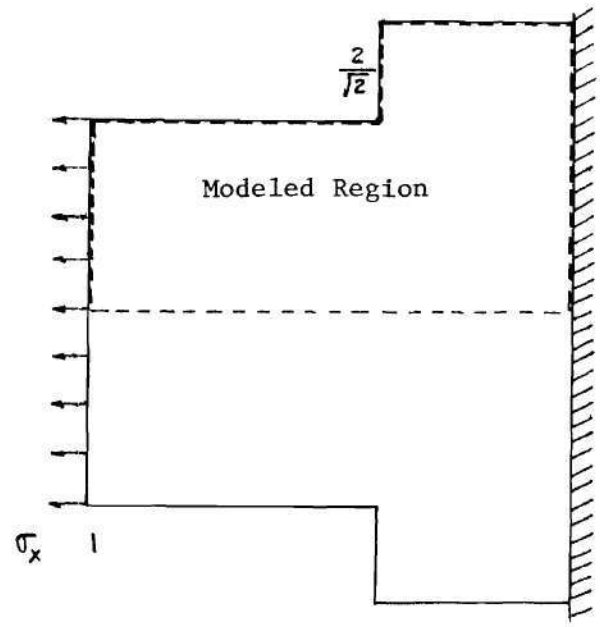

Figure 46. A Footing Plate.

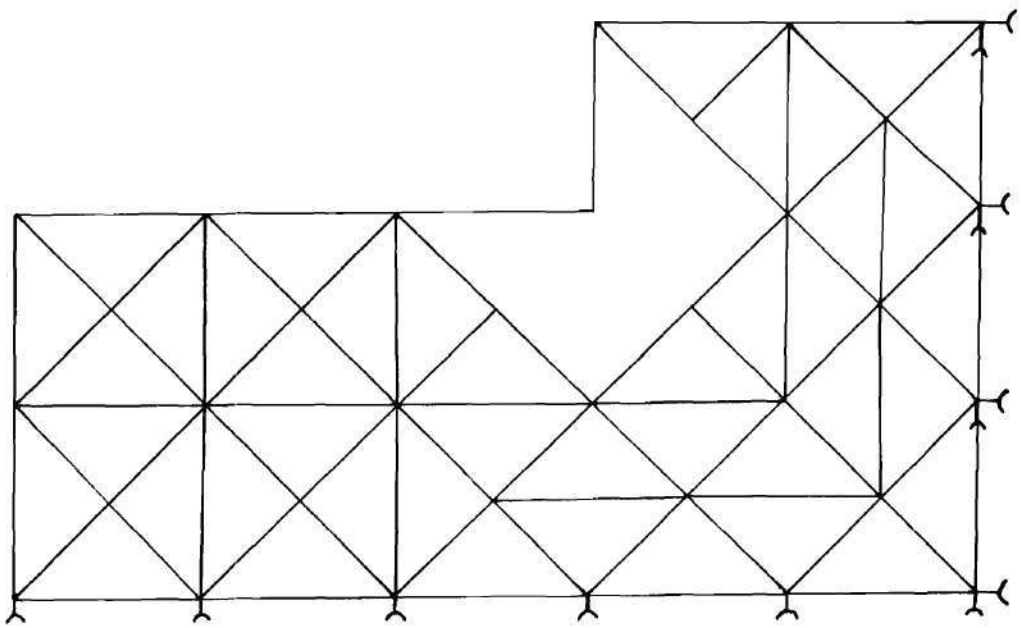

Figure 47. A Finite Element Model of One Half of the Footing Plate.

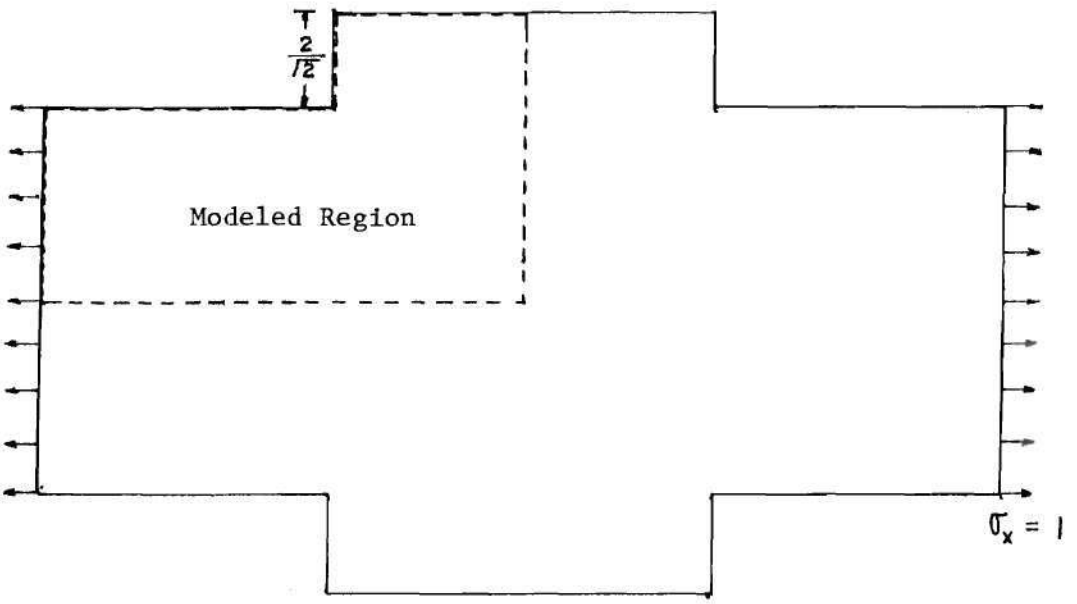

Figure 48. A Doubly Stepped Plate.

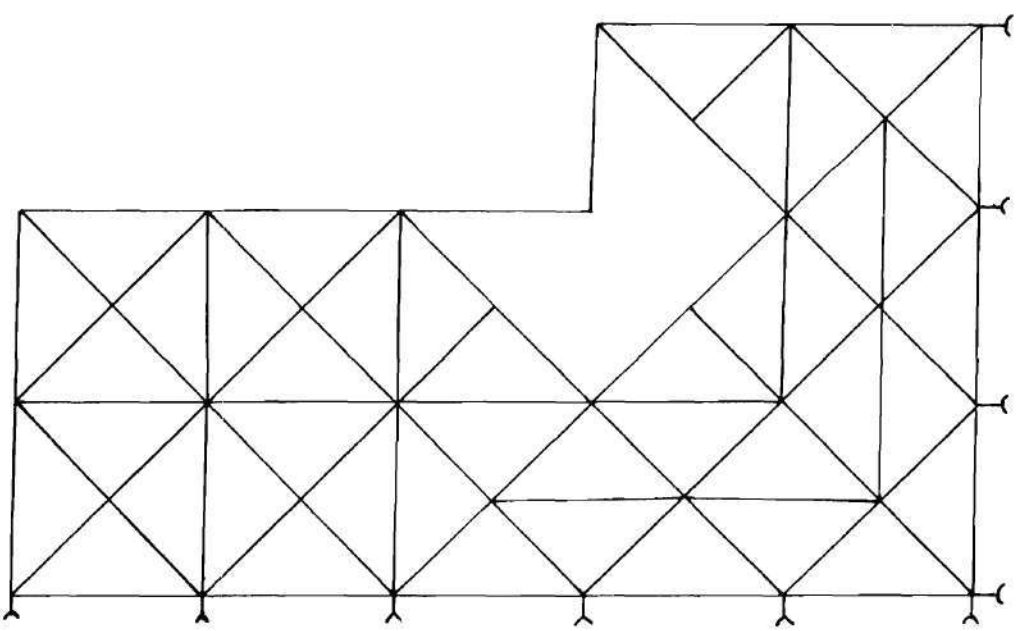

Figure 49. A Finite Element Model of One Quarter of the Doubly Stepped Plate.

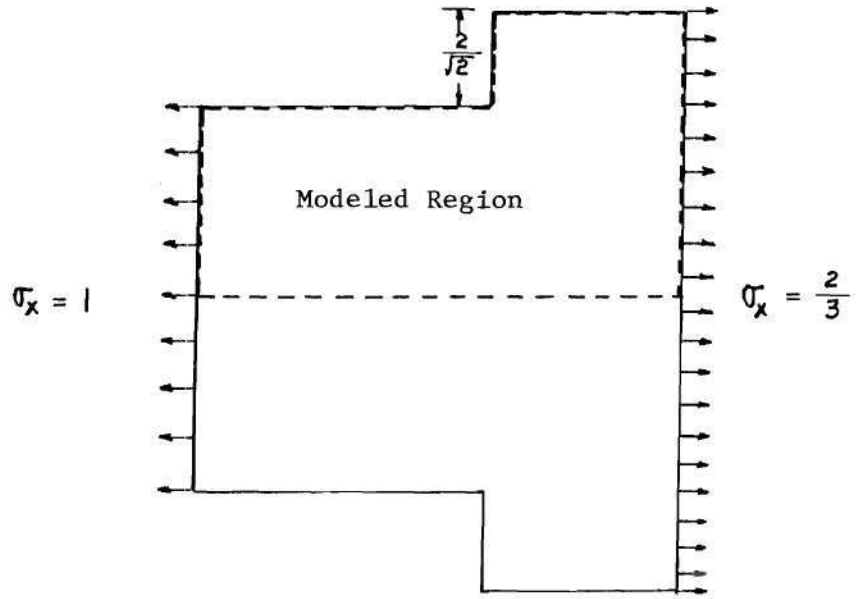

Figure 50. A Footing Plate with Free Ends.

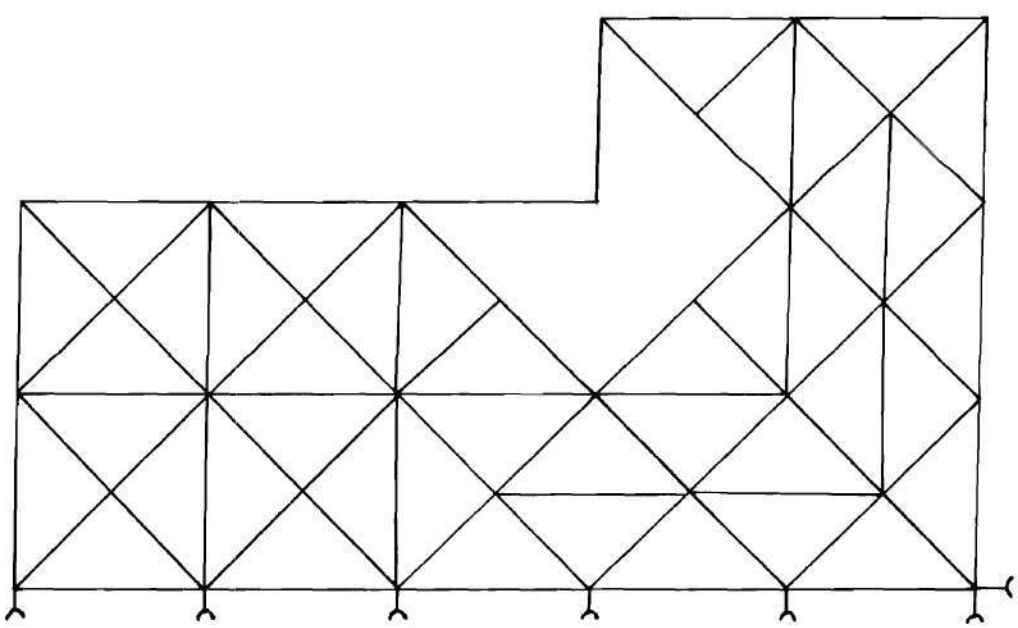

Figure 51. A Finite Element Model of One Half of the Footing Plate with Free Ends.

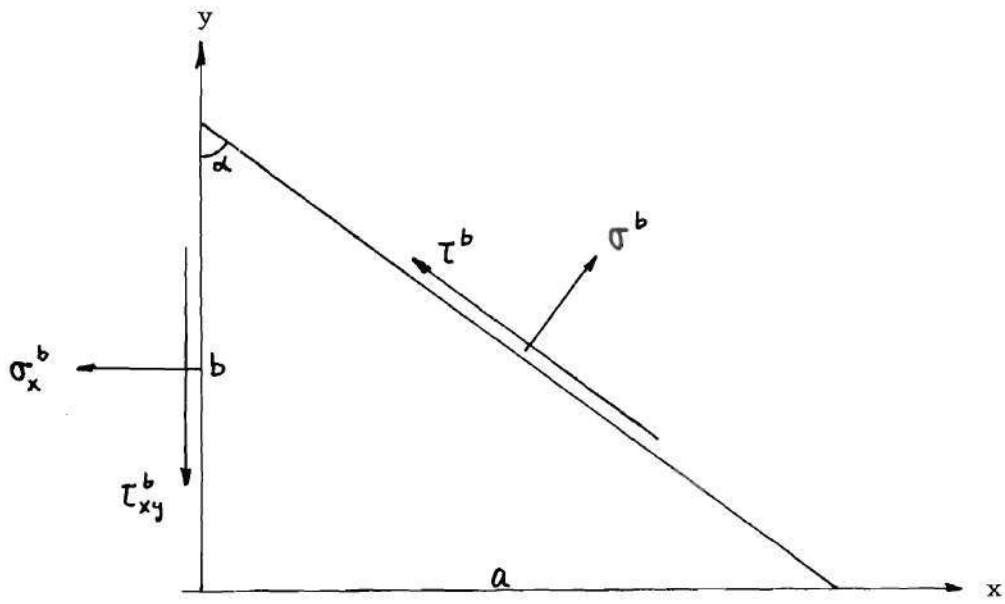

Figure 52. A Special Triangular Element with One Edge Free from Stresses.

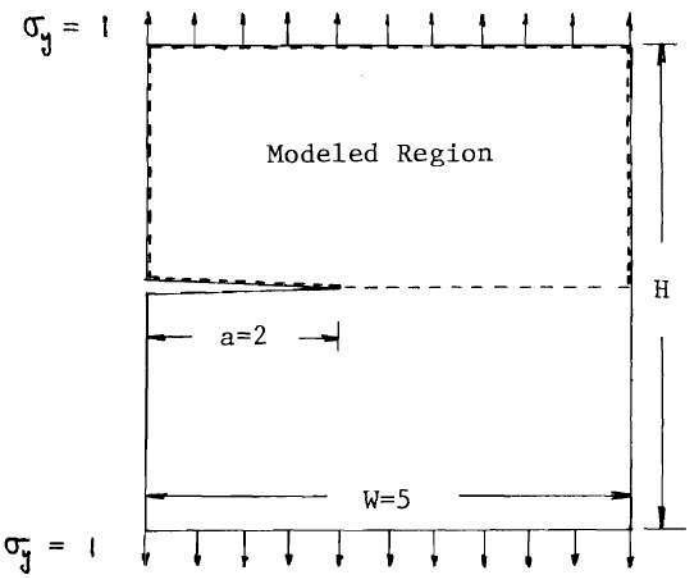

Figure 53. Single-Edge Cracked Plate with $\frac{a}{W} = 0.4$.

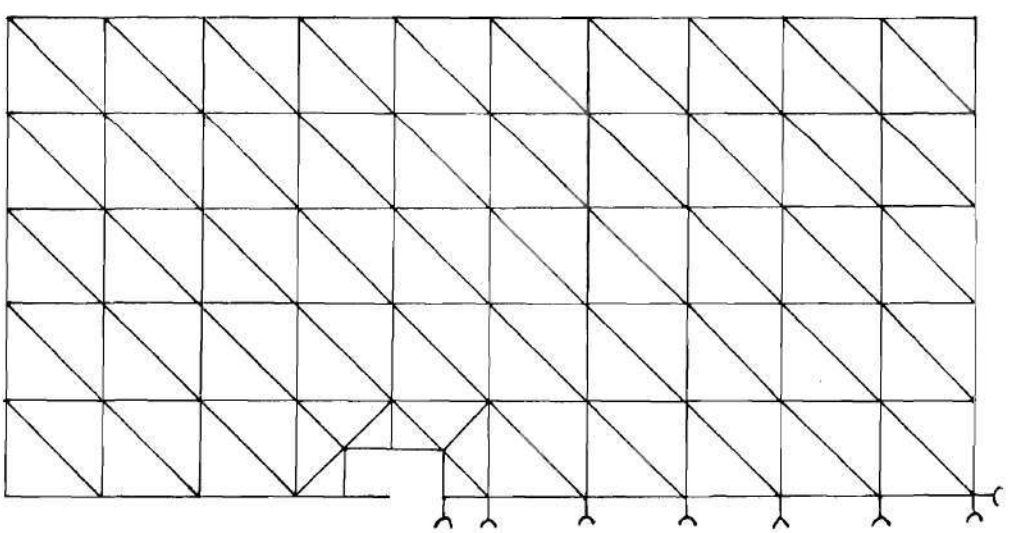

Figure 54. Finite Element Model of One Half of the Plate with $\frac{H}{W} = 1$ in Figure 53.

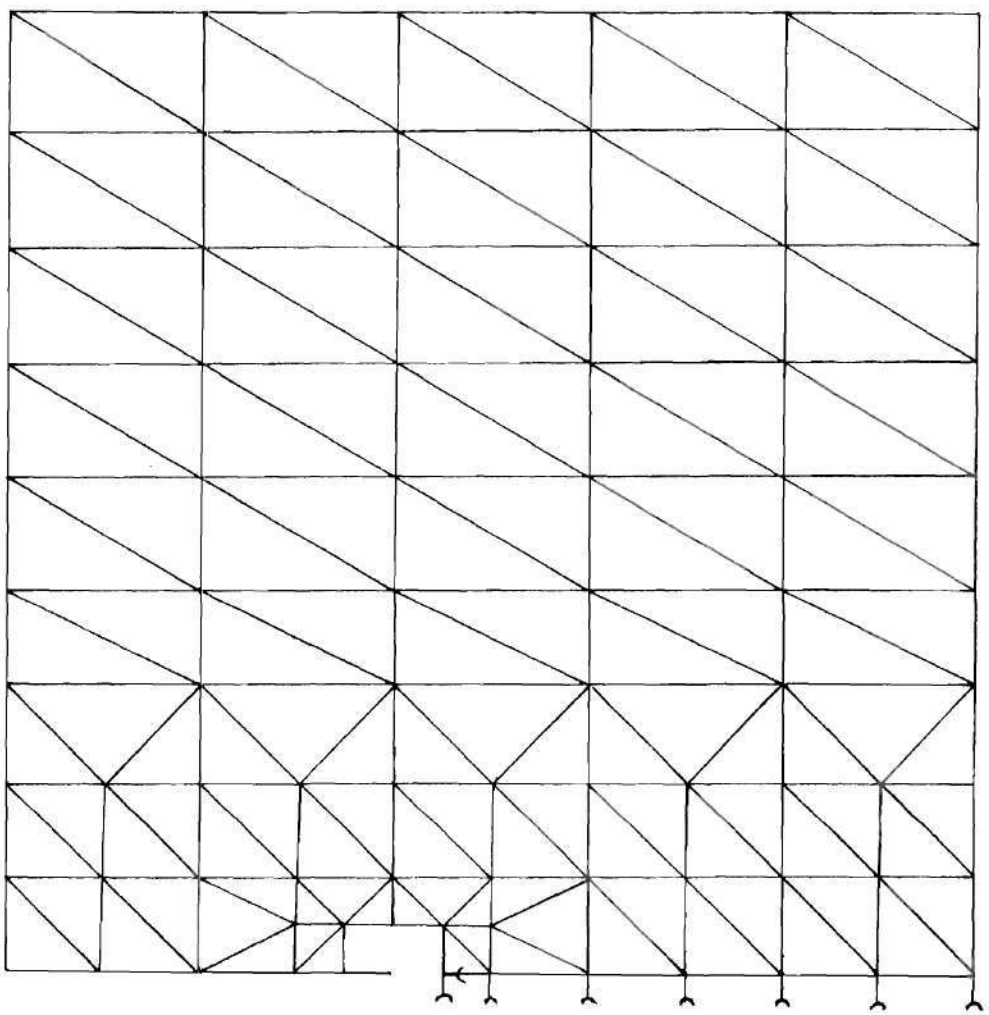

Figure 55. Finite Element Model of One Half of the Plate with $\frac{H}{W} = 2$ in Figure 53.

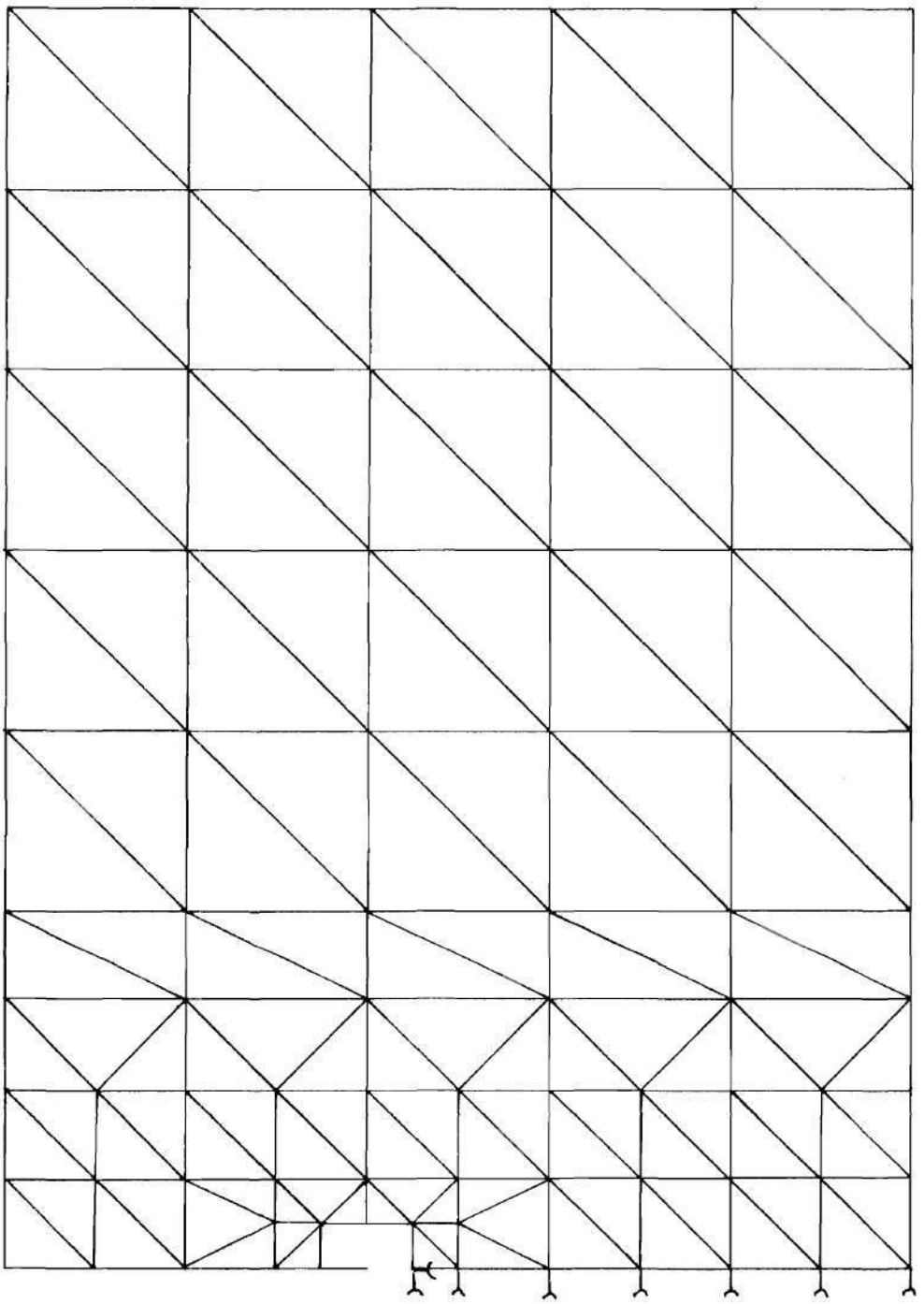

Figure 56. Finite Element Model of One Half of the Plate with $\frac{H}{W} = 3$ in Figure 53.

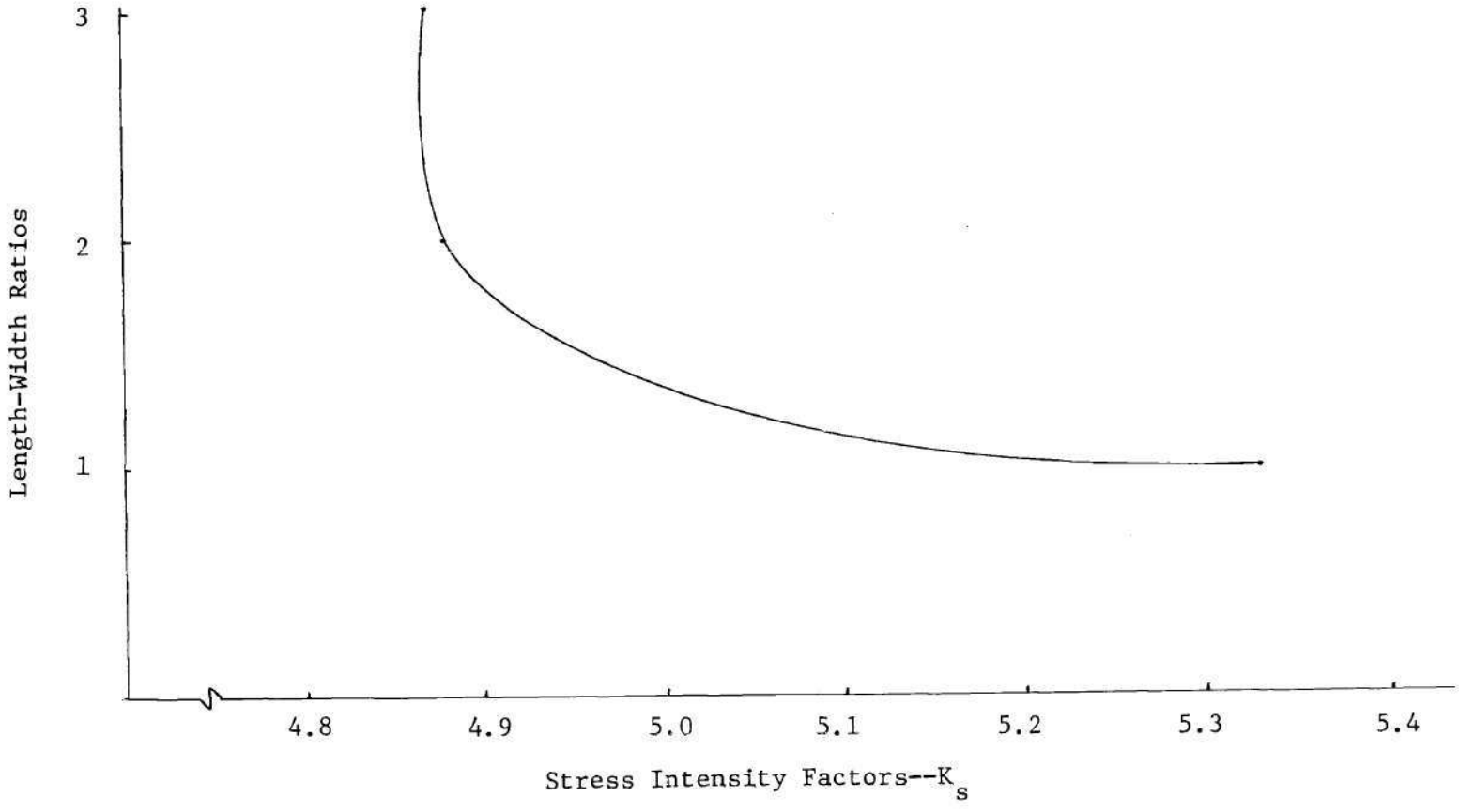

Figure 57 Effect of Length on the Stress Intensity Factors for Single-Edge Notch Plates.

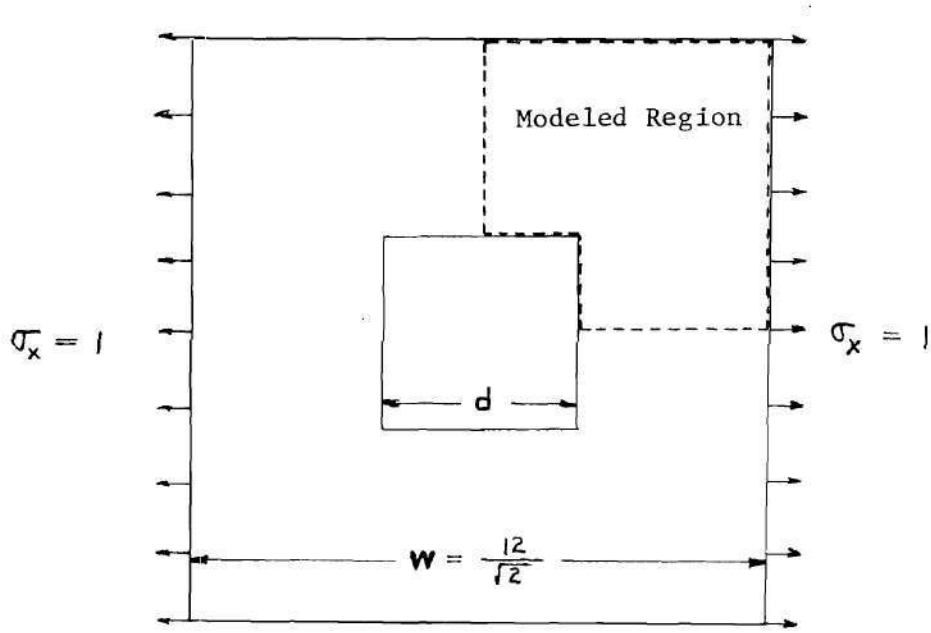

Figure 58. Square Plate with a Central Square Cutout.

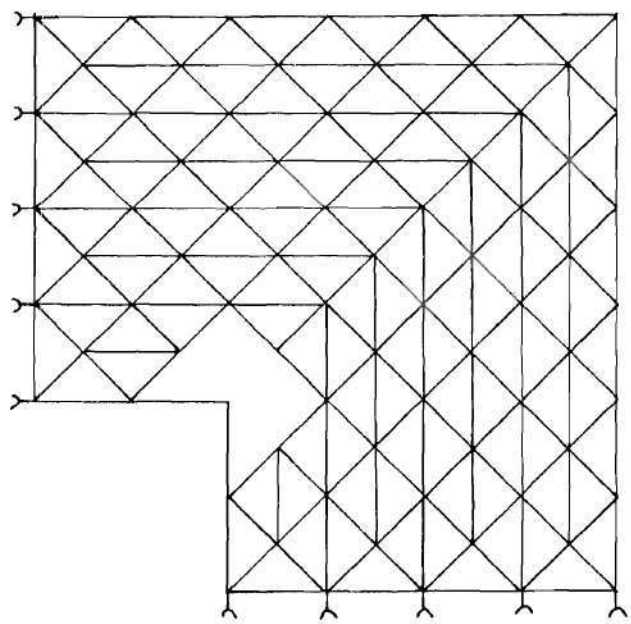

Figure 59. Finite Element Model of One Quarter of the Plate with $\frac{d}{W} = \frac{1}{3}$ in Figure 58.

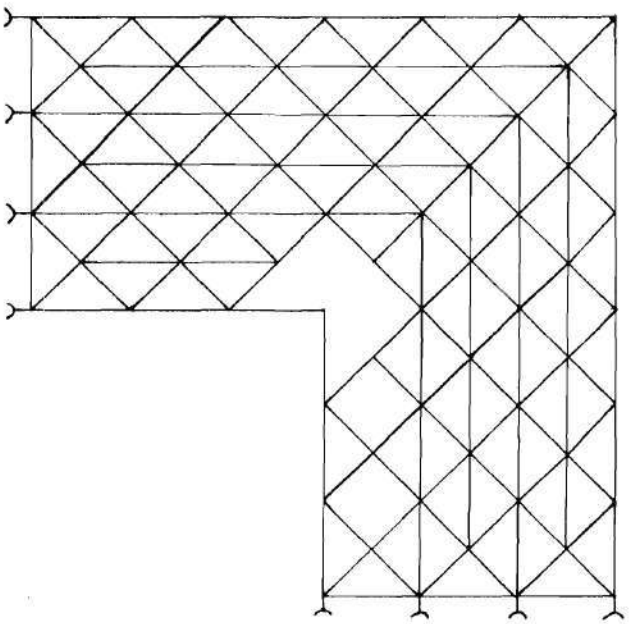

Figure 60. Finite Element Model of One Quarter of the Plate with $\frac{d}{W} = \frac{1}{2}$ in Figure 58.

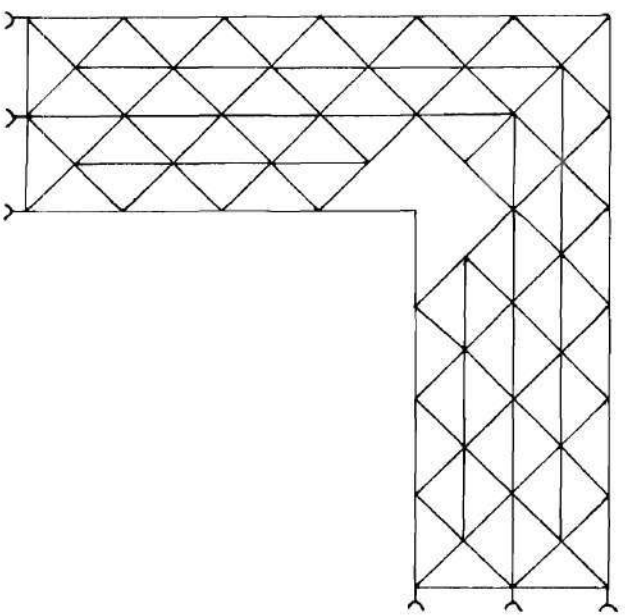

Figure 61. Finite Element Model of One Quarter of the Plate with $\frac{d}{W} = \frac{2}{3}$ in Figure 58.

APPENDIX B

DERIVATION OF A STIFFNESS MATRIX FOR A SPECIAL TRIANGULAR ELEMENT WITH ONE EDGE FREE FROM STRESSES

It is known that the stiffness matrix of a conventional triangular element is derived based on the assumption that the displacement functions are two linear polynomials which imply that stresses and strains are constant throughout the element. Thus the traction-free boundary conditions along the edges of the sharp corner will generally not be satisfied if the conventional triangular elements should be placed along the free edges. It is the purpose of this section to develop a special triangular element (see Figure 52) to replace a conventional triangular element along the free edge of a cracked plate as given in Figure 33.

In order to maintain adjacent element continuity, this special element will have linear displacements imposed on two edges. The third edge will be traction free. This elasticity problem will be solved approximately by again using the principle of stationary complementary energy. The stresses in the interior are assumed as follows:

$$\begin{Bmatrix} \sigma_x \\ \sigma_y \\ \tau_{xy} \end{Bmatrix} = \begin{bmatrix} 1 & x & y & 2xy & x^2 & y^2 \\ 0 & 0 & 0 & 0 & y^2 & 0 \\ 0 & -y & 0 & -y^2 & -2xy & 0 \end{bmatrix} \begin{Bmatrix} \beta_1 \\ \beta_2 \\ \beta_3 \\ \beta_4 \\ \beta_5 \\ \beta_6 \end{Bmatrix}$$

Note that the number of stress coefficients is selected equal to the total displacement degrees of freedom of the special triangular element. See Chapter III, "Comments on the Determination of Stress Coefficients" for a discussion of this approximation.

Again the set of assumed stresses satisfies the following conditions:

(1) Equilibrium equations;

$$\frac{\partial \sigma_x}{\partial x} + \frac{\partial \tau_{xy}}{\partial y} = 0$$

$$\frac{\partial \sigma_y}{\partial y} + \frac{\partial \tau_{xy}}{\partial x} = 0$$

(2) Traction boundary conditions;

$$\left.\begin{aligned} \sigma_y &= 0 \\ \tau_{xy} &= 0 \end{aligned}\right\} \quad @ \quad y = 0$$

The horizontal and vertical tractions along the edge between nodes 1 and 2 can be found through the equilibrium conditions on the surface, i.e.,

$$S_x = \sigma_x \cos\alpha + \tau_{xy} \sin\alpha$$

$$S_y = \sigma_y \sin\alpha + \tau_{xy} \cos\alpha$$

where the thickness of element is assumed to be unit.

Obtain the boundary stresses in term of the stress coefficients.

Therefore

$$S_x = (\cos\alpha)\beta_1 + (x\cos\alpha - y\sin\alpha)\beta_2 + (y\cos\alpha)\beta_3 +$$

$$(2xy\cos\alpha - y^2\sin\alpha)\beta_4 + (x^2\cos\alpha - 2xy\sin\alpha)\beta_5 + (y^2\cos\alpha)\beta_6$$

$$S_y = -(y\cos\alpha)\beta_2 - (y^2\cos\alpha)\beta_4 + (y^2\sin\alpha - 2xy\cos\alpha)\beta_5$$

The displacements along the edge between nodes 1 and 2 are assumed in linear form as follows:

$$\begin{Bmatrix} u_x \\ u_y \end{Bmatrix} = \begin{bmatrix} -\frac{y-b}{b} & 0 & +\frac{y}{b} & 0 \\ 0 & -\frac{y-b}{b} & 0 & +\frac{y}{b} \end{bmatrix} \begin{Bmatrix} q_1 \\ q_2 \\ q_3 \\ q_4 \end{Bmatrix} = [D]\{q\}$$

Evaluate [T] matrix along the edge between nodes 1 and 2 according to equation (3.12);

$$[T] = \int_{S_u} [B]^T[D]ds = \int_{y=0}^{y=b} \begin{bmatrix} \cos\alpha & 0 \\ x\cos\alpha - y\sin\alpha & -y\cos\alpha \\ y\cos\alpha & 0 \\ 2xy\cos\alpha - y^2\sin\alpha & -y^2\cos\alpha \\ x^2\cos\alpha - 2xy\sin\alpha & y^2\sin\alpha - 2xy\cos\alpha \\ y^2\cos\alpha & 0 \end{bmatrix}$$

$$\begin{bmatrix} \frac{y-b}{b} & 0 & \frac{y}{b} & 0 \\ 0 & \frac{y-b}{b} & 0 & \frac{y}{b} \end{bmatrix} ds \qquad (B.2)$$

Note that the equation along this edge is $\frac{x}{a} + \frac{y}{b} = 1$; therefore

$$ds = \frac{c}{b}\, dy$$

Then perform the integration for equation (B.2) and obtain the final form of matrix [T] between nodes 1 and 2;

$$[T] = \begin{bmatrix} \frac{b}{2} & 0 & \frac{b}{2} & 0.0 \\ \frac{ab}{6} & -\frac{b^2}{6} & \frac{-ab}{6} & \frac{-b^2}{3} \\ \frac{b^2}{6} & 0 & \frac{b^2}{3} & 0 \\ \frac{ab^2}{12} & \frac{-b^3}{12} & \frac{-ab^2}{12} & \frac{-b^3}{4} \\ \frac{a^2b}{12} & \frac{-ab^2}{12} & \frac{-a^2b}{12} & \frac{ab^2}{12} \\ \frac{b^3}{12} & 0 & \frac{b^3}{4} & 0 \end{bmatrix}$$

The horizontal and vertical tractions along the edge between nodes 2 and 3 are

$$\begin{Bmatrix} S_x \\ S_y \end{Bmatrix} = \begin{bmatrix} -1 & 0 & -y & 0 & 0 & -y^2 \\ 0 & y & 0 & y^2 & 0 & 0 \end{bmatrix} \begin{Bmatrix} \beta_1 \\ \beta_2 \\ \beta_3 \\ \beta_4 \\ \beta_5 \\ \beta_6 \end{Bmatrix}$$

The displacements are assumed in linear form as follows:

$$\begin{Bmatrix} u_x \\ u_y \end{Bmatrix} = \begin{bmatrix} \frac{y}{b} & 0 & -\frac{y-b}{b} & 0 \\ 0 & \frac{y}{b} & 0 & -\frac{y-b}{b} \end{bmatrix} \begin{Bmatrix} q_3 \\ q_4 \\ q_5 \\ q_6 \end{Bmatrix}$$

Similarly, evaluate matrix [T] along the edge between nodes 2 and 3. According to equation (3.12);

$$[T] = \int_{S_u} [B]^T [D] ds =$$

$$= \begin{bmatrix} -\frac{b}{2} & 0 & -\frac{b}{2} & 0 \\ 0 & \frac{b^2}{3} & 0 & \frac{b^2}{6} \\ -\frac{b^2}{3} & 0 & -\frac{b^2}{6} & 0 \\ 0 & \frac{b^3}{4} & 0 & \frac{b^3}{12} \\ 0 & 0 & 0 & 0 \\ -\frac{b^3}{4} & 0 & -\frac{b^3}{12} & 0 \end{bmatrix}$$

Now that the individual matrix [T] is evaluated along the two edges, the overall matrix [T] is generated by assembling the individual matrices at common node 2, as follows:

$$[T] = \begin{bmatrix} \frac{b}{2} & 0 & 0 & 0 & -\frac{b}{2} & 0 \\ \frac{ab}{6} & -\frac{b^2}{6} & -\frac{ab}{6} & 0 & 0 & \frac{b^2}{6} \\ \frac{b^2}{6} & 0 & 0 & 0 & -\frac{b^2}{6} & 0 \\ \frac{ab^2}{12} & -\frac{b^3}{12} & -\frac{ab^2}{12} & 0 & 0 & \frac{b^3}{12} \\ \frac{a^2b}{12} & -\frac{ab^2}{12} & -\frac{a^2b}{12} & \frac{ab^2}{12} & 0 & 0 \\ \frac{b^3}{12} & 0 & 0 & 0 & -\frac{b^3}{12} & 0 \end{bmatrix} \quad (B.3)$$

Next, matrix [H] obtained from integrating strain energy over the volume of the singular element will be evaluated according to equation (3.13).

According to equation (B.1), define matrix [L] from equation (3.4);

$$[L] = \begin{bmatrix} 1 & x & y & 2xy & x^2 & y^2 \\ 0 & 0 & 0 & 0 & y^2 & 0 \\ 0 & -y & 0 & -y^2 & -2xy & 0 \end{bmatrix} \quad (B.4)$$

Substitution of the matrices [L] and elasticity matrix [N] into equation (3.5) gives the following expression

$$[H] = \int_V [L]^T [N][L] dV$$

$$= \int_V \begin{bmatrix} 1 & 0 & 0 \\ x & 0 & -y \\ y & 0 & 0 \\ 2xy & 0 & -y^2 \\ x^2 & y^2 & -2xy \\ y^2 & 0 & 0 \end{bmatrix} \cdot \begin{bmatrix} \frac{1}{E} & -\frac{u}{E} & 0 \\ -\frac{u}{E} & \frac{1}{E} & 0 \\ 0 & 0 & \frac{1}{G} \end{bmatrix}$$

$$\cdot \begin{bmatrix} 1 & x & y & 2xy & x^2 & y^2 \\ 0 & 0 & 0 & 0 & y^2 & 0 \\ 0 & -y & 0 & -y^2 & -2xy & 0 \end{bmatrix} dV$$

Perform the integration over the area to get the expression for the matrix [H] shown on the following page:

$$
[H] = \begin{bmatrix}
\frac{ab}{2E} & \frac{a^2b}{6E} & \frac{ab^2}{6E} & \frac{a^2b^2}{12E} & \frac{a^3b - ab^3}{12E} & \frac{ab^3}{12E} \\
\frac{a^2b}{6E} & \frac{\frac{a^3b}{E} + \frac{ab^3}{G}}{12} & \frac{a^2b^2}{24E} & \frac{a^2b^2}{30E} + \frac{ab^4}{20G} & \frac{a^4b}{20E} + \frac{a^2b^3(\frac{\mu}{E} + \frac{2}{G})}{60} & \frac{a^2b^3}{60E} \\
\frac{ab^2}{6E} & \frac{a^2b^2}{24E} & \frac{ab^3}{12E} & \frac{a^2b^3}{30E} & \frac{a^3b^2}{60E} + \frac{-\mu ab^4}{20E} & \frac{ab^4}{20E} \\
\frac{a^2b^2}{12E} & \frac{a^3b^2}{30E} + \frac{ab^4}{20G} & \frac{a^2b^3}{30E} & \frac{a^3b^3}{45E} + \frac{ab^5}{30G} & \frac{\frac{a^4b^2}{E} + a^2b^4(\frac{-\mu}{E} + \frac{1}{G})}{60} & \frac{a^2b^4}{60E} \\
\frac{a^3b - \mu ab^3}{12E} & \frac{a^4b}{20E} + \frac{a^2b^3(2/G - \mu/E)}{60} & (\frac{a^3b^2}{60E} - \frac{ab^4\mu}{20E}) & \frac{\frac{a^4b^2}{E} + a^2b^4(\frac{1}{G} - \frac{\mu}{E})}{60} & \frac{a^5b}{30E} + \frac{a^3b^3(\frac{2}{G} - \frac{\mu}{E})}{90} - \frac{ab^5}{30E} & (\frac{a^3b^3}{180E} - \frac{ab^5}{30E}) \\
\frac{ab^3}{12E} & \frac{a^2b^3}{60E} & \frac{ab^4}{20E} & \frac{a^2b^4}{60E} & \frac{a^3b^3}{180E} - \frac{\mu ab^5}{E} & \frac{ab^5}{30E}
\end{bmatrix} \qquad \text{(B.5)}
$$

Now that the matrices [T] and [H] are generated and expressed in equations (B.3) and (B.5) respectively, the stiffness matrix [K] of the triangular element can be formulated according to the equation (3.19). Note that the numerical integration has not been necessary to determine the matrices [T], [H], or [K]. A numerical stiffness matrix [K] for the special case a = b, which is the shape used in this thesis, is presented in the following:

$$[K] = 10^5 t \begin{bmatrix} 53.0727 & 0.1453 & 0.1453 & 4.8960 & -53.2180 & -5.0413 \\ 0.1453 & 13.5494 & 13.5494 & 0.4534 & -13.6947 & -14.0028 \\ 0.1453 & 13.5494 & 13.5494 & 0.4534 & -13.6947 & -14.0028 \\ 4.8960 & 0.4534 & 0.4534 & 15.2793 & -5.3494 & -15.7327 \\ -53.2180 & -13.6947 & -13.6947 & -5.3494 & 66.9127 & 19.0441 \\ -5.0413 & -14.0028 & -14.0028 & -15.7327 & 19.0441 & 29.7355 \end{bmatrix}$$

based on $E = 10.3 \times 10^6$ psi and $\mu = 0.32$.

APPENDIX C

ALTERNATIVE FORMULATION OF THE COMPLEMENTARY STRAIN ENERGY

The complementary energy functional, π_c, as given in equation (3.1) has been used to formulate the stiffness matrix; the complementary strain energy, U_c can be rewritten in tensor form as follows:

$$U_c = \frac{1}{2}\int_V C_{ijkl}\,\tau_{ij}\,\tau_{kl}\,dV$$

The strains are defined in terms of stresses by using stress-strain relations $\epsilon_{kl} = C_{ijkl}\,\tau_{ij}$. Then the complementary strain energy expression can be written as

$$U_c = \frac{1}{2}\int_V \epsilon_{kl}\,\tau_{kl}\,dV$$

If the strains satisfy compatibility, then there exist displacements u_k which can be related to the strain by using strain-displacement equation, $\epsilon_{kl} = \frac{1}{2}(u_{k,l} + u_{l,k})$. Now the complementary strain energy equation becomes

$$U_c = \frac{1}{2}\int \frac{1}{2}\,(u_{k,l} + u_{l,k})\,\tau_{kl}\,dV$$

and since the stress tensor is symmetric,

$$U_c = \frac{1}{2}\int_V \tau_{ij}\,u_{j,i}\,dV$$

By divergence theorem;

$$\int_S n_i \tau_{ij} u_j \, dS = \int_V (\tau_{ij} u_j)_{,i} \, dV$$

i.e.,

$$\int_V \tau_{ij} u_{j,i} \, dV = \int_S n_i \tau_{ij} u_j \, dS - \int_V \tau_{ij,i} u_j \, d$$

Therefore, U_c can be expressed in the following form:

$$U_c = \frac{1}{2} \int_S n_i \tau_{ij} u_j \, dS - \frac{1}{2} \int_V \tau_{ij,i} u_j \, dV$$

Note that the second integral above can be dropped out since the stress expressions (2.37) satisfy the equilibrium conditions. It is also noted that $\tau_{ij} n_j$ is the surface traction ; therefore U_c can be reduced to the following simple form.

$$U_c = \frac{1}{2} \int_{S_u} S_i u_i \, dS$$

It is important to note that this boundary formulation of U_c is valid only when the stress state satisfies the compatibility equation as well as the equilibrium equations and traction boundary conditions.

Rewrite U_c in matrix form and denote U_c as U_c^u (in terms of displacements) in order to distinguish from U_c (in terms of stresses) in equation (3.2)

$$U_c^u = \frac{1}{2} \int_{S_u} [S]^T \{u\} \, dS$$

Now π_c as given in equation (3.1) becomes

$$\pi_c = U_c^u + V_c$$

$$\pi_c = \frac{1}{2}\int_{S_u} \{S\}^T \{U\}\, dS - \int_{S_u} \{S\}^T \{U^p\}\, dS$$

Incidentally π_c becomes identical with hybrid functional, π_m, as given in equation 16 in reference [16]. Note that U_c^u can be evaluated along the boundary provided that the interior displacements along the boundary are known. Of course the displacements have to be found manually from assumed stresses by stress-strain law and strain-displacement relations. However, evaluation of U_c in (3.2) involves no hand calculation of interior displacements; and the area integration can be very easily reduced to line integration (see evaluation of [H] in Chapter III). Therefore, in the formulation of the stiffness matrix, the advantages in using U_c rather than U_c^u are as follows:

(1) Both functionals involve only line integration numerically.

(2) The computer can be used to calculate U_c as easily as U_c^u.

(3) There is no need to calculate interior displacement manually in order to obtain U_c.

Furthermore the comparison of accuracy of numerical integration can be made between U_c (in terms of stresses) and U_c^u (in terms of displacements). The simplest rectangular approximation is used for the calculation of U_c and U_c^u based on 1 symmetrical singular term for hairline cracked singular element. The numerical results for various number of segments

between nodes are given in the following table.

n	U_c^u (10^{-7})	$U_c(10^{-7})$	Difference = $\frac{U_c^u}{U_c} - 1$
5	6.9166	6.9098	9.81×10^{-4}
10	6.9132	6.9110	3.11×10^{-4}
20	6.9123	6.9113	1.43×10^{-4}
30	6.9121	6.9113	1.13×10^{-4}

Note that the differences between U_c^u and U_c are reducing as the number of segments is increased. The error vs number of segments due to numerical integration is shown in Figure 62. It appears that in order to obtain accurate results, fewer segments are required for U_c than U_c^u and only very few number of segments are necessary to obtain accurate results for both U_c^u and U_c. However, it is easier to prepare computer program to evaluate U_c^u than U_c. As a result, it requires less computer time for U_c^u than U_c.

As mentioned earlier, there are only a finite number of real eigenvalues with the exception of notch angles of 0° and 180°. If the complex eigenvalues should be used to formulate the stiffness matrix, then the procedure becomes very complicated. Fortunately the real and imaginary parts of stress expressions for any complex eigenvalue can be easily obtained by the computer. These two parts of the stress expressions are the two independent solutions for the stresses associated with the one complex eigenvalue. In order to evaluate U_c^u for an arbitrary notch angle, the interior displacements must be known. Of course the displacements can

be found from the general expressions for stresses (3.2) through the stress-strain law and strain-displacements relations. Thus the displacement functions contain the eigenvalues α which can be either real or complex numbers. It seems that the real and imaginary parts of displacements for any complex eigenvalue still can be easily obtained by computer which performs the complex arithmetic in two locations for real and imaginary parts. These two parts of the displacement expression are the two independent solutions associated with one complex eigenvalue. Thus U_c^u is still possible to be evaluated by computer without explicitly separating the complex stress function into real and imaginary parts manually.

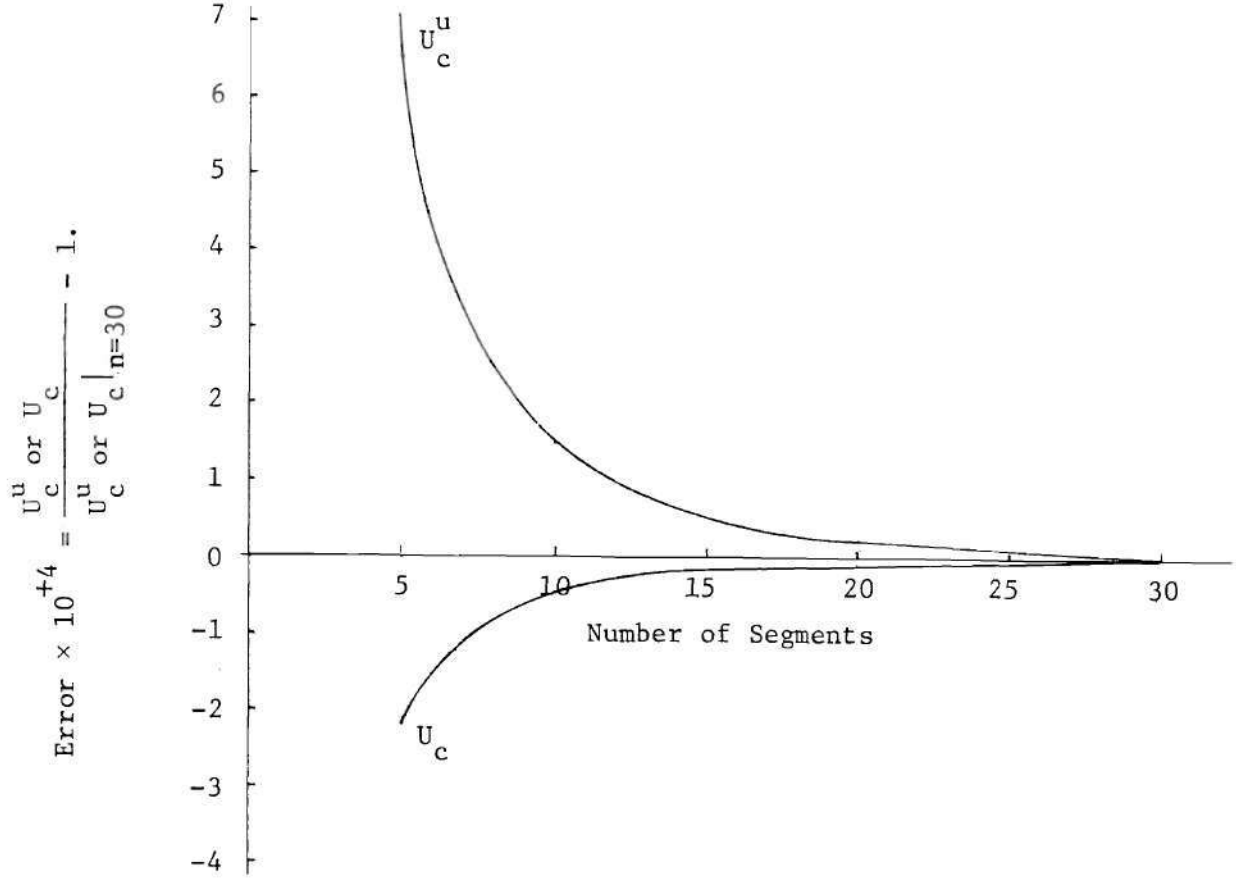

Figure 62. Comparison of Errors of U_c^u and U_c due to Numerical Integration

REFERENCES

1. Chan. S. K. et al., "On the Finite Element Method in Linear Fracture Mechanics," Engineering Fracture Mechanics, Vol. 2, July 1970, pp. 1-17.

2. Kobayashi, A. S., et al., Application of the Method of Finite Element Analysis to Two-Dimensional Problems in Fracture Mechanics, Department of Mechanical Engineering, ONR Contract Nonr-477(39), NR 064 478, TR No. 5, October 1968.

3. Anderson, G. P., et al., "Use of Finite Element Computer Programs in Fracture Mechanics," International Journal of Fracture Mechanics, Vol. 7, No. 1, 1971, pp. 63-76.

4. Watwood, V. B., Jr., "The Finite Element Method for Prediction of Crack Behavior," Nuclear Engineering and Design, Vol. II, 1969, pp. 323-332.

5. Hardy, R. H., "A High-Order Finite Element for Two-Dimensional Crack Problems," Ph.D. Dissertation, Georgia Institute of Technology, June, 1974.

6. Atluri, S., "A New Assumed Stress Hybrid Finite Element Model for Solid Continua," AIAA, Vol. 9, No. 8, August 1971.

7. Atluri, S. N., Kobayashi, A. S. and Nakagaki, M. "Application of an Assumed Displacement Hybrid Finite Element Procedure to Two-Dimensional Problems in Fracture Mechanics," AIAA, Paper No. 74-390, AIAA/ASME/SAE 15th Structures, Structural Dynamics and Materials Conference, Las Vegas, 17-19 April 1974.

8. Walsh, P. F., "The Computation of Stress Intensity Factors by a Special Finite Element Technique," International Journal of Solids and Structures, Vol. 7, 1971. pp. 1333-1342.

9. Byskov, E., "The Calculation of Stress Intensity Factors Using the Finite Element Method with Cracked Element," International Journal of Fracture Mechanics, Vol. 6, 1970, pp. 159-167.

10. Hilton, Peter D. and Hutchinson, John W., "Plastic Intensity Factors for Cracked Plates," Engineering Fracture Mechanics, Vol. 3, 1971. pp. 435-451.

11. Williams, M. L., "Stress Singularities Resulting from Various Boundary Conditions in Angular Corners of Plates in Extension," J. Appl. Mech., 1952, pp. 526-528.

12. England, A. H., "On Stress Singularities in Linear Elasticity," Int. J. Engng. Sci. Vol. 9, pp. 571-585, 1971.

13. Karp, S. N. and Karal, F. C., Jr., "The Elastic-Field Behavior in the Neighborhood of a Crack of Arbitrary Angle," Communication on Pure and Applied Mathematics, Vol. 15, 1962, pp. 413-421.

14. Timoshenko, S. P. and Goodier, J. N., Theory of Elasticity, McGraw-Hill Book Company, Third Edition.

15. Tada, H., Paris, P. E. and Irwin, G. R. The Stress Analysis of Crack Handbook, Del Research Corporation, Hellertown, Pennsylvania, 1973.

16. Tong, Pin, Pian, H.H. and Lasry, S.J., "A Hybrid-Element Approach to Crack Problems in Plane Elasticity," International Journal for Numerical Methods in Engineering, Vol. 7, 1973, pp. 297-308.

17. Bowie, O. L. and Neal, D. M., "A Modified Mapping-Collocation Technique for Accurate Calculation of Stress Intensity Factors," Army Materials and Mechanics Research Center, Watertown, Massachusetts, AMMRC TR 69-28, November 1969.

18. Bowie, O. L. and Freese, C. E., "Central Crack in Plane Orthotropic Rectangular Sheet," International Journal of Fracture Mechanics, Vol. 8, No. 1, March 1972.

VITA

The author of this dissertation, Wen-mo Chen, son of Mr. and Mrs. Mou-lin Chen, was born on June 20, 1939 in Taiwan, Formosa, Republic of China.

After graduating from the Civil Engineering Department of Taiwan Provincial Cheng Kung University in July, 1963, the author served in the Chinese Army, infantry division as a secondary lieutenant for one year.

In September, 1965, he came to the United States and entered into the Department of Engineering Mechanics, University of Missouri at Rolla. After receiving the degree of master of science in August 1966, the author worked for State of Illinois as a Civil Engineer for two years. While at Springfield, Illinois, he was a member of American Judo Association and a winner of second place light weight in Illinois State Judo tournament in 1968. During the period 1968-1974, he worked for the Lockheed-Georgia Company as an aircraft structural engineer, and continued his graduate work toward the degree of Doctor of Philosophy in the school of Aerospace Engineering. After resignation from Lockheed-Georgia Company, the author worked for Bell Aerospace Company as a Navy Surface Effect Ship Seal development method engineer for two years. The author has accepted a position as technical engineer with Hughes Aircraft Company in Culver City, California.

He was married to Pi-Ian in 1969. They have two children: Boris, born in 1970; and Jennifer, born in 1974.